LA-6850-C
Conference Proceedings

C.3

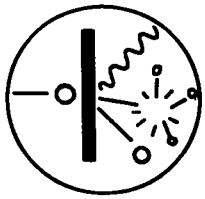

FIFTH ANNUAL CONFERENCE

OF THE

INTERNATIONAL NUCLEAR TARGET DEVELOPMENT SOCIETY

OCTOBER 19, 20, 21, 1976

PROCEEDINGS

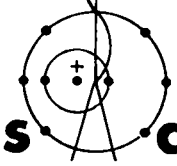

los alamos
scientific laboratory
of the University of California
LOS ALAMOS, NEW MEXICO 87545

UNITED STATES
ENERGY RESEARCH AND DEVELOPMENT ADMINISTRATION
CONTRACT W-7405-ENG. 36

Printed in the United States of America. Available from
National Technical Information Service
U.S. Department of Commerce
5285 Port Royal Road
Springfield, VA 22161
Price: Printed Copy $7.75 Microfiche $3.00

LA-6850-C
Conference Proceedings

UC-34c

Issued: June 1977

Fifth Annual Conference of the

International Nuclear Target Development Society

Held at the Los Alamos Scientific Laboratory

Los Alamos, New Mexico

October 19—21, 1976

Compilers

Judith C. Gursky
John G. Povelites

los alamos
scientific laboratory
of the University of California
LOS ALAMOS, NEW MEXICO 87545

An Affirmative Action/Equal Opportunity Employer

UNITED STATES
ENERGY RESEARCH AND DEVELOPMENT ADMINISTRATION
CONTRACT W-7405-ENG. 36

FOREWORD

Ideas and techniques on the preparation and standardization of nuclear targets were exchanged at the fifth annual conference of the International Nuclear Target Development Society held at the Los Alamos Scientific Laboratory (LASL) on October 19 - 21, 1976. The conference was sponsored jointly by the Physics Division and the Chemistry-Nuclear Chemistry Division. Participants were from LASL and twenty-one other laboratories including six from foreign countries.

These Proceedings represent a compilation of most of the papers presented at the Conference. Three papers presented orally are not included because they have been published elsewhere as noted in their abstracts. In addition, two papers were contributed for the Proceedings, but they were not presented orally (Stoner and Bashkin and Saettel). Papers are reproduced as received from the authors.

The discussions following the papers have been summarized and appear in the back of the Proceedings. Unfortunately the first morning's session was not recorded on tape; therefore these discussions are not available. Two of the planned discussion sessions are represented by papers in the body of the Proceedings (Anderl and Heagney), while the discussion following Heagney's paper appears in the back. The other discussion sessions (Perry, Riel, Gursky) include contributions from many people. In reporting the session, a presentation by the session leader is followed by a discussion summary. In addition, an abstract of J. Gallant's work, described by Wayne Perry, is included in the Proceedings.

Judith C. Gursky
John G. Povelites
Co-Chairmen

CONTENTS

Session D

THE SELECTION, CHARACTERIZATION AND COATING OF LASER-FUSION TARGETS*

by

R. Jay Fries

University of California
Los Alamos Scientific Laboratory
Los Alamos, New Mexico 87545

ABSTRACT

In this paper, I will describe some of the techniques we have developed to fabricate targets for the Los Alamos Laser Fusion program. These laser-fusion targets are essentially microminiature packages of 50:50 deuterium:tritium mixtures. They are zapped with our high-power short-pulse lasers to compress them to 10^3 to 10^4 times normal liquid density and to heat them to temperatures of several kilovolts. Under these conditions the deuterium and tritium undergo a fusion reaction to produce helium 4 plus a neutron plus energy. Calculations indicate that with sufficiently large lasers we will be able to get back more energy than we put in and therefore have a source of fusion power.

---

* Work performed under the auspices of the U. S. Energy Research and Development Administration.

Although our lasers have very high power outputs, their energy output per pulse is very small. As an example, we have under construction an eight-beam CO_2 laser, illustrated in Fig. 1, that will have a power output of from 10 to 40 terrawatts, which exceeds the power generating capacity of the entire United States. However, the energy per pulse is only 10 kJ which is just about enough to warm up your morning cup of coffee by about 10° C. As a consequence, laser-fusion targets cannot contain much mass and we find ourselves working in a microminiature world.

I will first describe in detail how we fabricate one type of laser-fusion target, known as the ball-and-disk type, to introduce you to our micro-mini world. Then I will describe some of the novel techniques we have developed to coat laser-fusion targets with metals and dielectrics.

A schematic of one of our ball-and-disk targets is shown in Fig. 2. This target was invented at LASL to overcome the problems of nonsymmetric illumination by only one or two laser beams. The DT fuel is contained as a high-pressure gas inside a glass microballoon. A disk of low-z material covers the area surrounding the pellet. In use, this disk is vaporized by a laser prepulse to form a plasma which has a very high energy conductivity. This high-conductivity plasma then allows the energy from the main laser pulse to couple uniformly to the pellet over its entire surface. The outside surface of the glass microballoon is heated by this plasma and streams away from the pellet like an ablator. This imparts a rocket reaction force to the remainder of the shell, called the pusher, and thus implodes it, compressing and heating the DT fuel. This technique is known as ablation-driven compression.

The glass microballoon is typically 40 to 60 microns in diameter with a one- to two-micron-thick wall. In order to avoid the development of instabilities during the compression, the microballoon must be highly spherical and have uniform wall thickness.

The support film should minimize the mass of extraneous material in the vicinity of the target. We have developed a duplex plastic film which supports the target rigidly, provides a substrate for the disk and acts as a glue to hold the microballoon in place. This film is a laminate of polystyrene and nitrocellulose with a total thickness of about 100 nanometers. The low-z absorber disk is usually one micron of polyethylene that is vapor deposited from the same direction as the laser beam. In Fig. 3, we show a photomicrograph of one of these ball-and-disk targets. In this case we used a gold disk to enhance its visibility.

The largest part of the effort required to fabricate this target is the selection and characterization of the glass microballoons. In Fig. 4 we show a close-up of one of these microballoons. This is 40-micron-diameter microballoon with a 1.5 micron wall. It weighs about 30 nanograms and is smaller than a human hair, as shown in Fig. 5.

And now, just to emphasize the lilleputian nature of our microballoons, we have threaded our hair through the eye of the smallest standard sewing needle as shown in Fig. 6.

Glass microballoons are made by several different companies for use as fillers and density-control additives for plastics. They are available in minimum orders of 2 to 10 pounds. And at a density of 10^{10} balls per pound, that is a lot of microballoons. However, most of these are not suitable for use as laser targets. Although we have not actually counted the bad ones, one in 10^6 or 10^7

is a conservative estimate for the fraction of good microballoons. That still leaves 1000 to 10,000 good balls in each one pound batch. So the only problem is how to find the good ones.

In Fig. 7 we outline the process we use to find the good microballoons. I will describe each one of these steps in detail below. For now, I want you to notice that we first use three batch processes to increase the fraction of good microballoons that are present in the batch; after these, we must start examining the microballoons one at a time for quality characterization and measurement. In all of these techniques we must account for the seemingly perverse character of these very light microballoons for which electrostatic, surface tension and aerodynamic forces greatly exceed gravitational effects.

The first batch process, shown in Fig. 8, is size separation. Normal screening methods are greatly hampered by the tendency of dry microballoons to agglomerate strongly when shaken and the tendency of wet microballoons to float. We have, therefore, used the bouyant forces in a float screening method as shown in the figure. The microballoons are introduced under an inverted screen stack which is immersed in ethanol in an ultrasonic cleaner. Bouyancy provides the driving force and the ultrasonic motion provides agitation. This method gives very efficient screening. It also eliminates broken pieces of microballoons and any microballoons containing large holes. The method is used a second time later after the crush test, described below, to separate good balls from broken pieces.

Once the microballoons are separated by size, their particle density is a measure of their wall thickness. The density of microballoons of interest is less than 0.5 g/cm^3, too light for the use of any liquid density separation

methods. Therefore, we use a gas density separation technique in an apparatus shown schematically in Fig. 9. We charge a batch of sized microballoons into this chamber and pressurize it with SF_6 gas until the desired density is reached. Microballoons with a density less than that of the gas float upward, up by the collector cone and gather at the top of the upper glass cap. A vibrator is used to help discourage agglomeration by providing periodic agitation to the vessel. Then, after all of the floaters have collected at the top of the vessel, the pressure is reduced and the microballoons fall into the collector cone. Again, a little buzz from the vibrator is helpful. These microballoons are then removed from the cone prior to repressurizing to a higher pressure for the next density cut. Here again, since we collect only microballoons that float, those with small holes are removed from the batch in this step.

After the float screening and this density separation, the diameter and average wall thickness are known and the spheres can be sorted for use as targets. However, we would like to obtain the highest possible yield of good microballoons from our one-at-a-time inspection. Therefore, we employ one additional batch process, and subject the microballoons to a high external gas pressure. As shown schematically in Fig. 10, this creates larger stresses in the imperfect microballoons than in the perfect ones and we can thereby preferentially crush the lower quality balls. We generally choose a pressure that crushes 90 to 95% of the microballoons. This increases the number density of good microballoons in the surviving batch by a factor of 3 to 4.

As mentioned above, after this crush test, the spheres are separated from the shards in a separatory funnel and the microballoons are then rescreened by float screening under ethanol to remove small adherent chips.

At this point, we have completed the batch processing and must now go to the one-at-a-time inspection technique, as shown in the processing flow diagram in Fig. 7. If the microballoons are transparent glass such as we have been discussing, we use optical interferometry to select high-quality microballoons and measure their wall thickness. If, on the other hand, the microballoons are metal or otherwise opaque we use x-ray microradiography for this purpose.

In this latter case, we lay out a 10 by 10 array of microballoons on a thin film of mylar that is stretched across a frame. A microdrop of light oil holds each ball in place by surface tension. The array is made by removing microballoons from a dish under the microscope with a tool made from a single piece of camel's hair glued to the end of a dissecting needle. Then we slide the array holder under the microscope and deposit the microballoon into its proper place in the array with our camel's hair. When complete, the array is placed against the emulsion side of a Kodak HRP plate and irradiated in vacuum by an x-ray source about one-half meter away. In Fig. 11, we show typical radiographic images of a good microballoon on the left and a bad one on the right.

Now, with glass microballoons, we have found that it is faster and more precise to quality select and measure wall thickness by optical interferometry. For this inspection we spread out the microballoons on a glass microscope slide and use a Jamin-Lebedev interferometer attachment on our Zeiss research microscope to examine the balls. A field of balls on the stage of the interferometer is shown in Fig. 12. If the microballoon is spherical with uniform walls, we will see circular interference fringes that are concentric with the outside of the microballoon. If the microballoon is not spherical or if the walls are not

uniform, the fringes will be noncircular and/or nonconcentric. There is only one high-quality microballoon in this figure, the one in the upper left corner. Most of the rest range from bad to horrible. In Fig. 13, we illustrate one of the oddities that we sometimes encounter. This microballoon has a very nonuniform wall thickness but the nonuniformity is very symmetrical. We might be able to use this type to compensate for some asymmetries in the laser energy input. Except that we'll probably never find another one like it.

Acceptable microballoons are removed from the interferometer microscope stage with our camel's hair tool or from the radiograph array with a micro vacuum pipette. If necessary, they are cleaned in acetone and then placed into a glass capillary to be loaded with DT fuel.

The microballoons are filled with the desired density of DT fuel gas by permeation through the wall at elevated temperature. The capillary containing the selected microballoons is placed in a steel vessel that is then pressurized with DT gas and heated to the desired temperature. Usually 24 h at 400° C is sufficient to fill any of the glass microballoons that we use. And in this case, nature smiles on us because at room temperature these glass microballoons retain the DT fuel gas with a half-life in excess of one year. Following cooling and depressurization, the microballoons are floated out from the capillary in acetone and mounted for use as targets.

The target holder consists of a strip of molybdenum foil with a 4-mm hole near one end where the target is mounted. A thin polystyrene film is picked up from a water surface so that it covers the hole in the molybdenum sheet. A thin nitrocellulose film is then laminated to the polystyrene, also by picking it up from a water surface. A DT-filled microballoon is then placed

near the center of the 4-mm hole on the polystrene side of the film. Here again, our camel's hair tool is used to position the microballoon on the plastic film. With the ball in place, the target holder is placed on a hot plate at 150° C for about 30 seconds. This heating stretches the plastic films tautly across the hole and softens the polystyrene which serves to glue the ball to the films. The nitrocellulose supports the entire assembly during this processing.

The mounted target is then placed in an x-ray counter shown schematically in Fig. 14 to assay the tritium content of the microballoon. If this is satisfactory, the absorber disk is then applied. To do this, a mask with a 200 micron diameter hole is centered over the ball and this assembly is then mounted in a vacuum evaporator. Polyethylene is boiled in a resistance-wire-heated crucible located below the target mask assembly. This creates the polyethylene vapor beam that deposits through the mask to create the disk and the cap on the front of the ball.

Figure 15 shows another completed ball-and-disk target. The ball has been nickel coated here to increase its mass. The colored rings in the polyethylene disk arise because of light interference effects. In Fig. 16, we show a two-beam ball-and-disk target using a plain glass ball and a polyethylene disk. In this case, the microballoon is supported by sandwiching it between two nitrocellulose films so that the equator of the ball is in the plane of the support film, and polyethylene disks are deposited on both sides of the support film.

Sometimes, for other types of experiments we mount microballoons on glass posts or stalks, as shown in Fig. 17. The stalk tapers down to be about 5 microns where it attaches to the ball. The two are glued together with a fast-setting epoxy.

Alternatively, we can use a glass fiber as shown in Fig. 18. In this case, we can use a much thinner fiber - down to one or two microns diameter - because the fiber is immobilized at both ends by gluing to the molybdenum frame.

That concludes my description of the fabrication of these laser targets. Now I want to describe several novel techniques that we have developed for coating microspheres with metals and dielectrics.

In Fig. 19 we show a schematic of a generalized laser-fusion target that might be useful with our large, multibeam laser systems in the future. We start with a preexisting glass or metal microballoon for a mandrel and then coat that with a high-z, high-density metal to serve as the pusher and then overcoat this pusher with a low-z, low-density material to serve as the absorber-ablator.

A plastic coating is frequently desired for this absorber-ablator layer. Thus, we developed a glow discharge polymerization technique, shown schematically in Fig. 20, to put uniform coatings of polymerized paraxylene plastic onto microsphere substrates. We place two flat parallel-plate electrodes in our vacuum system and admit a mixture of argon and paraxylene vapor to get a pressure of about 400 millitorr. Then we drive the electrodes with about 400 volts at one kiloherz which creates a glow discharge between the two electrodes. This glow discharge activates the paraxylene to form ions and free radicals which then deposit on any surfaces in the vicinity, reacting and polymerizing in the process. We found that if we put glass microballoons on the lower electrode, the plasma causes them to bounce. This keeps the balls in motion to prevent agglomeration and to allow a uniform coating of plastic to be deposited over their entire surface. Figure 21 shows a picture of the apparatus, which was mounted in an 18 inch bell jar vacuum system. Figure 22 is a close-up view of a set of electrodes. We put a mylar fence around the bottom electrode to prevent the balls from bouncing away.

We found that metal microballoons didn't bounce nearly as well in the plasma as the glass microballoons and as a result, they didn't coat as well. As shown in Fig. 23, we overcame this difficulty by mounting a set of electrodes on an electromagnetic vibrator. With the combined plasma and vibrator agitation we can now coat metal microballoons as well as the glass ones. Figure 24 is a microradiograph of a plastic coated glass microballoon. It illustrates the good adherence and coating thickness uniformity that we obtain with this technique.

Now I want to describe our techniques for coating microballoons with metal. We have tried all of the usual methods with our microspheres, including physical vapor deposition, sputtering, electroless deposition and electroplating. In all of these methods, the trick is to keep the microspheres moving so that they don't agglomerate together or stick to the apparatus and so that they are coated uniformly with the metal. I will limit my discussion to electroplating and to electroless deposition because we have developed novel techniques to coat microspheres with metal by both of these processes. Both of these techniques were developed by Tony Mayer in LASL Group CMB-6.

Let's start with electroless plating. In this technique, the metal is generated by chemical reduction in an aqueous solution. The metal then plates out onto surfaces in contact with the solution.

The method we used in the past for electroless plating was to disperse the microspheres in the vortex of a vigorously-stirred plating solution until the desired deposit thickness was obtained.

As shown in Fig. 25, useful coatings were obtained by this method. However, agglomeration was a serious problem; coating thickness uniformity from ball-to-ball in the same batch varied widely as the figure illustrates, and, it was difficult

to obtain good surfaces on coatings thicker than about 5 microns. In addition, rather different stirring techniques were required for microspheres more dense or less dense than the plating solution.

These difficulties prompted us to develop this new technique, in which the microspheres are dispersed in the plating solution by pumping. We show a schematic of the apparatus in Fig. 26. The microspheres to be plated are contained in a cylindrical reaction chamber between two end screens. This chamber is driven up and down over a stationary piston which effectively pumps the solution through the reaction chamber. The motion of the pumped solution imparts a random stirring motion to the microspheres regardless of their relative density.

For example, when the cylinder moves down, the plating solution is forced up through the reaction chamber which lifts, rotates and disperses any sinking particles. Conversely, when the cylinder moves up, the solution is pulled into the cavity through the top screen. This rotates and disperses any floating particles. An additional advantage of this system is ready removal of any gases that are formed in the plating process.

Figure 27 shows an overall view of the apparatus. The motor assembly that drives the reaction cylinder up and down is above the apparatus but it is not connected in this view.

Figure 28 shows cross sections and surfaces of electroless nickel coatings deposited onto Solacel metal microballoons with this new technique. Note that we have obtained very thick coatings with good ball-to-ball uniformity and good surface quality.

Finally, I want to describe our electroplating technique. Electroplating was of particular interest to us because of the wide range of high-strength metals and alloys that can be deposited by this technique. A schematic of the apparatus

is shown in Fig. 29. Here again, we contain the microballoons in a cylindrical reaction cavity that is closed off at each end with a plastic screen. A cathode wire is mounted adjacent to each screen inside the reaction chamber. Plating solution is pumped through this chamber - first downward and then upward - which forces the particles alternately against each end of the chamber.

A switching system is used so that the only cathode that is activated is the one against which the particles are being pumped. Note that most of the volume of the cavity is filled with large, 3-mm-diam plastic spheres. As the much smaller microspheres are pumped from one end of the chamber to the other, they tumble and bounce against these big plastic spheres, which breaks up any agglomerates that are forming.

Figure 30 is an overall view of the apparatus showing the reaction chamber, the pumps and the timing and switching circuitry.

In Fig. 31, we show a close up of the reaction chamber and you can see the tiny black microspheres that we are plating mixed in with the big white plastic balls.

We have found this apparatus to be very useful. With it, we can plate thick, high-quality layers of metal onto microsphere substrates regardless of their density relative to the plating solution. Figure 32 shows a 14-micron-thick bright-nickel coating applied to Solacel metal microballoons. We have also plated copper and gold/copper alloys and we are now working on a high-strength nickel/iron alloy.

Acknowledgements

The techniques described above represent the work of many people. We have a group of twelve people here in the Laser Division at LASL, who are responsible for the detailed target fabrication and assembly. Of these, Gene Farnum deserves special recognition for the development of many of the separation and characterization techniques that we use. In addition to this "in-house" effort, as shown in Fig. 33, we have been aided by people in 29 different groups spread across 11 LASL divisions, as well as by the Advanced Engineering Department of Bendix, Kansas City Division. The successes we have achieved are, in large measure, a direct result of this very broad base of support on which we have been able to call.

Figure Captions

Fig. 1. LASL's eight-beam, 10 kJ CO_2 laser system.

Fig. 2. Schematic diagram of a one-beam ball-and-disk target.

Fig. 3. Photomicrograph of a one-beam ball-and-disk target. Metallic disk employed to enhance visibility.

Fig. 4. Close-up view of a glass microballoon, $\sim$ 40 μm diameter with a $\sim$ 1.5 μm-thick wall.

Fig. 5. Photomicrograph of a glass microballoon on a hair, which is a useful tool for manipulating microballoons.

Fig. 6. Glass microballoon on a hair that is threaded through the eye of a sewing needle to illustrate the scale.

Fig. 7. Flow diagram for glass microballoon processing.

Fig. 8. Schematic diagram of inverted liquid screening technique for size separation of microballoons.

Fig. 9. Schematic diagram of gas-density separation apparatus used to separate previously-sized microballoons according to their wall thickness.

Fig. 10. Schematic diagram of wall stresses in symmetric and assymetric microballoons resulting from an external gas pressure.

Fig. 11. X-ray microradiographs of symmetric and assymetric microballoons.

Fig. 12. Glass microballoons as viewed in an optical interferometer. A good microballoon exhibits circular fringes that are comentric with the outside surface of the microballoon.

Fig. 13. Interferometer fringe pattern of a glass microballoon that has an unusually symmetric wall-thickness nonuniformity.

Fig. 14. Schematic diagram of x-ray counting system used to assay tritium content of microballoons.

Fig. 15. Photomicrograph of a one-beam ball-and-disk target with a metal-coated microballoon and a polyethylene disk mounted on a thin ($\sim$ 1000 Å) plastic film. (Disk location indicated by interference fringes.)

Fig. 16. Photomicrograph of a two-beam ball-and-disk target using a glass microballoon mounted between thin plastic films ($\sim$ 500 Å), onto which polyethylene disks are deposited.

Fig. 17. Photomicrograph of a glass microballoon target glued to a thin glass stalk.

Fig. 18. Photomicrograph of a bare glass microballoon target glued to a very thin (1 to 2 μm) glass fiber.

Fig. 19. Schematic diagram of a generalized, multilayered laser-fusion target.

Fig. 20. Schematic diagram of the apparatus used for glow-discharge polymerization (GDP) method of applying plastic coatings to laser-fusion targets.

Fig. 21. Photograph of the glow-discharge-polymerization apparatus.

Fig. 22. Photograph of stationary electrode assembly used in the GDP apparatus for coating glass microballoons and stationary mandrels.

Fig. 23. Photograph of vibratory electrode assembly used in the GDP apparatus for coating metal microballoons.

Fig. 24. X-ray microradiograph of a GDP plastic-coated glass microballoon.

Fig. 25. Metallographic sections of nickel coatings (on Solacel metal microballoons) applied by the stirred-vortex dispersion technique of electroless plating.

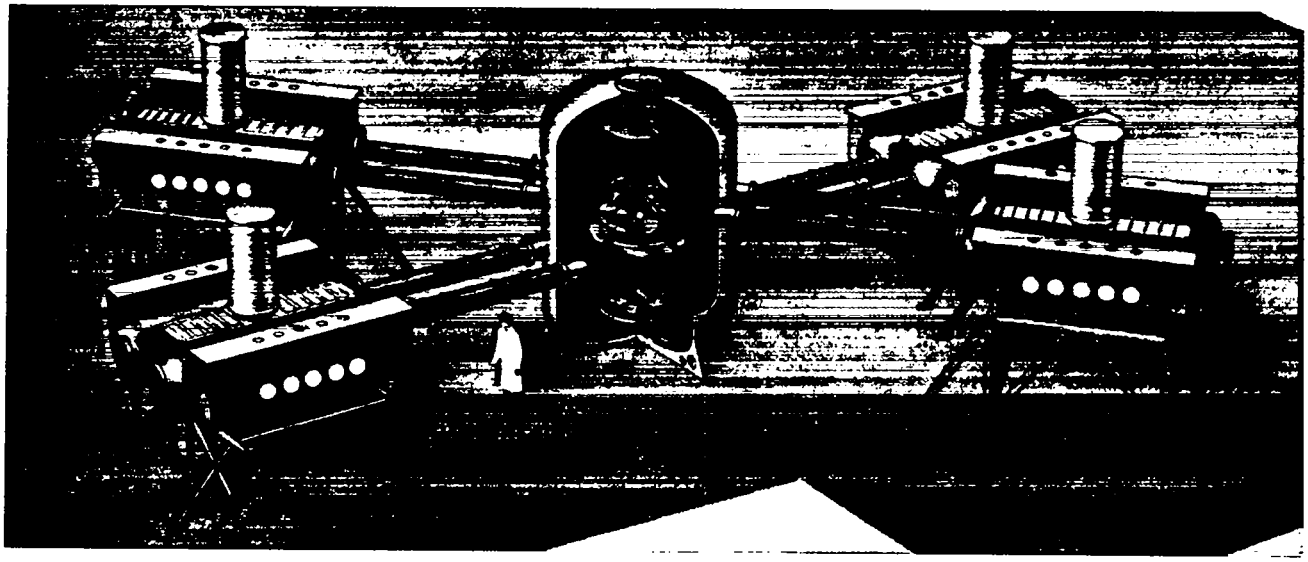

Fig. 1

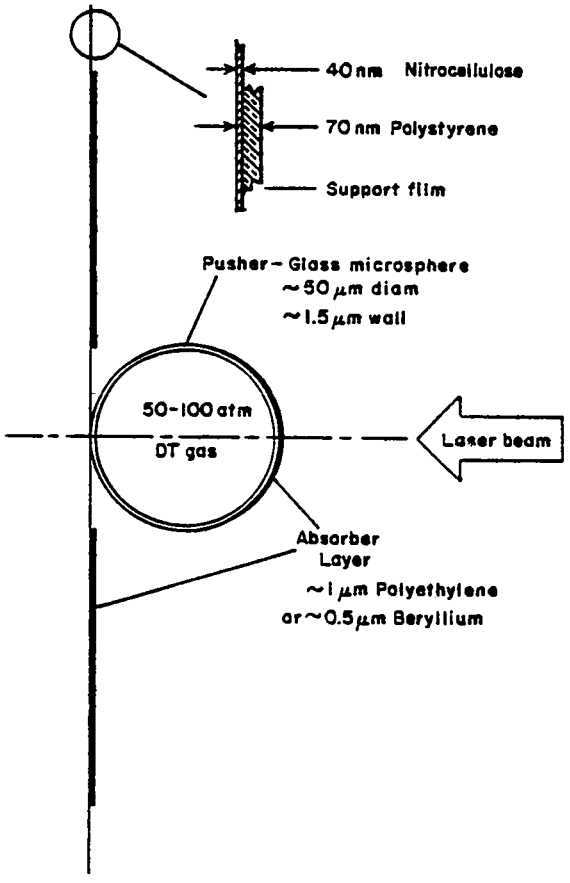
40 nm Nitrocellulose
70 nm Polystyrene
Support film
Pusher – Glass microsphere
~50 μm diam
~1.5 μm wall
50-100 atm
DT gas
Laser beam
Absorber
Layer
~1 μm Polyethylene
or ~0.5 μm Beryllium

Fig. 2

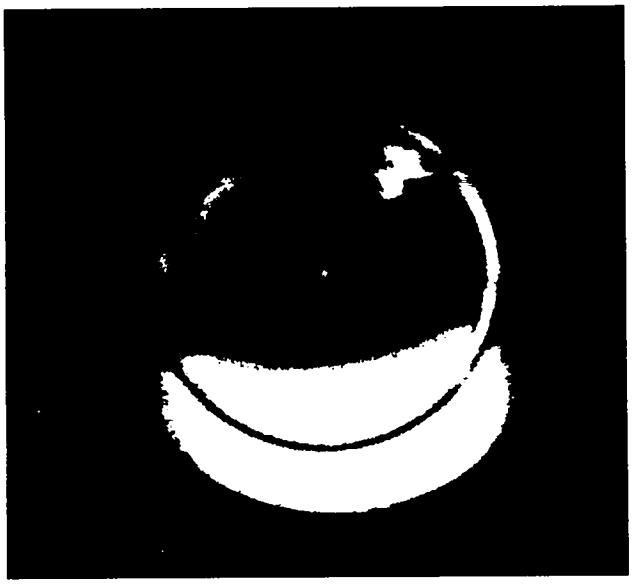

Fig. 3

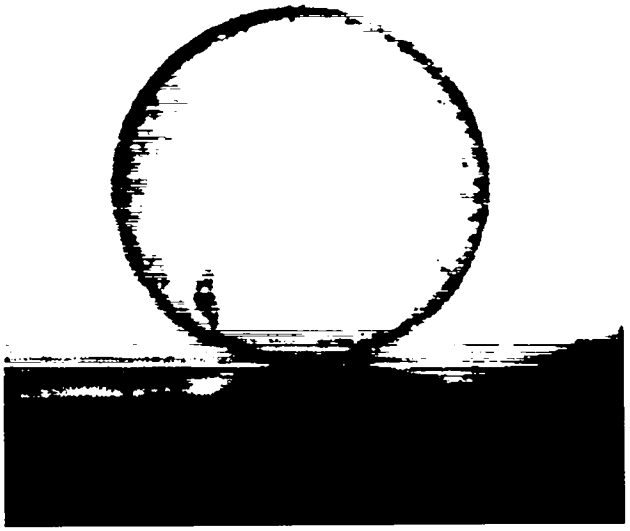

Fig. 4

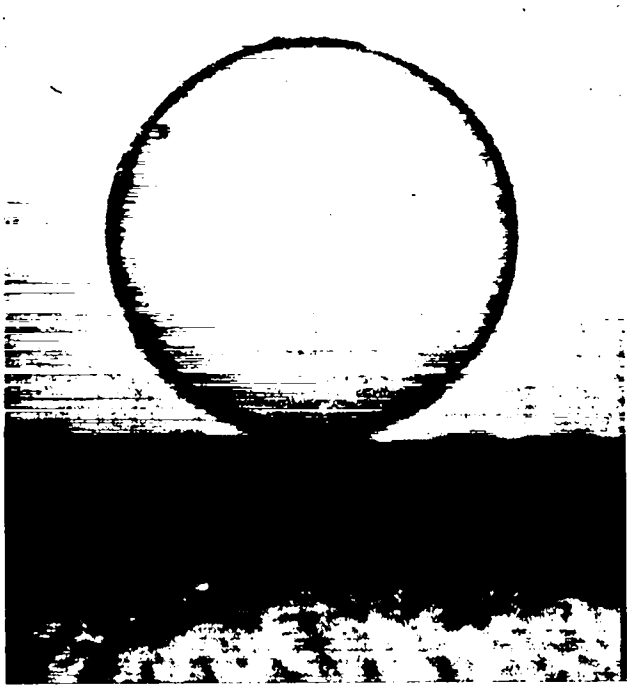

Fig. 5

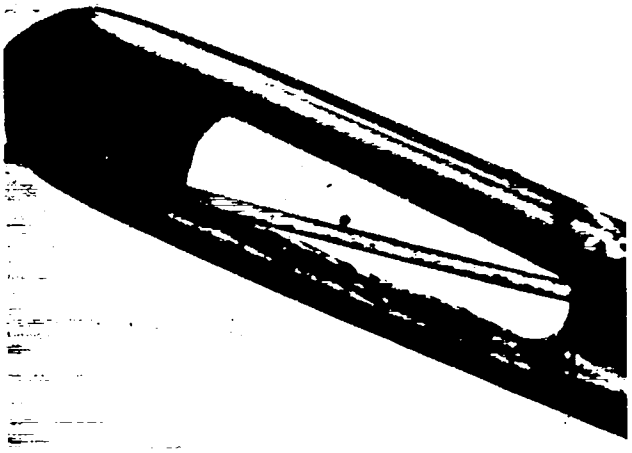

Fig. 6

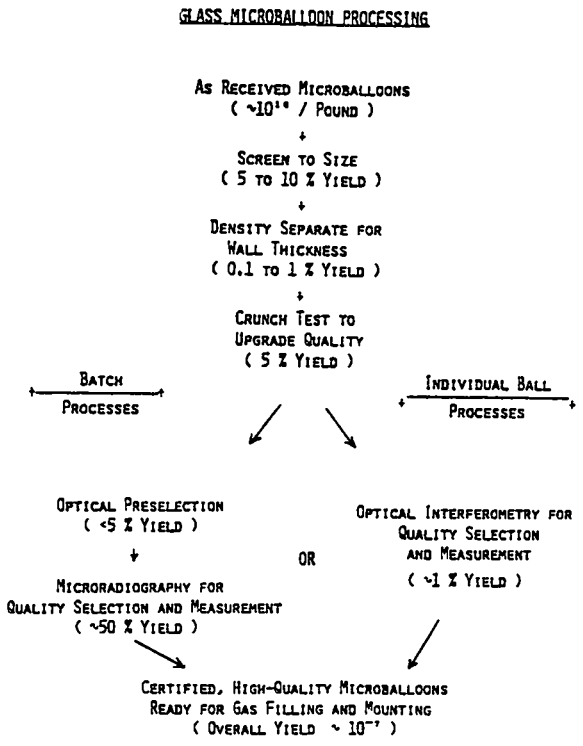

Fig. 7

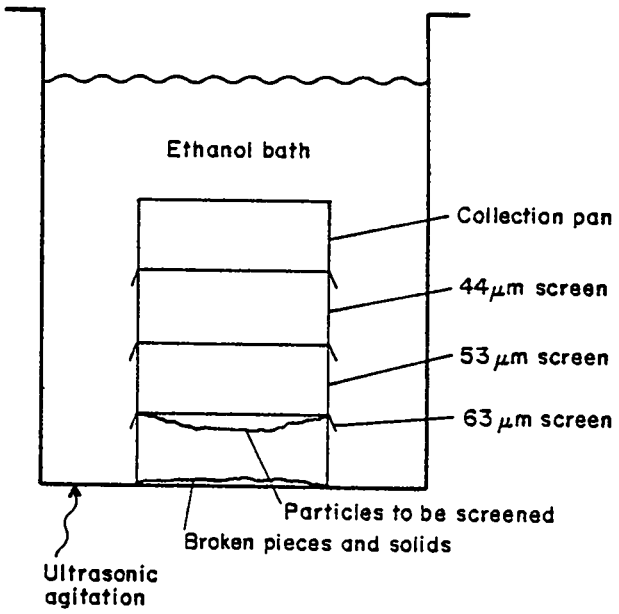

Fig. 8

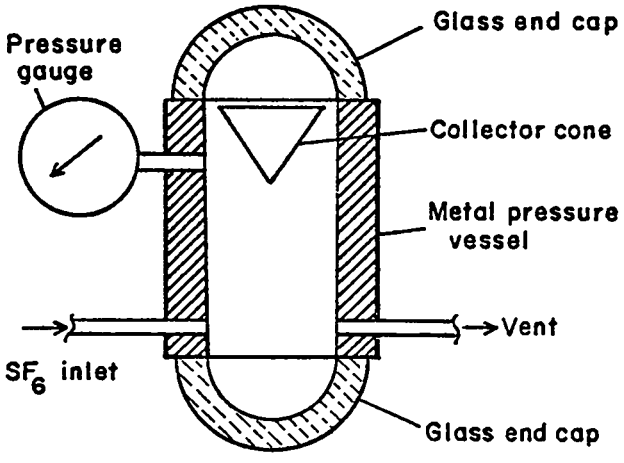

Fig. 9

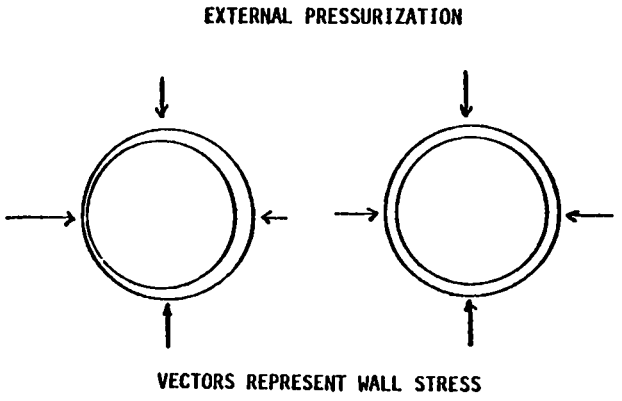

Fig. 10

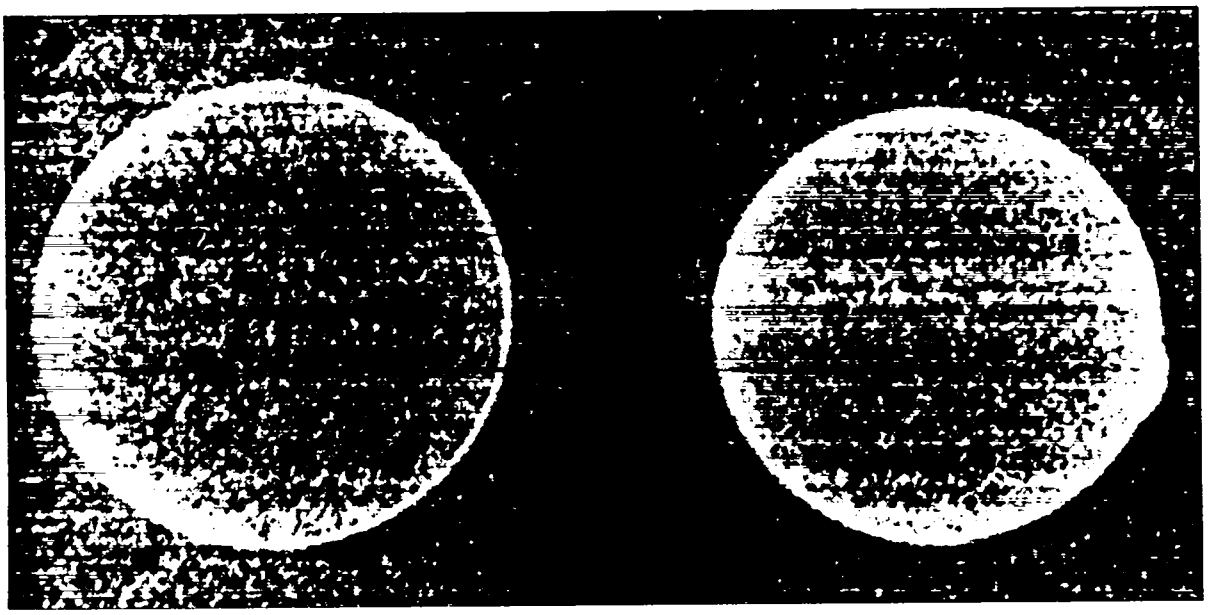

Fig. 11

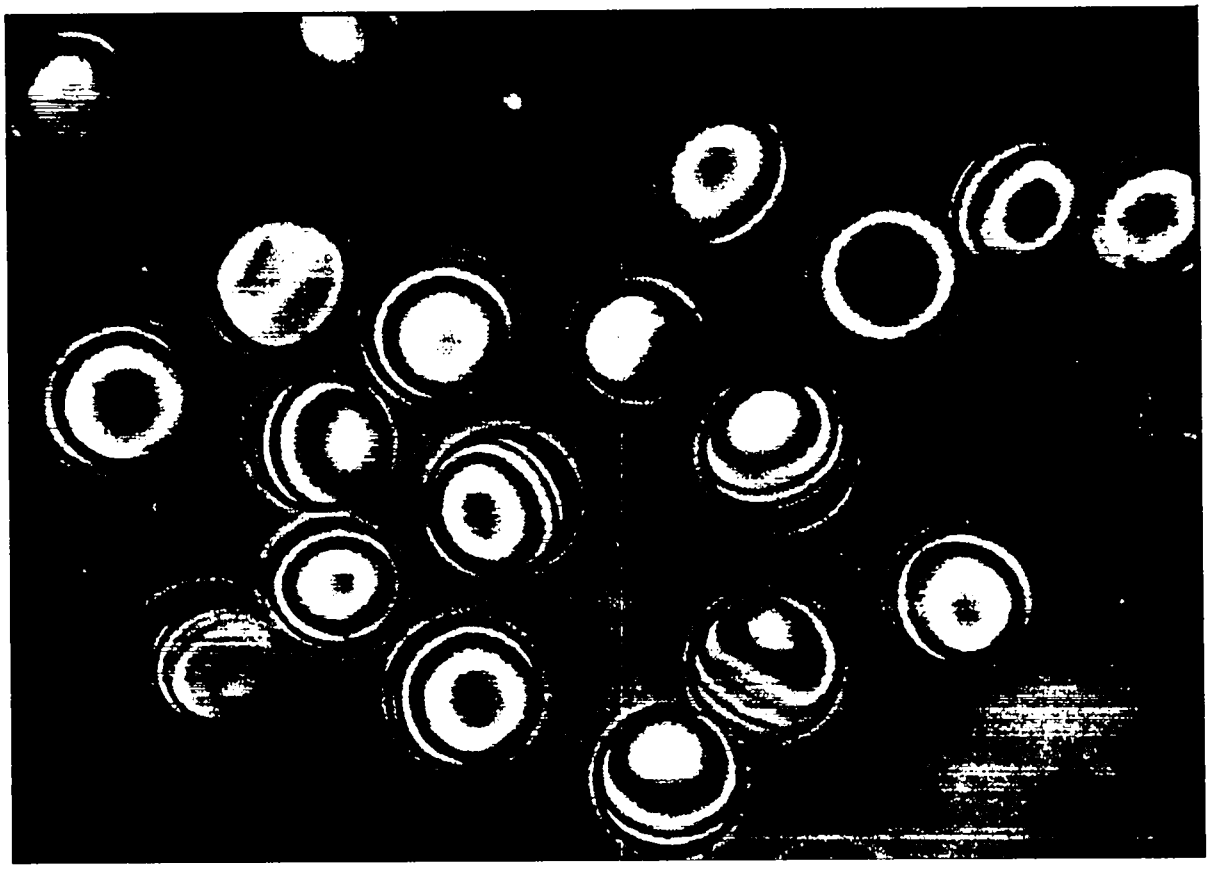

Fig. 12

Fig. 13

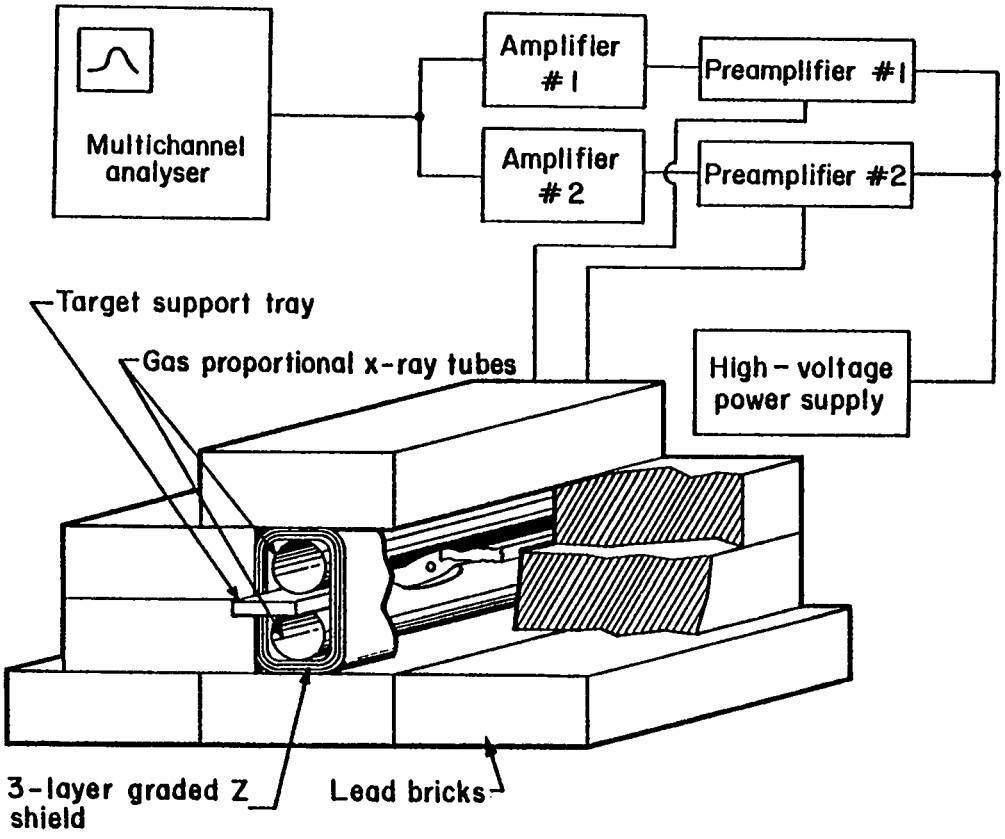
Multichannel analyser
Amplifier #1
Amplifier #2
Preamplifier #1
Preamplifier #2
High - voltage power supply
Target support tray
Gas proportional x-ray tubes
3-layer graded Z shield
Lead bricks

Fig. 14

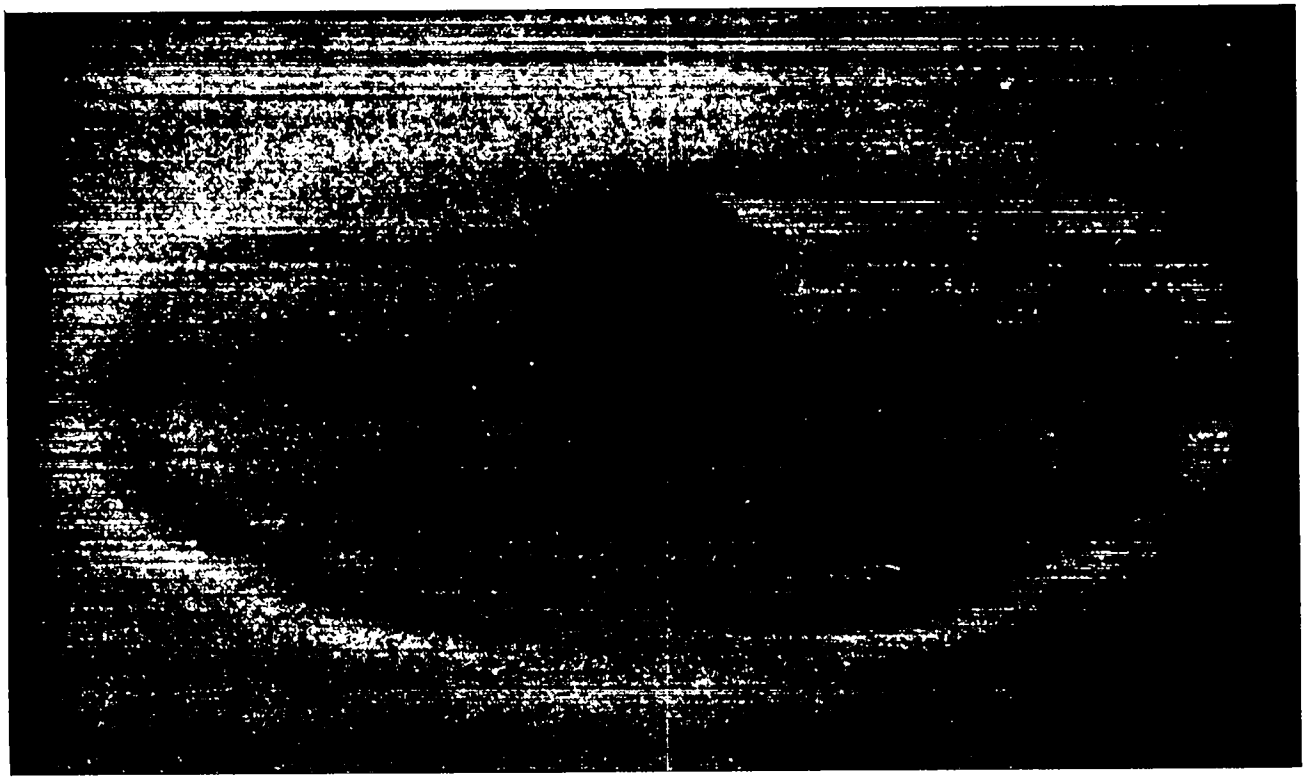

Fig. 15

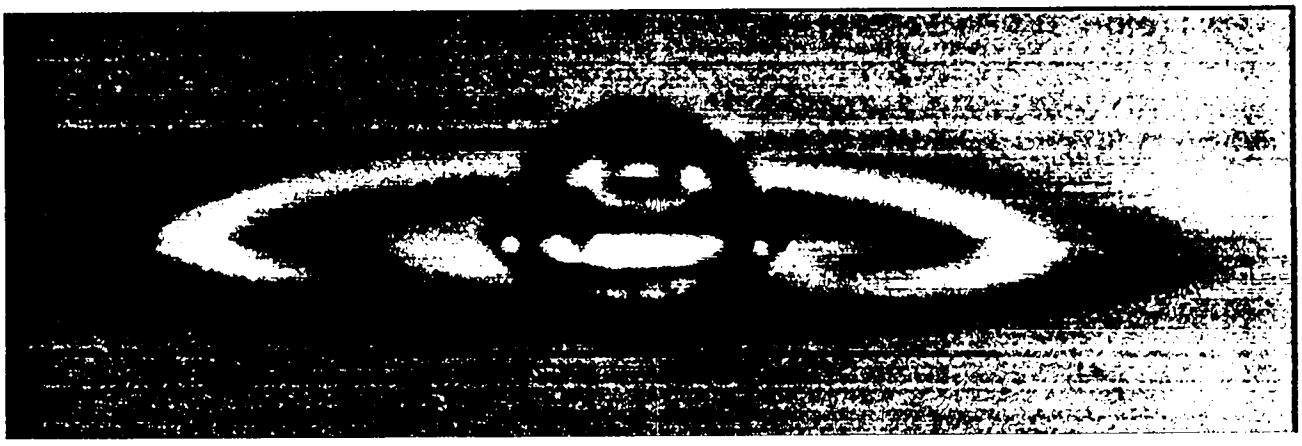

Fig. 16

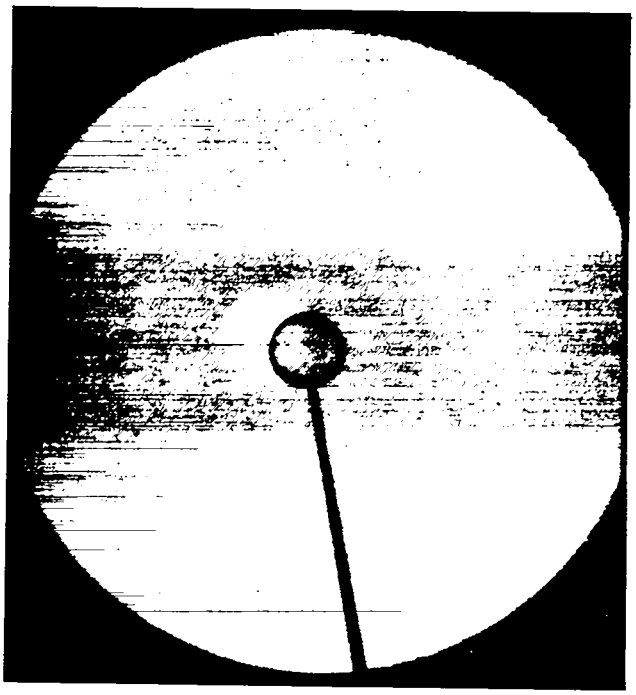

Fig. 17

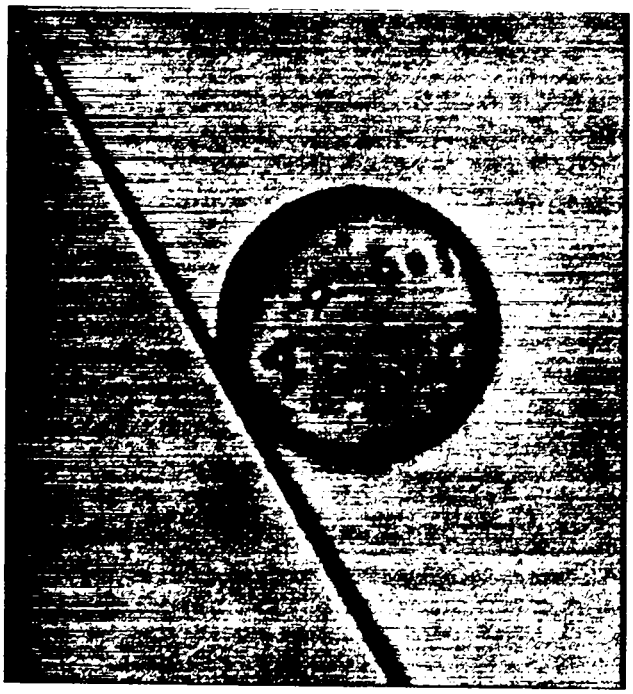

Fig. 18

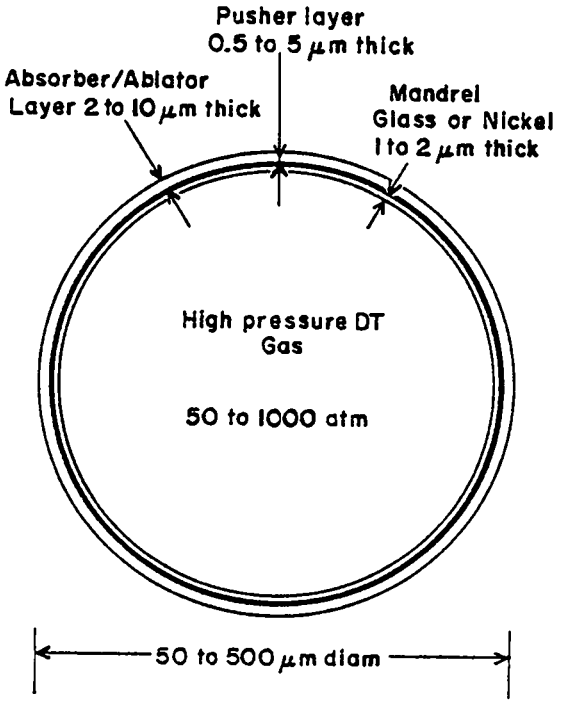

Fig. 19

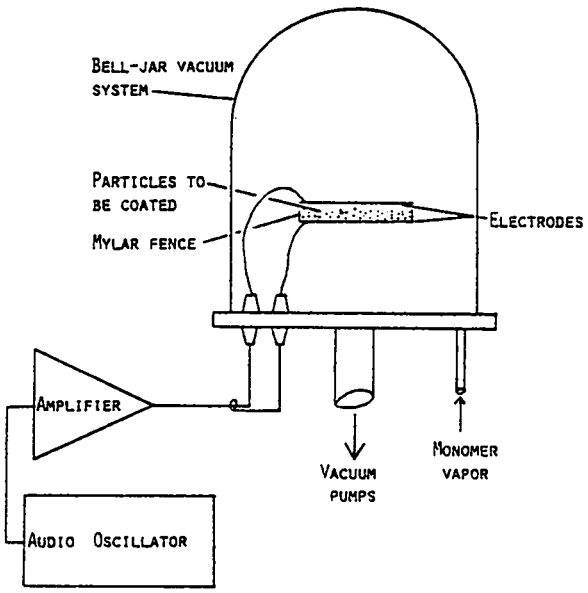

Fig. 20

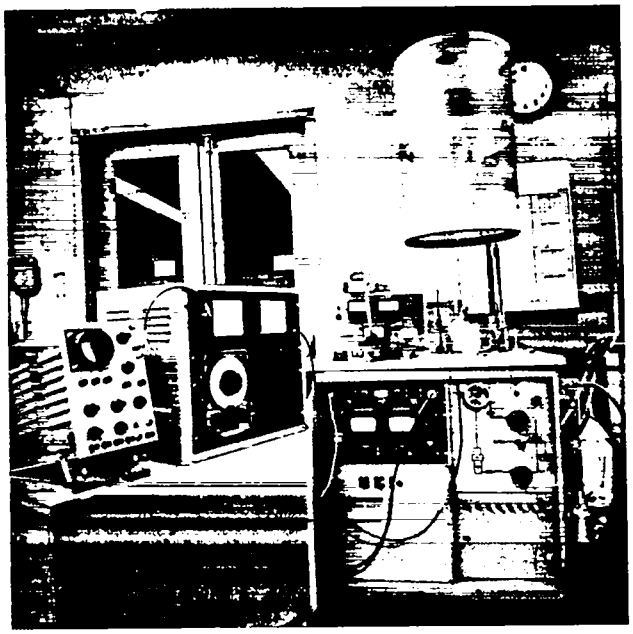

Fig. 21

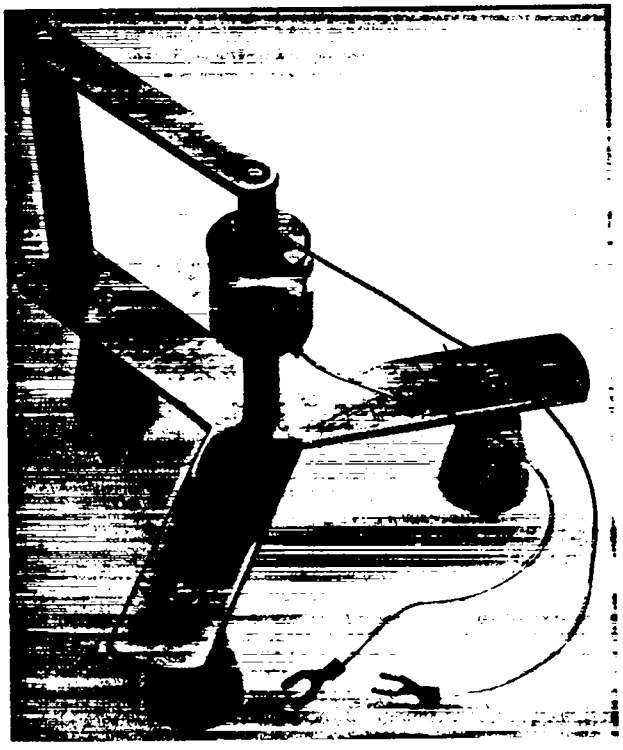

Fig. 22

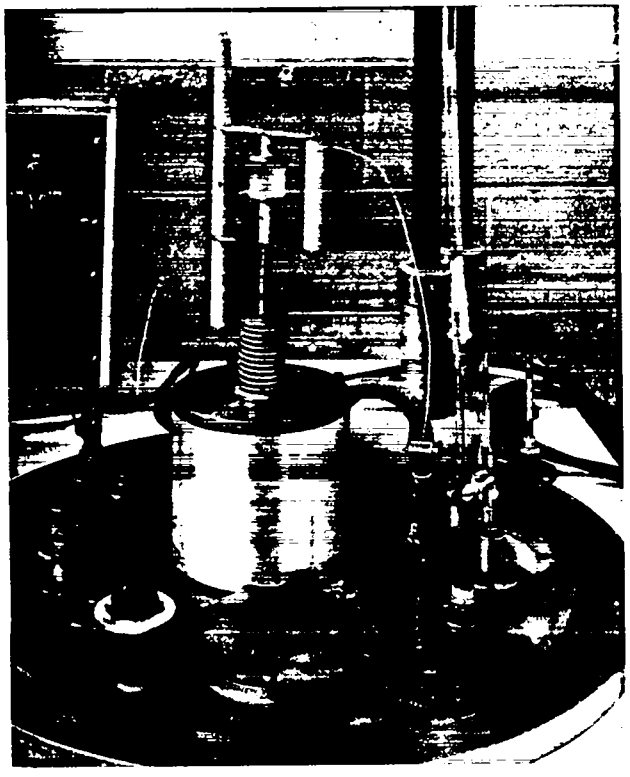

Fig. 23

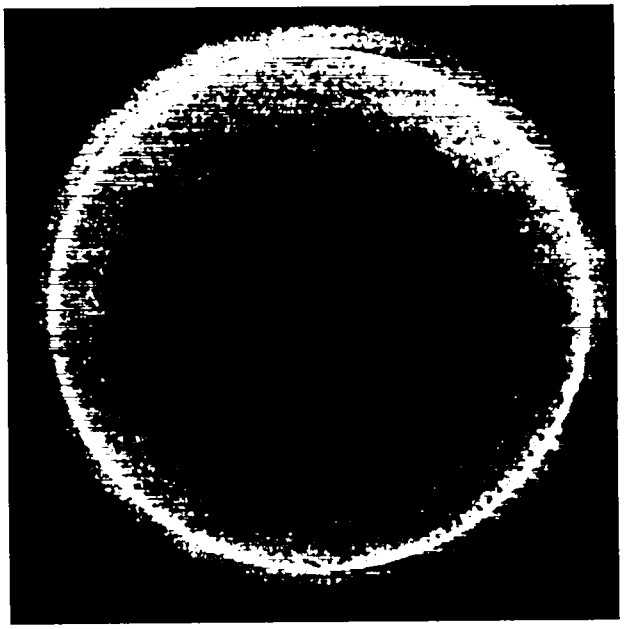

Fig. 24

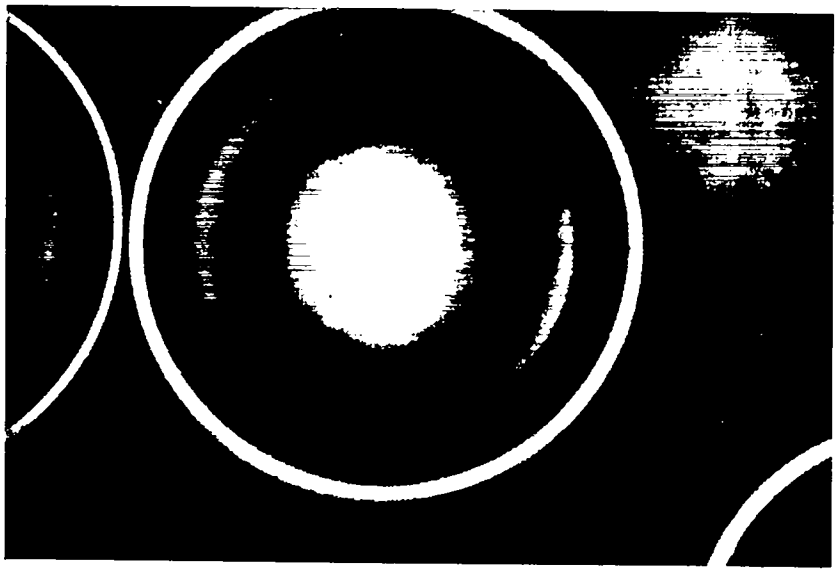

400X

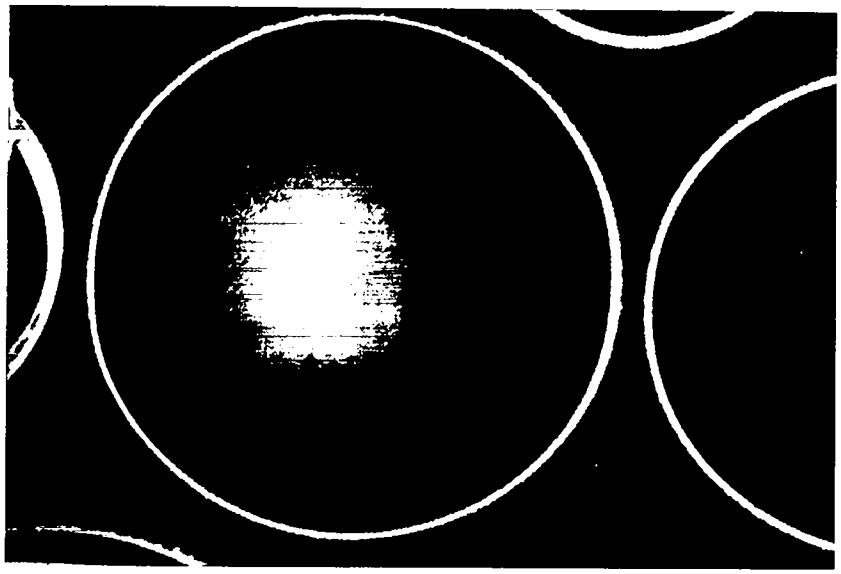

400X

Fig. 25

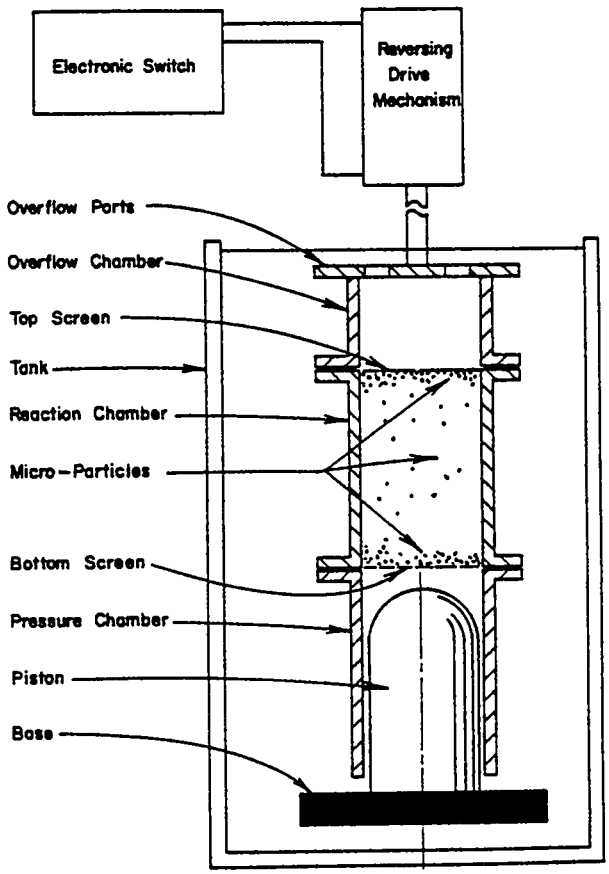
Electronic Switch
Reversing Drive Mechanism
Overflow Ports
Overflow Chamber
Top Screen
Tank
Reaction Chamber
Micro-Particles
Bottom Screen
Pressure Chamber
Piston
Base

Fig. 26

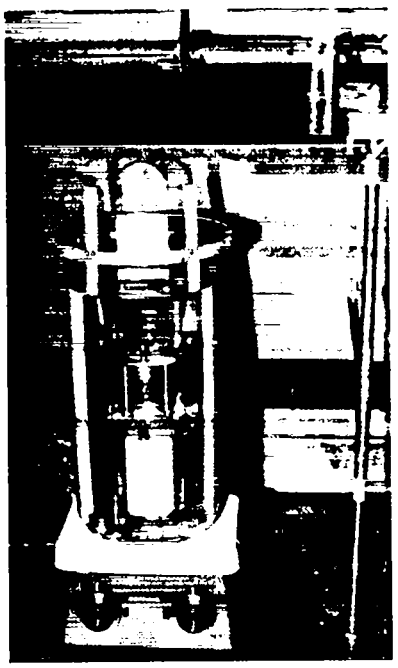

Fig. 27

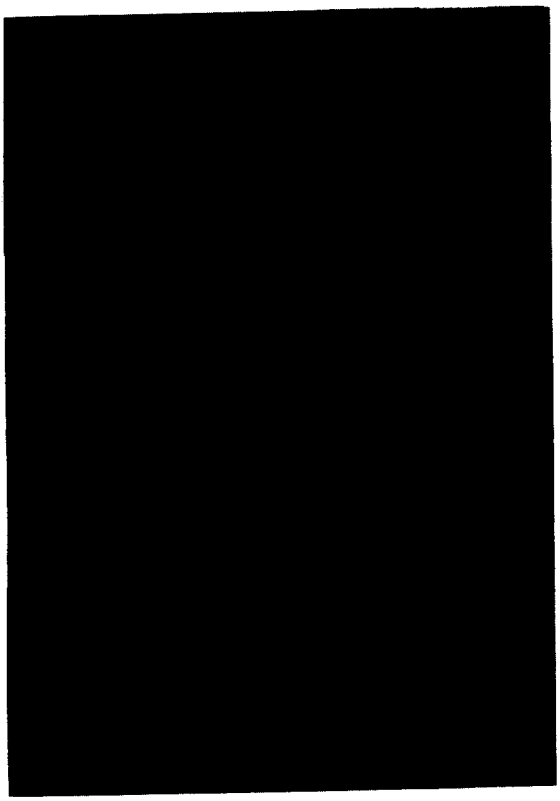

400X

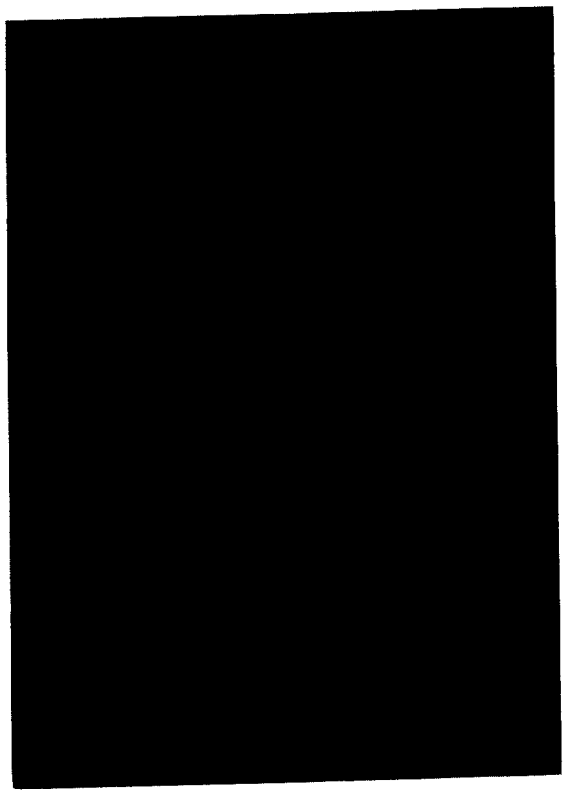

400X

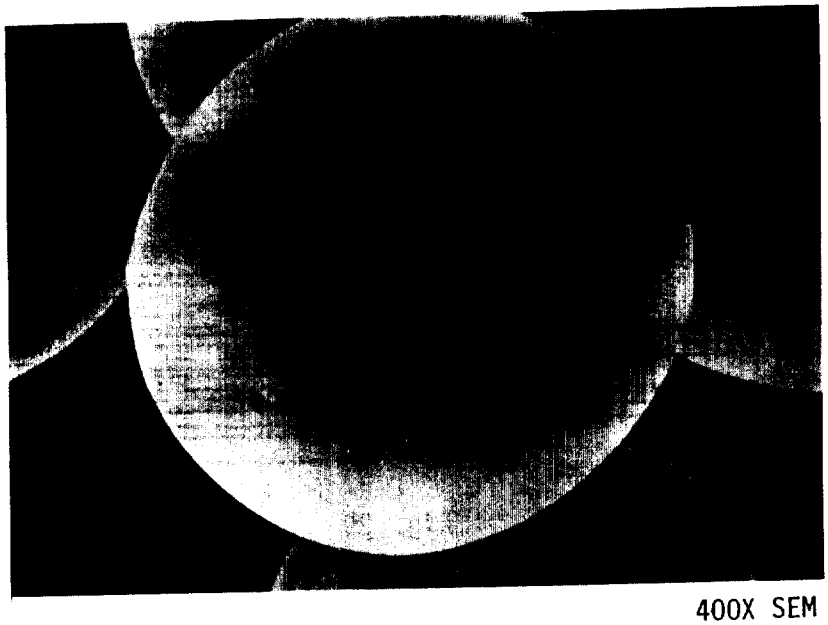

400X SEM

Fig. 2E

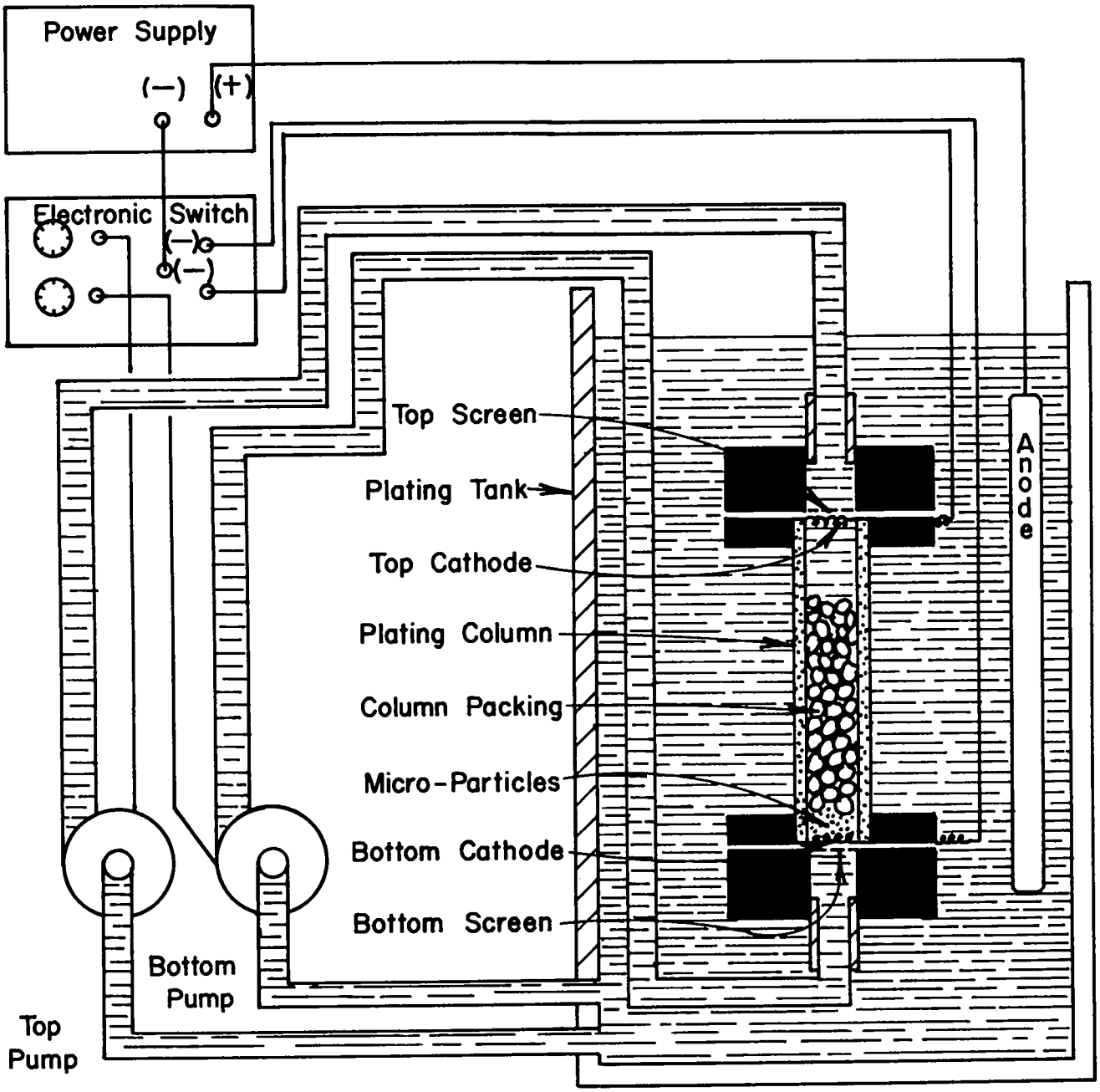
Power Supply
(−)
(+)
Electronic Switch
(−)
(−)
Top Screen
Plating Tank
Top Cathode
Plating Column
Column Packing
Micro-Particles
Bottom Cathode
Bottom Screen
Anode
Bottom Pump
Top Pump

Fig. 29

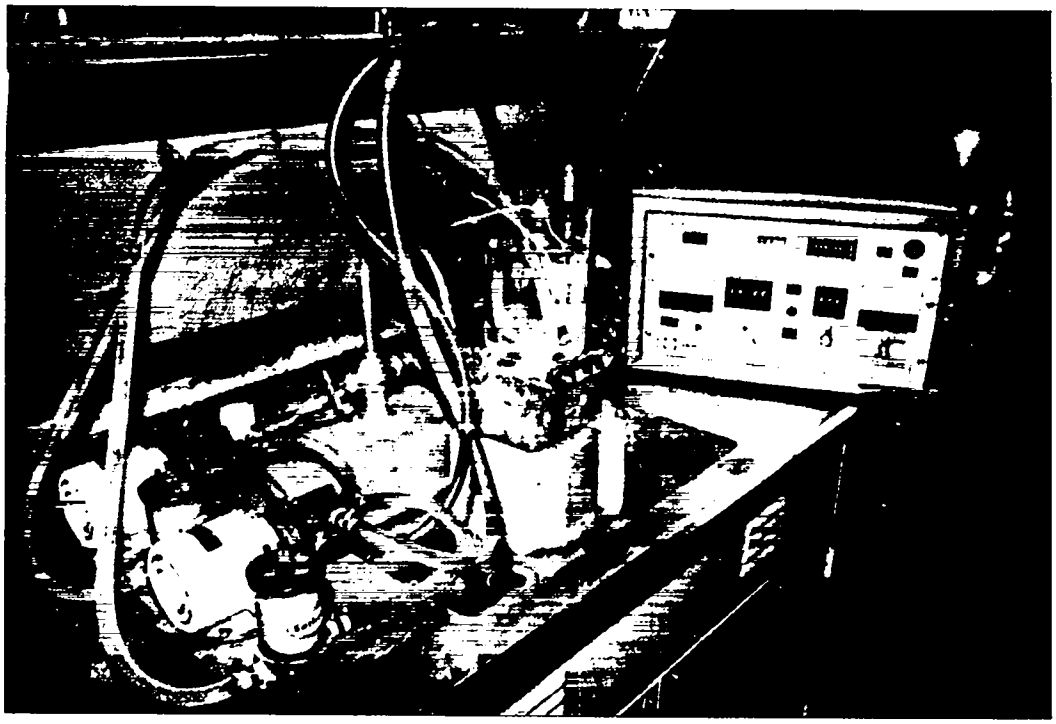

Fig. 30

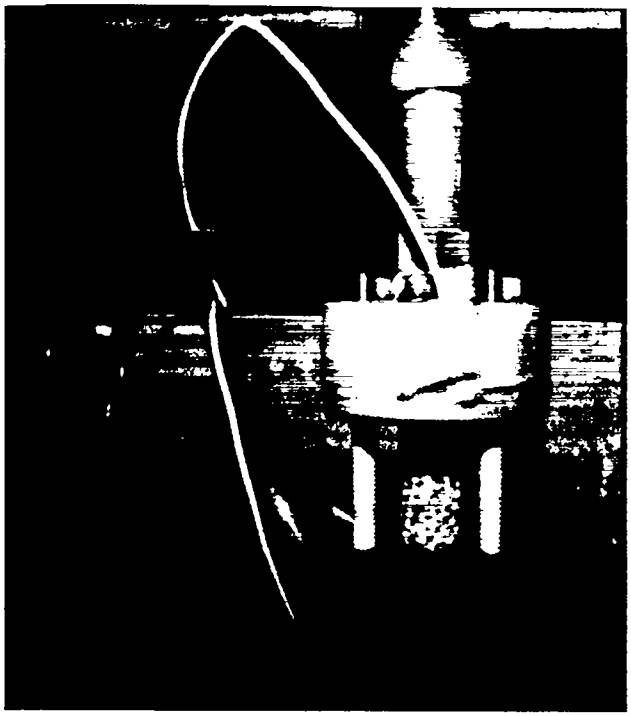

Fig. 31

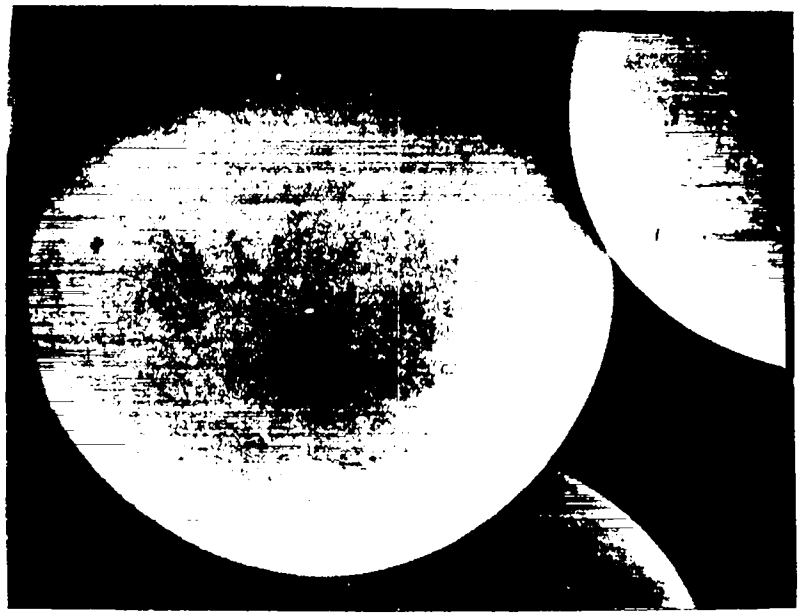

400X

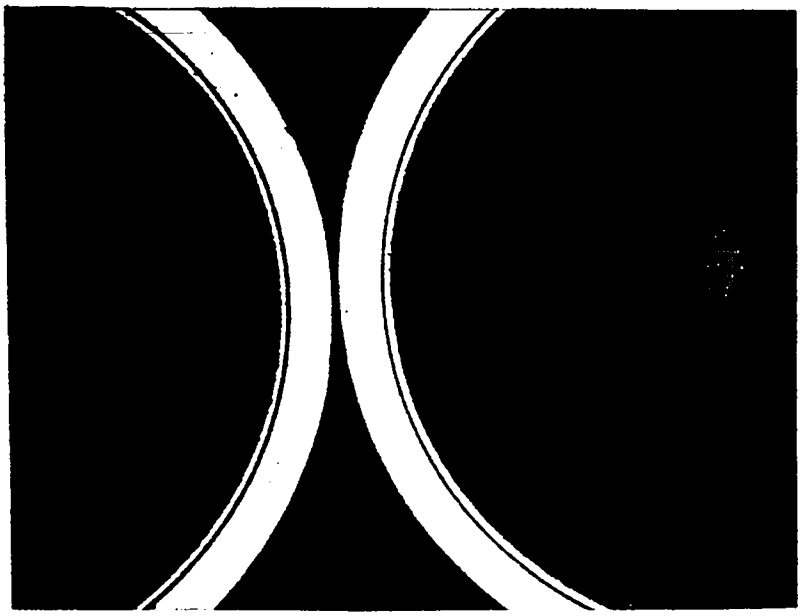

500X

Fig. 32

LASER TARGET FABRICATION PROGRAM

A LARGE FRACTION OF TARGET FABRICATION EFFORT IS OUTSIDE OF L-DIVISION PROPER.

WE HAVE RECEIVED MAJOR SUPPORT FROM:

CMB-1, -3, -6
J-14
M-1, -8
P-9, -12, -DOR
Q-26
R-2
WX-5
ADVANCED ENGINEERING DEPT., BKC

WE HAVE ALSO BENEFITTED SIGNIFICANTLY FROM THE SUPPORT OF:

CMB-7, -8
E-4
ENG-6, -7
H-5
P-2, -3
R-1
SD-1, -2, -3, -4, -5, -6
WX-1, -2

Fig. 33

ETCHING OF THIN SILICON FILMS*

by

S. C. Stotlar, C. J. Maggiore, C. R. Gruhn

ABSTRACT

Silicon films 1 μm to 6 μm thick can be fabricated by an etching technique similar to one developed by R. L. Meek and others. Diameters greater than 5 mm are achieved. Surface barrier detectors fabricated from these thin windows have been used for heavy ion detection. The etching technique used by the Los Alamos Scientific Laboratory (LASL) to obtain these thin films is described.

I. INTRODUCTION

Self-supporting epitaxial silicon films < 1 μm thick have been produced using an electrochemical etch technique. R. L. Meek first introduced the technique of thinning n/n^+ silicon wafers by selective anodic dissolution of the substrate.[1,2] The electrochemical etch rate of n^+-type silicon in HF solution is much higher than for n-type silicon. This fact is used to etch the n^+-type substrate (.01 Ω-cm) from the n-type epitaxial layer (> 1 Ω-cm) leaving a thin epitaxial film supported at the edge by the substrate. The films produced in this manner have been used to fabricate epitaxial silicon Schottky barrier (ESSB) detectors.[3,4,5]

II. METHOD

The apparatus required to electroetch epitaxial silicon wafers consists of a power supply and holders for the wafer and platinum electrode. Figure 1 shows a picture of the holder assembly. The sapphire plate holding the wafer is

---

*Work performed under the auspices of the U. S. Energy Research and Development Administration.

mechanically positioned relative to the electrode and the entire wafer-electrode apparatus lowered into the etch with a portable laboratory jack.

An electrical contact was made to the n^+ substrate side of the wafer with conductive silver epoxy. To insure a uniform low resistivity contact and uniform polishing, the n^+ side of the wafer was pre-etched with 20:1 HNO_3:HF for three minutes. This removed $\sim$10μm of the silicon substrate. The wafer with its electrical contact was then mounted epi side against a clean sapphire plate with paraffin. The n^+ substrate was coated with wax (Apiezon W) except where etching was to occur. This surface preparation yielded an etching mask with well-defined edges that was stable over the relatively long etching times required.

After alignment of the wafer relative to the electrode, the wafer was immersed in a 5% (weight percent) aqueous HF solution. A +8V bias was applied to the wafer and the current and voltage monitored until the etch was complete. During the etch a magnetic stirrer and nitrogen bubbler were used to keep the etch concentration uniform in the vicinity of the electrode. The etch was performed in the dark because photo induced charge in the substrate will cause non-uniform etching. Similarly photo induced charge in the epitaxial layer may result in holes in the finished film. The temperature of the etch was 20°C.

Table I shows the properties of the n/n^+ wafers used in this study. The ability to produce the thin films relies on the fact that the etch rate in the n-type epitaxial layer is >1000 times slower than in the substrate due to the difference in resistivities. If the substrate is etched away to the edge of the mask, etching will still proceed in the epitaxial film. It was observed that the epitaxial film etched through preferentially at this edge. Meek has

TABLE I

CHARACTERISTICS OF STARTING MATERIAL

Resistivity of Epi δ (Ω-cm) ±10%	Thickness t (μm) ±10%	Substrate δ (Ω-cm)	Substrate t (μm) ±25%
1	1	.005 - .020	200
1	2	.005 - .020	200
9	3	.005 - .015	250
9	4.4	.005 - .015	300
9	6.2	.005 - .020	250

pointed out that this is due to diffusion of holes into the n-type region from the n^+ substrate. To minimize this problem it is desirable to have the etch proceeding radially toward the edge of the mask at the time the etch is terminated.

A number of different probe-wafer geometries were tried. To produce 5mm diameter films it was found that either a flat or hemispherical electrode 3mm in diameter placed 1mm from the wafer yielded the most consistent results. Figure 2 shows two of the platinum electrodes in their teflon holders.

As the etching proceeds, the current drops after the epitaxial layer is reached and will continue to drop as the etched pattern increases in size. However, this drop in the etching current is not reproduceable enough to be used as a means of timing the etch termination. A periodic visual inspection was made to determine when the etch should stop. The size of the film was determined by shining a light through the sapphire plate and the partially transparent film. Typical etching currents were 200ma/cm^2 initially and 120ma/cm^2 at termination. Typical etch times were 60±15 minutes.

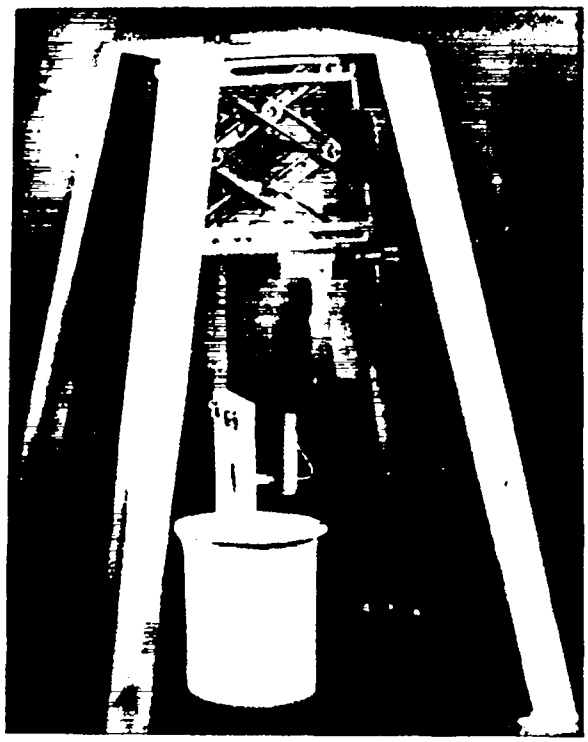

Fig. 1
Etching apparatus used to support the wafer and electrodes in the etch.

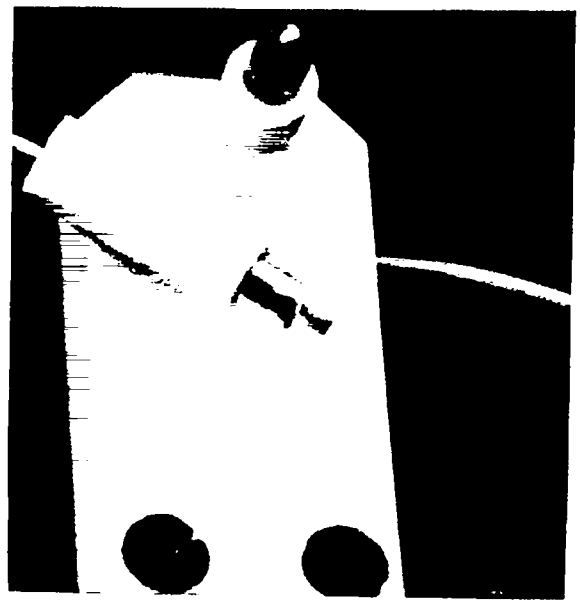

Fig. 2
Platinum electrodes used for etching.

To produce the thin films efficiently the technique outlined above was generalized to a multiple point apparatus. A square array of nine flat electrodes was mounted opposite a two inch wafer masked with nine holes 5mm in diameter. Since termination of the etch is critical to prevent etch through at the edge of the film, each pattern was terminated by masking with wax when indicated by visual inspection. There were no problems associated with possible crosstalk between electrodes and adjacent films. After etching and cleaning the wafer was diced into separate self supporting films with a diamond scriber.

The yield of suitable films from multiple etching depended on the thickness of the epitaxial film and care in handling. Yields of ∿50% for the 1μm material and >80% for films thicker than 3μm were obtained. For 1μm material the largest films obtained were 5mm in diameter, but films up to 2.5cm in diameter have been produced with 50μm material. These large area patterns require the use of a flatscreen electrode.

III. RESULTS

The thin films have been fabricated into surface barrier detectors. Their responses to α particles, ^{16}O ions, and fission fragments have been measured.[3] The thickness uniformity of the ESSB detectors was measured with an α thickness gauge and by the α response of the detector. Table II shows the results of the uniformity measurements. The α beam was collimated to 0.5mm diameter and measurements were taken in a square matrix with 0.5mm spacing.

TABLE II

UNIFORMITY MEASUREMENTS

Detector	Total Thickness[a] (μm of Si)	Thickness Minus Electrodes[b]	Thickness Observed[c]
26-4	4.39±.15	4.13±.16	4.18±.06
40-1	2.88±.13	2.66±.13	2.52±.04
28-2	.97±.08	.71±.10	

[a]The thickness determined by the standard surface barrier detector.

[b]The total thickness minus the thickness due to the front and back contacts as measured at the time of evaporation.

[c]Thickness measured by the alpha response of the ESSB detector itself.

IV. CONCLUSIONS

Selective anodic dissolution of the substrate of m/m^+ epitaxial silicon wafers has been shown to be a viable processing technique for the production of thin self-supporting epitaxial films. The technique has been used to produce simultaneously up to nine films 5mm in diameter on a single two inch wafer. The uniformity of films produced in this manner is determined primarily by the uniformity of the epitaxial growth process. The specifications of the commercially prepared epitaxial material were ±10% thickness and resistivity over the two inch diameter surface. The resultant films have been processed into ESSB detectors uniform to ±3% for thicknesses >3μm and ±14% for a 0.71μm detector.

ACKNOWLEDGMENTS

The authors wish to thank J. Gursky for help in evaporating the contacts on the detectors fabricated from the thin films.

REFERENCES

1. R. L. Meek, "Electrochemically Thinned N/N^+ Epitaxial Silicon - Method and Applications," Electrochemical Technology (July 1971).
2. R. L. Meek, W. M. Gibson, and R. H. Braun, "Preparation of Supported, Large-Area, Uniformly Thin Silicon Films for Particle-Channeling Studies," Nuclear Instruments and Methods 94 (1971).
3. C. Maggiore, P. Goldstone, C. Gruhn, H. DeHaven, S. Stotlar, and N. Jarmie, "Thin Epitaxial Silicon for dE/dX Detectors," IEEE Trans. Nucl. Sci. NS-24 (February 1977).
4. A. Tetefort, "Etude d'cm Nouvean Procede de Preparation de Detecteurs Nucleaires dE/dX Minces," Thesis University Clermont-Ferrand, France (1976).
5. J. P. Ponpon, P. Siffert, F. Vazeille, "Thin dE/dX Detectors of Uniform Thickness Made on Epitaxial Silicon," NIM 112, 465-467 (1973).

A FAST TAPE TRANSPORT SYSTEM FOR USE WITH ON-LINE SEPARATORS

J.A. Macdonald, J.C. Hardy, H. Schmeing, N.C. Bray,
W. Perry, R.B. Walker and M. Wightman

Atomic Energy of Canada Limited
Chalk River Nuclear Laboratories
Chalk River, Ontario, Canada K0J 1J0

ABSTRACT

A fast tape transport system has been developed for transporting samples collected from the ion beam of an isotope separator to a low background area. The unusual features of the system are its tape speed (up to 585 cm s^{-1}) and the fact that the tape system operates entirely in air except for the collection point on the tape at the end of the beam line.

Published in Nucl. Instr. and Meth. 139 (1976) 355.

TARGET PREPARATION WITH THE LASL ISOTOPE SEPARATOR #1

Gregory M. Kelley CNC-11
Bruce J. Dropesky CNC-11

I. Introduction

The vacuum evaporation method of target preparation is currently in widespread use. Its limitations become apparent when, for example, a chemically pure, highly enriched target of a naturally low abundance isotope is desired. The demand for such targets has made the electromagnetic separation, electrostatic retardation technique more and more attractive.

Basically, an isotope or mass separator (the terms tend to be used interchangeably) consists of; an ion source, electrostatic lenses for controlling beam shape, an electromagnetic analyzer stage, and a collection or retardation/collection system. The Swedish built machine used here at LASL for the past eleven years is shown in Figure 1.

Five high voltage supplies are used. One supplies the 50-60 kV acceleration potential. Three others provide necessary lens voltages. The fifth is connected in series with the acceleration supply. It provides a 0-2 kV net voltage which is brought through an overhead conduit to the retardation/collection assembly.

The analyzer magnet is a 90° sector, with a 1.6 m radius. Its power supply is rated at 10 kW with a current stability of 1 part in 10^4 per hour. It provides a field of up to 0.35 T (3500 gauss).

Three, freon baffled, oil diffusion pumps keep the system pressure in the low 10^{-6} region. Figure 2 shows a titanium sublimator pump and a L(N_2) cold surface used to further reduce the pressure in the post-analyzer section to the low 10^{-7} region. To the right of the photo is the grounded shield around the high voltage cable and ceramic feedthrough used to bring the retardation potential to the lens.

The ion source most generally used is of the Nielsen or oscillating electron type shown in Figure 3. Its anode and end plates are of high purity, high density graphite. In order to reduce memory effects, and maintain sample purity, the internal components of the source proper are usually replaced before use with a different charge material. The integral, plug in design of the source allows us to dedicate sources to specific charge materials.

II. Charge Vaporization and Ionization

Table 1 lists several targets, charge materials, and methods of charge vaporization and ionization.

TABLE I

TARGET	CHARGE MATERIAL	VAPORIZATION METHOD	
^{9}Be	BeO	Internal Chlorination	(a)
^{237}U	U_3O_8		
^{121}Sb	Sb (metal)	Charge Heating	(b)
^{210}Pb	Pb (metal)		
^{50}Ti	$TiCL_4$	High Vapor Pressure Compound	(c)

a. The internal chlorination method, first described by Sidenius and Skilbreid[1], wherein CCl_4 vapor is passed through a heated rare earth oxide, thus converting it to a volatile chloride which is then dissociated in the plasma discharge and ionized.

b. Heating one of the more volatile metals such as Pb or Sb, to a temperature where its vapor pressure is high enough to provide a plasma discharge and thus, an ion beam of the desired intensity.

c. Introduction of vapor from a highly volatile compound, such as $TiCl_4$, into the ion source plasma region where dissociation and ionization occur.

III. Retardation Lens

Figure 4 shows our retardation lens in place in the collector chamber. Retardation potential is brought to the lens by the vertical tube seen in the

center of the photo. The rectangular slot in which the target holder is mounted allows adjustment of the foil in the "X" direction. The small central tube allows "Z" axis corrections in order to achieve the desired spot size. Focusing of stable mass beams is accomplished by deflecting the beam to either of two fluorescent screens. The horizontal lines delineate the height of the lens entrance slit.

IV. Target Preparation

a) The neutron induced fission cross section of ^{237}U was measured by exposing a chemically purified, isotopically separated sample to the neutron pulse from an underground nuclear explosion. The short half life of ^{237}U ($t_{1/2}$ = 6.70 ± 0.02 d) and the rigid timing of the Pommard event called for unusually smooth scheduling and a high degree of interlaboratory cooperation so that the target could be properly placed on the experimental tower shortly before the detonation. Forty-two mg of enriched ^{236}U were irradiated in the high flux isotope reactor (HFIR) at Oak Ridge National Laboratory for a period of 22 days. The irradiated sample containing ∿ 1.9% ^{237}U was directly air shipped to LASL for chemical purification, (chiefly to remove fission products and curie quantities of Np) prior to isotopic separation and air shipment to the Nevada Test Site.

As shown in Figure 5, a concentrated solution of the purified uranium was transferred to a quartz wool wad in a quartz tube, evaporated to dryness, and converted to U_3O_8 by heating in air to 800°C. (The purification and transfer were done in a hot cell because of the high radiation levels involved.)

After the charge was placed in the ion source, it was volatized using the internal chlorination technique. Ion beams of the uranium isotopes were produced and accelerated at a potential of 50 keV. Figure 6 shows the simple cup and galvanometer arrangement which was provided to monitor the 5-10 μA ^{236}U beam. The adjacent slit was provided to allow the ^{237}U ions to enter the retardation lens. Ion energy was reduced to 300 eV to prevent sputtering and allow a deposit to build up. A second view of the lens (Figure 7) shows the 25-μm thick, .5-cm diam. stainless steel backing onto which the ^{237}U was deposited and its support ring being inserted prior to the separator run.

Three charges totalling ∿ 34 mg ^{236}U and ∿ 50 Ci of ^{237}U were processed through the separator in a period of 40 h, to provide the final target for the Pommard event. The deposit consisted of 18.1 μg of ^{237}U, covered an area of ∿ 1 cm^2, and lay totally within the area through which the collimated neutron beam passed.

b) The target used to study the $^{210}Pb(p,d)^{209}Pb$ reaction at 20.6 MeV[3] with the LASL Tandem Van de Graaff and particle spectrograph was produced as follows.

The charge material for the ion source was a metallic lead sample enriched in 22.3-y ^{210}Pb. It was prepared from a nitric acid solution of ^{210}Pb(Ra-D) whose decay products were in approximate equilibrium.

Shortly before the separator run, a chemical separation was performed on the starting material. Its purpose was to reduce the level of activity introduced into the ion source by removing the daughter products ^{210}Bi and ^{210}Po.

The purified solution had 0.5 mg of normal lead added to insure an adequate charge size for the ion source. The combined lead was reduced to the metal, compacted to a pellet, dried, and weighed. The pellet weighed 1.1 mg and contained $\sim$ 10 mCi of ^{210}Pb. It was placed in the ion source and heated to a temperature sufficient to produce approximately 5 μA of lead ions which was then accelerated to 50 keV.

In order to produce a usefully thick ^{210}Pb deposit on the 50 μg/cm^2 carbon foil, it was necessary to retard the beam entering the lens to a net voltage of approximately zero.

The resulting ^{210}Pb deposit covered a nearly square area $\sim$ 3 mm on a side. It weighed $\sim$ 22 μg (as determined by γ-ray counting), and constituted $\sim$ 25% of the amount in the charge. A target thickness of $\sim$ 240 μg/cm^2 was achieved.

c) The target used to study the (t,p) and (t,α) reactions on ^{50}Ti[4] at the Tandem was prepared in this manner.

A standard CCl_4 flask was filled with $\sim$ 5 cc of the highly volatile liquid $TiCl_4$. Flow of the $TiCl_4$ vapor into the ion source was controlled by our normal CCl_4 needle valve. The Ti ion current was brought to $\sim$ 20 μA or $\sim$ 1 μA of the 5.3% abundant ^{50}Ti. Ions entering the lens were slowed to 300 eV.

Attempts to build up a thick deposit on a 50-μg/cm^2 carbon foil were frustrated by persistent foil breakage. Finally, a rather thin ($\sim$ 10 μg/cm^2) deposit thickness was obtained and the target was brought to the Van de Graaff facility for scattering experiments.

d) Attempts to produce a ^{10}Be target in the 50-100 μg/cm^2 thickness range have been carried out.

During the past few years we have made many attempts to produce a Be target in the 50-100 μg/cm^2 thickness range on thin C foil backings for in-beam nuclear reaction spectroscopy at the Tandem Van de Graaff. The most reliable charge material has been found to be BeO from a $BeCl_2$ solution

which has been pipetted onto a quartz wool pad, dried, and heated to $\sim$ 800°C in air.

The usual internal chlorination process easily produces 5-20 μA of Be^{+} ions which, after entering the retardation lens are slowed to 600 eV. When the buildup approaches fractions of a microgram, a stretching of the carbon foil which usually results in breakage is observed. This phenomenon is quite severe, and has been noted in the literature[5]. Various techniques, such as heating the foil during deposition or laminating the foils (as suggested by Jerry Lerner during last year's meeting), have produced no significant improvement, as the deposit on carbon is apparently limited to $\sim$ 2 μg or a maximum thickness of $\sim$ 16 $\mu g/cm^2$.

Preliminary tests on thicker (400 $\mu g/cm^2$) Pt foils indicate that even this comparatively high Z (78) material is subject to severe stressing. Three attempts to deposit Be have produced only a single target. Although a visual inspection of the target showed promise, when it was later irradiated at the Van de Graaff, the Be deposit proved to be a disappointingly thin 10 $\mu g/cm^2$.

In conclusion, I'd like to point out that while the production of certain targets approaches the routine, others can present great difficulties because of the little known, but often encountered, deposit-substrate interactions.

References

1. G. Sidenius and O. Skilbreid, Proc. 1960 Int. Symp. On Separation of Radioactive Isotopes p. 243 Springer - Verlag, Wien 1961.
2. J. H. McNally, J. W. Barnes, B. J. Dropesky, P. A. Seeger, and K. Wolfsberg, "Neutron-Induced Fission Cross Section of ^{237}U", Phys. Rev. C 9, 717 (1974).
3. G. Igo, E. R. Flynn, B. J. Dropesky, and P. D. Barnes, "$^{210}Pb(p,d)$ ^{209}Pb Reaction at 20.6 MeV", Phys. Rev. C 3, 349 (1971).
4. D. C. Williams, J. D. Knight, and W. T. Leland, "The (t,p) and (t,α) Reactions on ^{48}Ca and ^{50}Ti," Phys. Letters, 22, 162 (1966).
5. D. L. Auton, "Direct Readings on ^{10}Be," Nucl. Phys. A157, 305-322, (1970).

FIGURE CAPTIONS

Figure 1. The LASL Isotope Separator #1.

Figure 2. Titanium sublimator and LN_2 cold surface.

Figure 3. LASL plug-in ion source.

Figure 4. The retardation lens in place.

Figure 5. Loading the charge.

Figure 6. Entrance slit configured for ^{237}U.

Figure 7. Target foil being inserted.

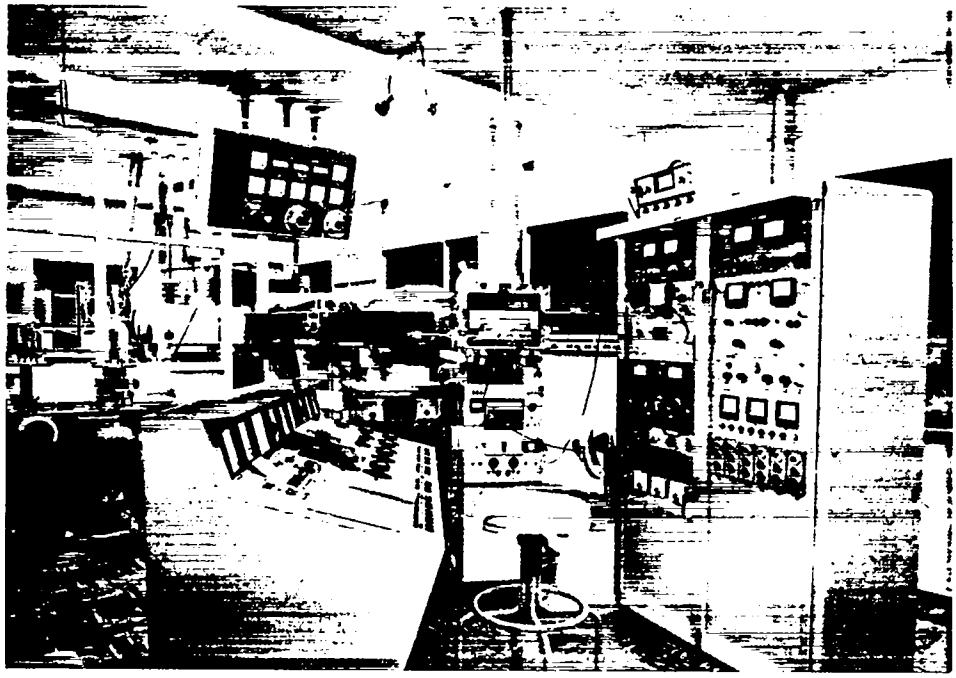

Fig. 1

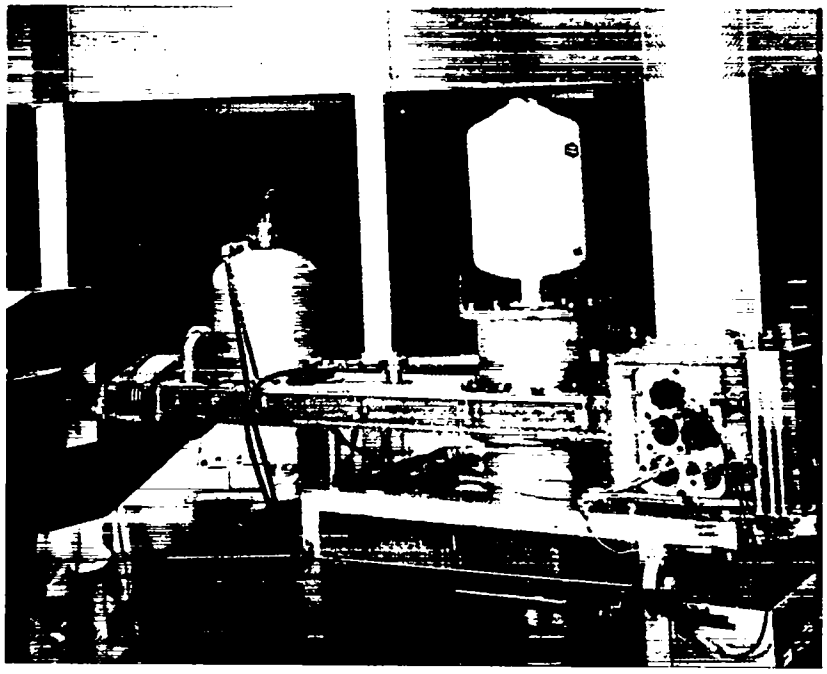

Fig. 2

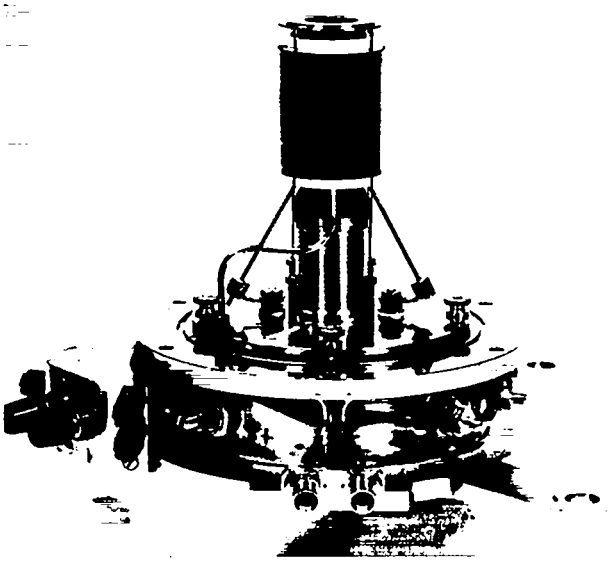

Fig. 3

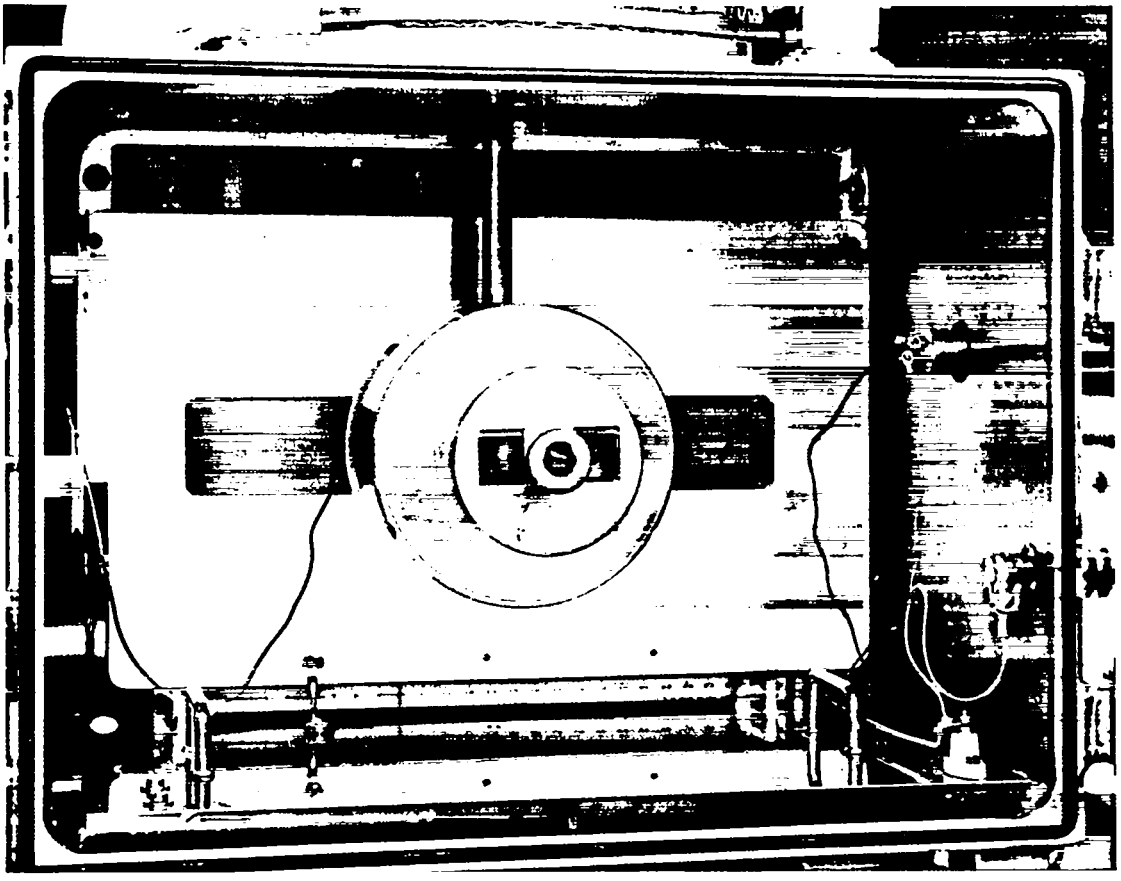

Fig. 4

Fig. 5

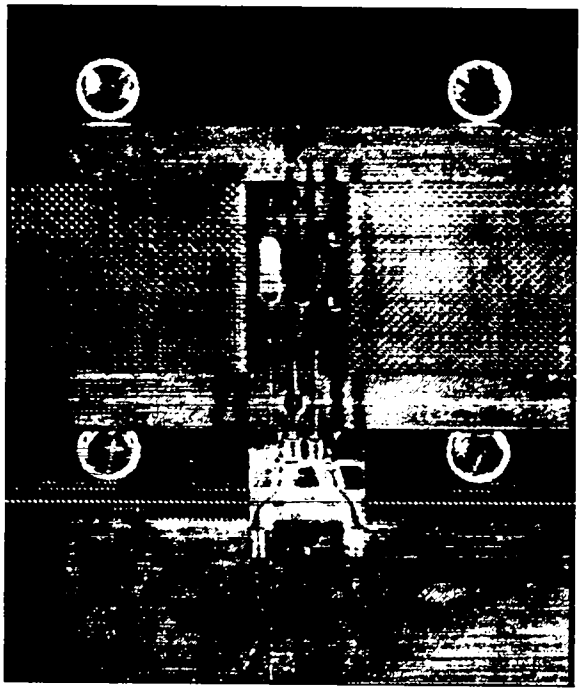

Fig. 6

Fig. 7

USE OF AN ISOTOPE SEPARATOR AT THE INEL*

R. A. Anderl
EG&G Idaho, Inc., Idaho National Engineering Laboratory

INTRODUCTION

Two major programs in our Nuclear Physics Branch are concerned with the measurement of the decay properties of fission product isotopes and with the measurement of integral capture cross sections for isotopes of interest to advanced fast reactor systems. Central to efforts in both of these programs is a "laboratory-type" electromagnetic isotope separator located at the Test Reactor Area, INEL.

Under development at the present time is the capability for performing "on-line" mass separation of fission products transported by a gas-jet technique from a ^{252}Cf spontaneous fission source to the ion source of the isotope separator. Using this capability in conjunction with a tape transport collector system, decay properties of short-lived fission products will be studied.

Of more interest to this conference is the use of the isotope separator for preparation of highly-enriched rare-earth samples for our cross-section measurement program. Hence, this discussion will center on this latter application and will include a sketch of the cross section experiment with an emphasis on sample requirements, a brief description of our isotope separator and a more detailed description of the collection apparatus used in the preparation of the majority of the samples for the experiment.

Briefly, the cross section experiment involves an EBR-II irradiation of selected isotopes of Nd, Sm, and Eu to a fluence of approximately 5×10^{21} n/cm^2, a post-irradiation measurement of the products of neutron absorption in each sample, and a determination of the integral capture cross section for each isotope. EBR-II is a liquid-sodium-cooled fast reactor which is used principally for irradiation experiments pertaining to the development of advanced fast reactor systems. The cross sections measured in this experiment will contribute to the evaluation of the fission-product-poison effect in fast reactors, the evaluation of the long-term capture worth of Eu_2O_3 as a fast reactor control material, and the development of a reliable burnup monitor for advanced fast reactor fuels.

Because standard activation and gamma spectrometric techniques are not applicable for most of the isotopes of interest in this experiment, mass spectrometric techniques will be used to determine the products of neutron absorption for each sample. In this perspective and noting that

---

*Work performed under the auspices of the U. S. Energy Research and Development Administration.

most of the materials are expected to have integral capture cross sections ranging from 100 mb to 3 barns, post irradiation (A+1)/A ratios are expected to be 100 ppm to 10,000 ppm. It is evident that for many of the samples high chemical purity and high isotopic enrichments are required.

Off-the-shelf enriched isotopes from ORNL, with primary isotopes enriched from 90% to 99%, are by-and-large unsatisfactory without additional enrichment. The required high enrichments (99.999% A, 10 ppm A+1) can be obtained by additional isotope separation of the ORNL enriched stock. At the present time this additional enrichment is being done using the INEL isotope separator equipped with a retardation lens. The following paragraphs describe the apparatus used for this sample preparation.

EXPERIMENTAL

Isotope Separator

Our electromagnetic isotope separator was designed and built by Nucletec S. A., Geneva, Switzerland, and was first operational in 1972.

Ion sources used with the separator are the oscillating electron ion source (Nielsen-type)[1] and the high-temperature-surface-ionization ion source (Johnson-type).[2] The Nielsen source is used for gaseous elements, for elements which are easily vaporized and for elements of high ionization potential which cannot be run with the Johnson source. The Johnson source is used routinely for high efficiency (~40%) production of alkali metal and lanthanide ions and can be used for actinides.

The ion beam is formed with an electrostatic lens assembly consisting of an extraction electrode, three cylindrical electrodes for cylindrical focus, and quadrupole singlet for beam compression. With the ion source operated at a positive 50 kV to 60 kV, the extraction voltage is 10 kV to 15 kV, the focus voltage is 10 kV to 25 kV, and the quadrupole voltage is 100 V to 200 V. Typical extracted ion currents are 10 μA to 100 μA.

Mass dispersion is obtained with a water-cooled, 90° sector electromagnet which has a mean radius of 150 cm, a magnet pole gap of 50 mm, and fringing field terminators at entrance and exit boundaries. Powered by a transistorized 0 to 150 A power supply (current stability better than 1 part in 10^4), the magnet has a field strength ranging from 0 to 5000 Gauss. Therefore, it is possible to collect mass-separated species over a mass range of 0 to 265 amu. The mass range for simultaneous collection is given by

$$M_{max} - M_{min} = 0.15\ M_{min}$$

and the mass dispersion is approximately 9 mm for mass 150 and 50 keV ions.

The beam shape is variable from a 3 mm circular spot to a 2 mm X (1 cm to 3 cm high) line spot. Enhancement factors with respect to adjacent masses of 1000 to 10,000 at mass 150 can be attained.

For direct viewing of the ion beam shape a transmission fluorescent screen coated with K Br is used. An electronically driven vibrating probe with current signal displayed as an oscilloscope trace at the console is used for indirect viewing of the beam.

Collector assemblies of interest to this conference are discussed in detail in the next section.

A vacuum of less than 5 X 10^{-7} torr is maintained throughout the separator vacuum chamber with three Edwards oil diffusion pumps which have dual water-cooled chevron baffles on each pump inlet. Two 6 inch diffusion pumps provide differential pumping at the ion source-electrostatic lens assembly and a single 9 inch diffusion pump is used at the collector. To further improve the vacuum quality at the collector end, a liquid nitrogen cold trap is located in the dispersion chamber between the magnet and the collection chamber.

Collection Apparatus

The collection apparatus used for the sample preparation is shown in Figures 1 and 2 which are photos of the collection chamber interior as seen through the top opening and the rear opening, respectively. The setup includes a vibrating probe beam scanner, a rotatable-collection-frame assembly, and a retardation lens.

Mounted on a movable carriage, the vibrating probe unit can be located at any position along a line perpendicular to the ion beam direction. Movement of the carriage is accomplished by a remote control outside the vacuum chamber. The probe vertical pin swings through an arc which is approximately 1.75 inches from the ion beam focal plane.

The rotatable-collection-frame system consists of 16 inch by 2.4 inch collection frames which are attached to two "wheels," each "wheel" supported in a vertical upright by a stainless shaft and Delrin bearing assembly. As shown in Figure 2, the right-hand shaft is coupled to a vacuum-rotary-motion feedthrough which permits remote control of the rotation of a collection frame into the focal plane of the ion beam. The rotatable system provides for interchangeable mounting of up to three collection frames, each of which can incorporate one or more of the following:

(1) a foil for direct collection of small quantities of mass-separated isotopes at full energy,

(2) a foil that can be used as a beam stop for all but one or more selected isotopic beams which pass on through apertures to other collection devices,

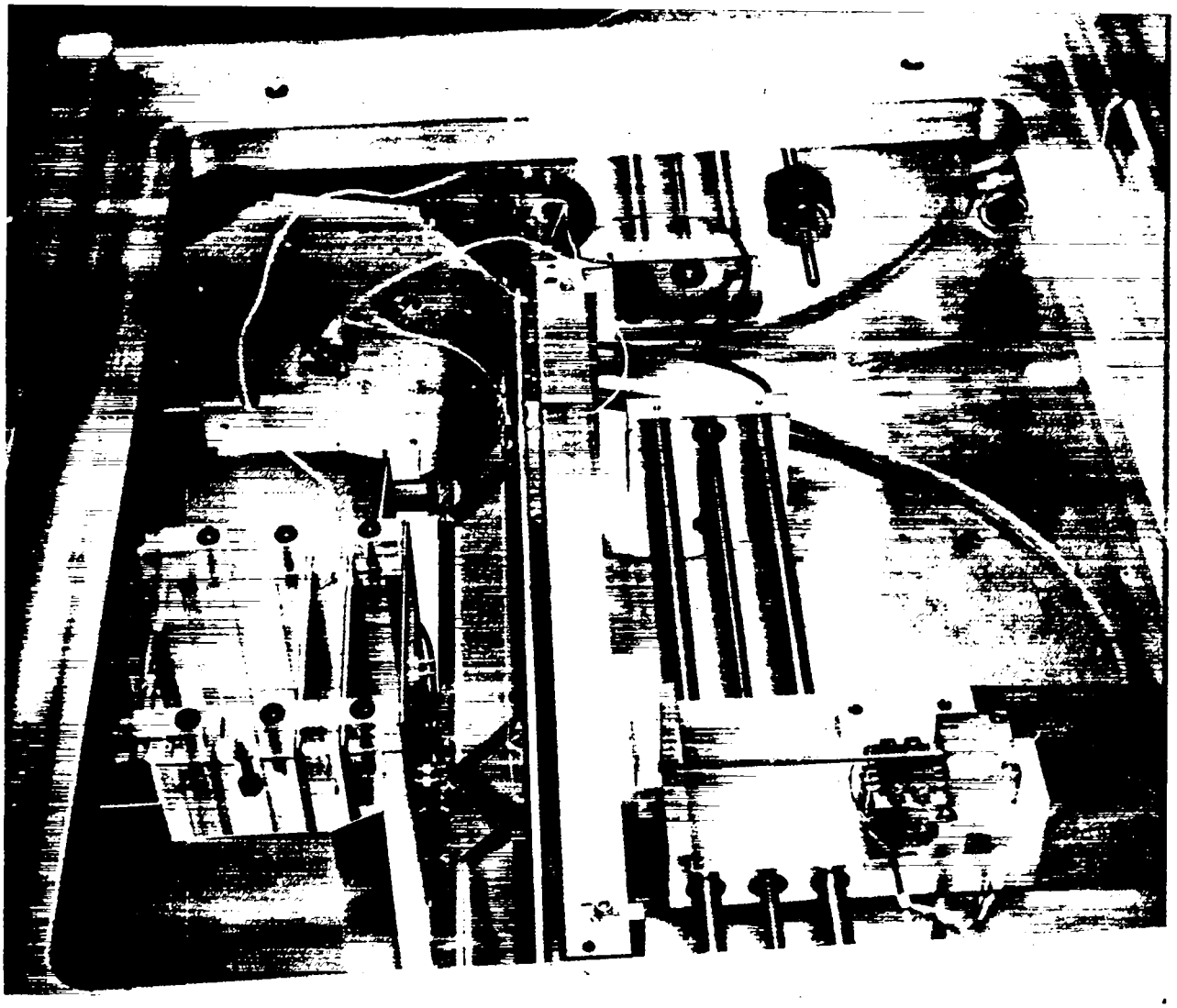

Figure 1. View of the rotatable collection-frame assembly and the retardation lens through the top opening of the collection chamber.

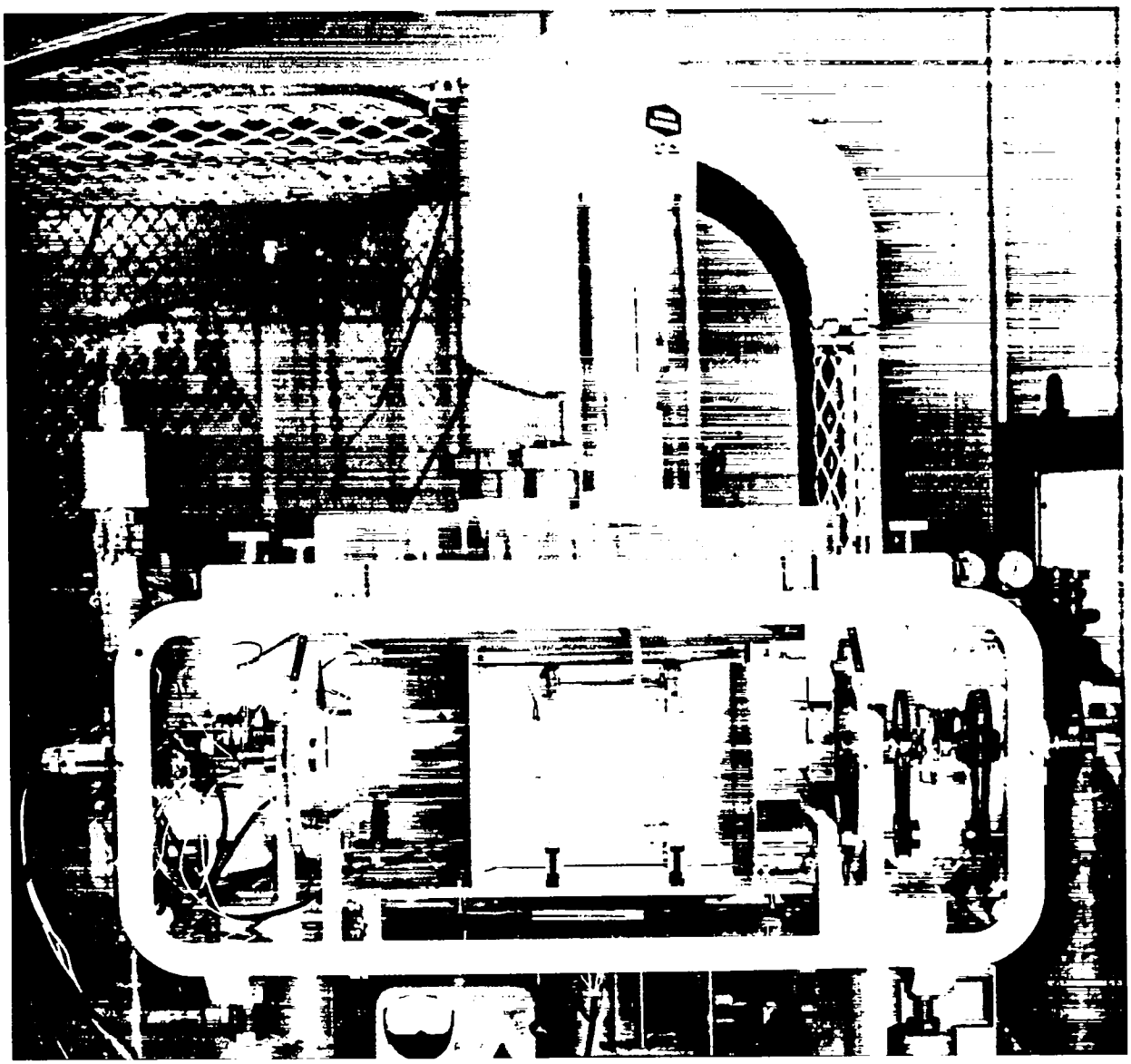

Figure 2. View of the rotatable collection-frame assembly and the retardation lens through the rear opening of the collection chamber.

(3) a transmission fluorescent screen for direct viewing of the ion beam shape,

(4) a Faraday cup for measuring ion beam currents.

For the setup used here with the retardation lens, two collection frames are mounted on the system "wheels." One frame supports a foil used as a beam stop for all ion beams but the one entering the retardation lens. The second contains a transmission fluorescent screen for viewing the beam shape and a Faraday cup for measuring the isotopic ion current entering the retardation lens.

The design of the retardation lens, as illustrated by the schematic in Figure 3, is based on the study by Dionisio and DeLima[3] and corresponds to their system D_5. This particular design was selected because it is used easily with line-focused beams and can provide either sharply-defined narrow deposits when the focus electrodes are used or broader deposits when the focus electrodes are removed. As shown in Figures 1 and 2, the focus lens elements were removed for the present application.

The beam defining electrode, with a .187 inch by 2.0 inch slot aperture, the electron suppression electrodes, with .40 inch by 2.0 inch slot apertures, and the retardation electrode are each 4 inch by 4 inch square. The focus electrodes are 4 inches high and are separated by a 2 inch gap. With the exception of the beam defining electrode which is constructed from stainless steel, all other lens elements are fabricated from Type 6061 aluminum alloy. To minimize arcing all corners are rounded and the surfaces of the elements are polished. A foil holder which slips into the T-slot in the retardation electrode is used to collect the isotopically enriched deposit.

The assembled lens is installed as two parts on the platform shown in the photographs. Mounted in one set of Plexiglass supports which provide for electrode alignment and spacing and attachment to the platform are the first three electrodes. Providing alignment and spacing of the focus and retardation electrodes is another set of Plexiglass supports which are mounted to nylon screws which serve as electrical standoff insulators with respect to the grounded platform. Two pins mounted on electrical insulators attached to the beam defining electrode are used to provide, via a difference amplifier, a correction signal to the acceleration supply for beam position stabilization.

As shown by the photographs in Figures 2 and 4, the retardation voltage is transmitted to the retardation lens through a specially designed high-voltage feedthrough located on the top cover-plate of the collection chamber. Fabricated from Plexiglass, the high voltage feed-through insulator is 7 inches long with approximately 4.25 inches extending above the 7.6 inch X 15.7 inch X 2 inch thick Plexiglass cover plate and .75 inch extending below the cover plate. The insulator body protruding above the cover plate is 1.75 inches in diameter. This system has been successfully tested at 62 kV.

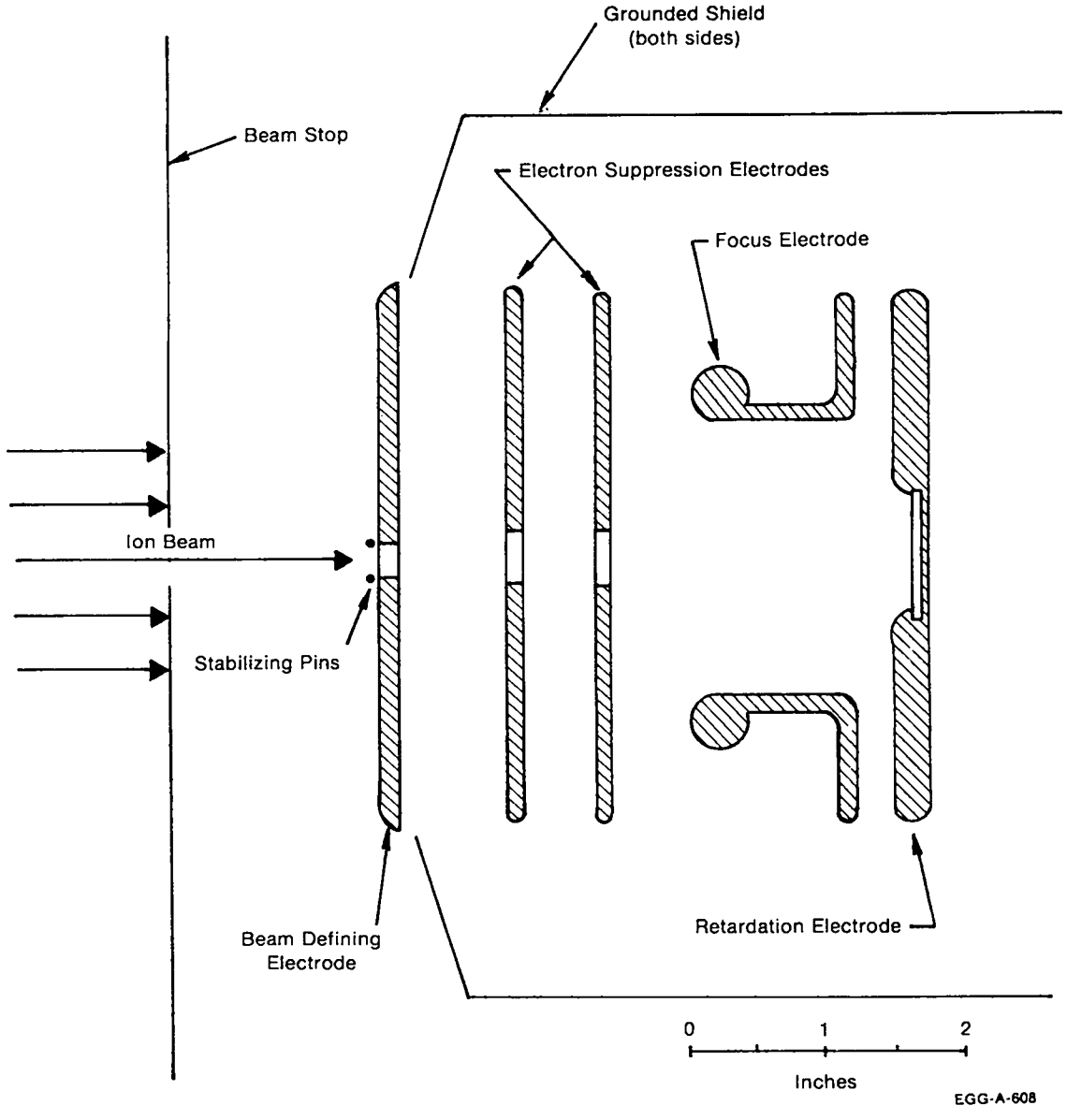

Figure 3. Schematic Illustration of Retardation Lens.

It should be noted that although Plexiglass (an acrylic plastic) is not the most desirable material to use in a vacuum environment because of its vapor pressure and outgassing properties, the mass-separator vacuum system is able to maintain the vacuum in the collection chamber at less than 3×10^{-7} torr. Lexan (a polycarbonate plastic) is a superior material to use in the vacuum environment but is considerably more expensive.

Grounded metal plates are used to shield as much of the collection chamber from the high voltage feedthrough, the high voltage lead to the retardation electrode, and the lens itself. These plates are situated as close as possible to the respective high voltage components.

Illustrated in Figure 5 is a schematic of the electrical layout of the power supplies used with the mass separator when operated in the retardation mode. Typical operating voltages are: (1) 50 kV, acceleration supply; (2) 12 kV, extraction supply; (3) 20 kV, focus supply; (4) 200 V, quadrupole supply; (5) 200 V, beam stop supply; (6) 1200 V, electron suppression supply; (7) 300 V, retardation supply.

Sample Preparation

Isotopically enriched samples prepared with the separator retardation system include the following: ND-143, -144, -145, -146, -148, -150; Sm-147, -149; Eu-151, -152, -153, -154. For the Nd, Sm and stable Eu isotopes, rare earth oxide material previously enriched to 90% to 99% at ORNL was used as charge material in the Johnson ion source. The mass-separated primary isotopic beam was deposited on 1 mil nickel foil or 0.5 mil vanadium foil mounted in a foil holder which slipped into the T-slot of the retardation lens. Approximately 50 μg to 75 μg deposits which measured from 2 mm to 3 mm wide by 30 mm to 35 mm high were collected. Typical isotopic ion currents ranged from 6 μA to 10 μA and the collection time per run was 90 minutes.

Isotope dilution mass spectrometry was used to measure the sample mass and sample enrichment for representative samarium samples. These analyses indicated that there was negligible loss of material in the collection of the decelerated ion beam and enhancement factors with respect to adjacent masses of better than 4000 were achieved.

SUMMARY

An electromagnetic isotope separator with a retardation lens as a collector was used to prepare highly enriched samples of Nd-143, -144, -145, -146, -148, -150; Sm-147, -149; Eu-151, -152, -153, -154. The 50 μg to 75 μg samples, deposited on 1 mil nickel foil or 0.5 mil vanadium foil, are part of a sample set to be irradiated in EBR-II as part of an integral-capture cross-section measurement program at the INEL. This discussion presented a description of the isotope separator and the apparatus used for the sample preparation.

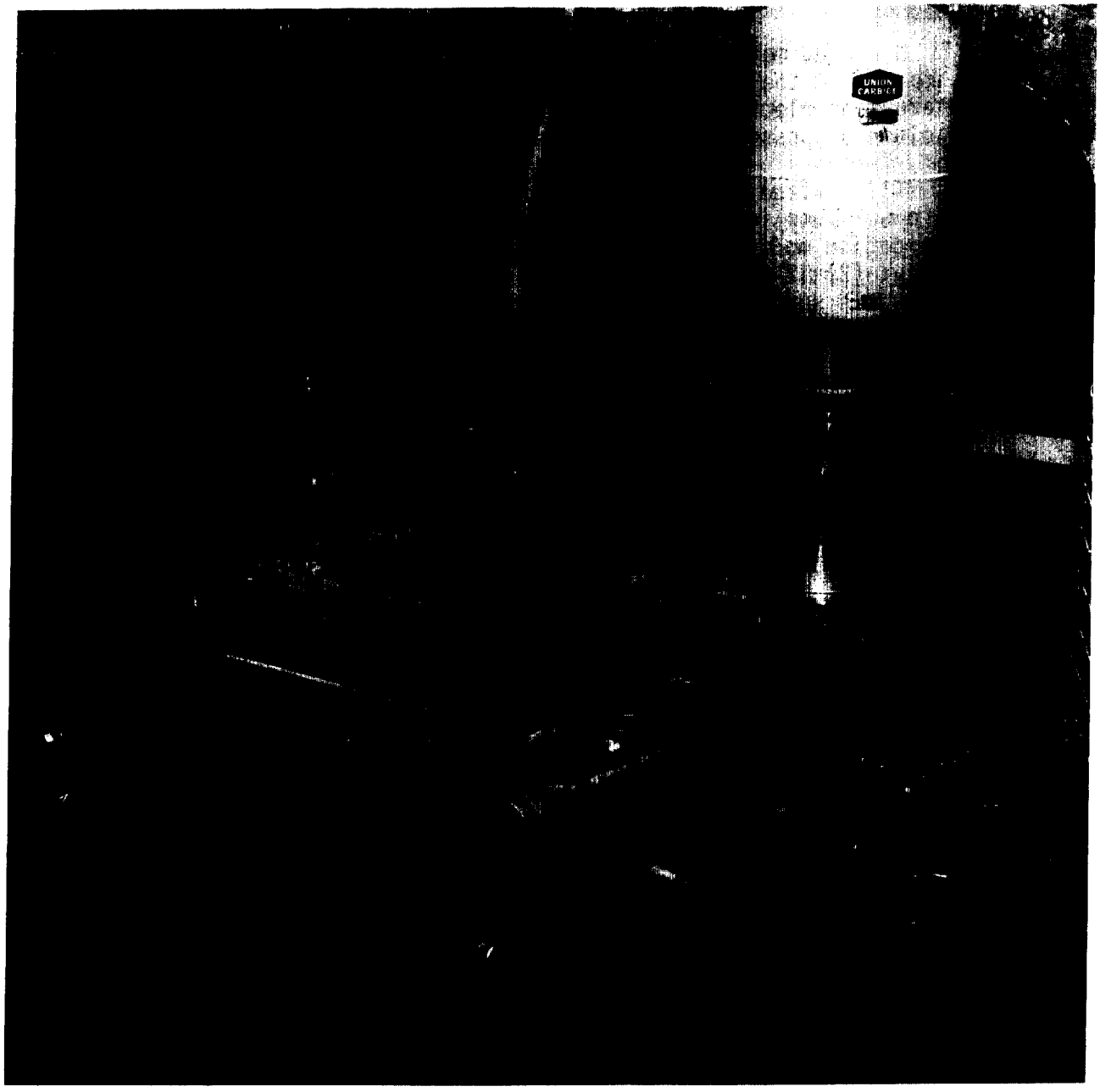

Figure 4. Photograph of the high-voltage feedthrough as-installed on the top of the collection chamber.

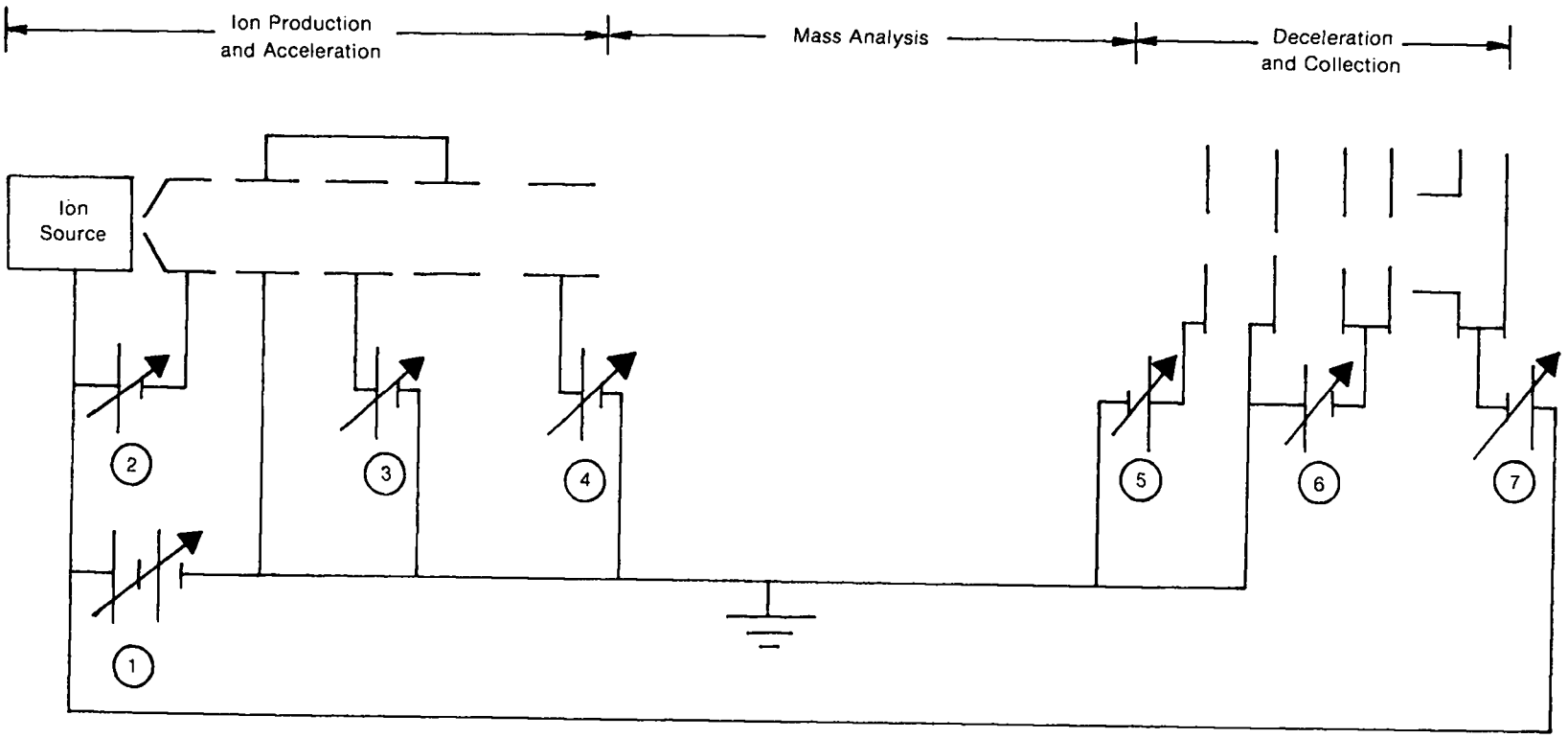

1 - Acceleration HV Supply (0-80 kV, positive).

2 - Extraction HV Supply (0-25 kV, negative, floating at acceleration voltage).

3 - Focus HV Supply (0-60 kV, positive).

4 - Quadrupole Singlet HV Supply (0-2 kV, positive).

5 - Beam Stop HV Supply (0-2 kV, positive).

6 - Electron Suppression Electrode HV Supply (0-2 kV, negative).

7 - Focus and Retardation Electrodes HV Supply (0-5 kV, negative, floating at acceleration voltage).

EGG-A-607

Figure 5. Schematic of Electrical Layout for HV Supplies Used in the Acceleration and Deceleration of an Ion Beam with the Mass Separator.

REFERENCES

1. K. O. Nielsen, Nuclear Instruments and Methods 1 (1957) 289.

2. P. O. Johnson et al, Nuclear Instruments and Methods 106 (1973) 83.

3. J. S. Dionisio and D. X. DeLima, Nuclear Instruments and Methods 61 (1968) 260.

VAPOR DEPOSITION OF LARGE AREA NpO_2 AND UO_2 DEPOSITS*

H. L. Adair, J. R. Gibson, E. H. Kobisk, and J. M. Dailey

Union Carbide Corporation, Nuclear Division
Oak Ridge National Laboratory, Solid State Division
P. O. Box X, Oak Ridge, Tennessee 37830

ABSTRACT

Deposition of NpO_2 and UO_2 thin films over an area of 7.5- to 10-cm diameter has become a routine operation in preparation of fission chamber plates. Vacuum evaporation or electroplating has been used for this purpose. The "paint brush" technique has been used as well; however, uniformity requirements normally eliminate this procedure. Vapor deposition in vacuum appears to be the most suitable technique for preparing NpO_2 and UO_2 deposits of >200 cm^2. This paper describes the procedures used in preparing uniform large area deposits of NpO_2 (226 cm^2) and UO_2 ($\sim$2000 cm^2) by vacuum evaporation using electron bombardment heating and several substrate motion and heating methods to achieve uniformity and adhesion.

INTRODUCTION

Small and large area deposits of actinide materials on a variety of substrates are important to experimentalists who need such materials for precision cross-section measurements, for sources of neutrons or fission fragments, and for standard calibration sources. Normal requirements for actinide deposits are that they should be adherent, uniform, and well defined in terms of areal density and contained impurities.

---

*Research sponsored by the Energy Research and Development Administration under contract with Union Carbide Corporation.

Two techniques used most often for preparing actinide deposits are electroplating and vacuum evaporation.[1] The electroplating procedure is limited in areal density (normally ≤ 2 mg/cm^2) and in the area possible to coat. The previous two limitations are overcome when physical vapor deposition is used; however, the deposition efficiency for this process is usually <1 percent (depending upon uniformity requirements).

The preparation of $^{235}UO_2$ deposits of ≤ 8 cm in diameter by the physical vapor deposition process has been described.[2] At that time, this area of $^{235}UO_2$ deposit was considered to be large compared with previously fabricated specimens. Within the past year, however, the Isotope Research Materials Laboratory (IRML) at the Oak Ridge National Laboratory (ORNL) has prepared considerably larger area targets of $^{235}UO_2$ (2000 cm^2) and $^{237}NpO_2$ (226 cm^2) to be used as sources of fission fragments under neutron bombardment and for use in precision cross-section measurements, respectively. Techniques and systems used in preparing actinide deposits will be described in this paper.

LARGE AREA DEPOSITS OF UO_2

There exists a large demand for well-defined, small pore size, membrane filters for use in blood research, cellular separation, tissue culture, and in other similar areas of research.[3] The membrane filters must have precise pore size distribution and possess chemical and thermal stability under a wide range of applications. One such procedure used to prepare such filters is to pass a plastic material over a $^{235}UO_2$

target while the target is being bombarded by neutrons. Resultant ^{235}U fission causes fission fragments to penetrate the filter material leaving sensitized tracks which can then be preferentially etched into uniform, cylindrical pores. The pore size is controlled by the length of the etching process.[4]

To be economically attractive, exposure of large areas of filter material is desired, within restraints of target fabrication technology and neutron irradiation capability. It was determined that the desired $^{235}UO_2$ deposits needed for this purpose would be approximately 51 cm wide and 76 cm long and contain 800 to 1000 $\mu g/cm^2$ of ^{235}U. As one can see, this represents a considerable extrapolation in area from the 8-cm diameter deposits previously prepared in our laboratory.

The procedure used to generate large area uranium targets was simply a modification of the one described in Reference 1. Since the targets were required to be uniform within ± 3 percent of the mean areal density, it was determined that the best approach would be to use two electron bombardment evaporation sources and a substrate mounted on a rotating drum assembly. Both electron bombardment sources were similar to the one shown in Fig. 1. As is shown, the electron beam is accelerated through an angle of 270° and impinges on a pressed UO_2 pellet. The electron beam can be programmed to sweep the pellet surface in a predetermined pattern to achieve maximum uniformity of evaporation.

To determine the system configuration for locating two electron beam guns under a rotating drum to give the desired uniformity of ± 3

percent, the following equation was used.[5]

$$t = \frac{mh_v^2}{\pi\rho} \left\{ \frac{1}{[h_v^2 + (D + X)^2]^2} + \frac{1}{[h_v^2 + (X - D)^2]^2} \right\} \qquad (1)$$

where

t = film thickness,

m = total mass of material evaporated,

h_v = source to substrate distance,

ρ = density of material,

D = distance from center line to center of electron beam crucible,

X = distance from center line to a point on the substrate where the film thickness is determined.

In addition, information provided by the Airco-Temescal Corporation concerning the uniformity of deposits from dual electron bombardment sources was used.[6] Equation 1 was derived from Holland's equation

$$t = \frac{mh_v^2}{\pi\rho(h_v^2 + \delta_j^2)^2} \qquad (2)$$

where

δ_j = the perpendicular distance from the center line of the evaporating beam and the point on the substrate where the deposition thickness is determined,

and the other terms are as defined for Equation 1. Thus, the following equation can be derived from Equation 1:

$$t = \frac{mh_v^2}{\pi\rho} \left\{ \frac{1}{(h_v^2 + \delta_1^2)^2} + \frac{1}{(h_v^2 + \delta_2^2)^2} \right\}. \qquad (3)$$

Since $\delta_1 = D + X$ and $\delta_2 = D - X$, Equation 1 can be obtained by substituting these terms in Equation 3.

The 51-cm x 76-cm targets were prepared using 25.5-cm x 76-cm substrate segments mounted on the rotating drum. A schematic representation of the preparative setup assumed in making the uniformity calculations is shown in Fig. 2. The terms shown in Fig. 2 are defined as for Equation 1 with

t_o = deposited film thickness at the center of the substrate,

t_e = deposited film thickness at the edge of the substrate.

The desired uniformity range is illustrated by the dashed lines in Fig. 3. Curve 1 in Fig. 3 was computed from Equation 1, whereas curve 2 was obtained from information provided by Airco-Temescal Corporation.[7] Thus, as is shown in Fig. 3, a distance from the center line to the source of approximately 20 cm together with h_v = 45.7 cm should theoretically yield the desired uniformity.

A schematic representation of the experimental equipment assembly used for the $^{235}UO_2$ evaporation is shown in Fig. 4. Pellets containing approximately 20 g of UO_2 were pressed and placed in each of the electron bombardment evaporation sources. The chamber was evacuated to the low 10^{-5} or high 10^{-6} torr range by using a 0.4 m^3/min. roughing pump in tandem with a 15-cm diameter oil diffusion pump. The substrate

was heated to 200-250°C and the evaporation was begun; substrate heating was necessary to insure an adherent bond between the titanium substrate and the UO_2 layer. Uniformity as well as average thickness of the UO_2 deposit was determined by weighing test plates placed on each side of the substrate as shown in Fig. 5. A resonating quartz crystal thickness monitor, shown in Fig. 6, was calibrated and used to determine in situ when the approximate desired film thickness was obtained. Also in Fig. 6 can be seen the electron bombardment heat sources, $^{235}UO_2$ pellets, quartz-iodide heating lamps, and the mounted titanium substrate. Since, as was shown in Fig. 4, two separate power supplies were used (one for each electron bombardment gun) it was anticipated that perhaps it would be difficult to maintain exactly the same evaporation rate from each source and consequently the uniformity requirements of ± 3 percent would be difficult to achieve. The desired mean thickness range was 0.8 to 1 mg/cm^2. It was decided to evaporate until approximately 0.8 mg/cm^2 of UO_2 deposit had been attained, and then determine the real thickness using the tared test plates as well as to verify the uniformity of deposit across the titanium substrate. If the desired uniformity was not obtained, the evaporation source on the side containing the lowest areal density could then be adjusted and more material evaporated to bring the total areal density across the substrate to within the desired uniformity range.

After two such titanium substrates were coated, they were glued to a thick aluminum substrate in a specified pattern. One such pattern is

illustrated in Fig. 7. As shown, one plate was attached in the central region and the other plate was sheared and glued to each side of the central diagonal plate. During neutron irradiation, as the membrane moved over the source surface, it was highly desirable not to have a straight line discontinuity in the membrane pore distribution resulting from few or no fission fragment tracks. This is the purpose for angling the deposits as shown in Fig. 7.

Uniformity of deposition obtained for two UO_2 evaporations is shown in Fig. 8. These uniformities were obtained very simply by counting the alpha disintegrations over a 2.54-cm diameter area at various locations on each substrate. As is shown, the desired uniformity (for the most part) was obtained for the 0.8 mg/cm^2 coating with slightly larger variations for the 1.0 mg/cm^2 coating. Both coatings were deemed acceptable.

LARGE AREA DEPOSITS OF NpO_2

One of the chief concerns of today is our national energy problem. The United States is trying to become energy self-sufficient by relying heavily on research in geothermal, coal gasification, solar and nuclear processes. Many believe the energy problem can best be alleviated or reduced through an enhanced reliance on nuclear power. Thus, more and more research is being conducted to better characterize existing and proposed future reactor materials. The goals of this research are to make power reactors efficient and safe for use on a large scale to meet the energy needs of the future.

One phase of the reactor research effort involves determining accurate cross-section data for the various reactor fuel materials. It is important to know, for example, the ratio of the neutron capture cross section to that for fission for certain reactor fuel materials. A high ratio would mean that more neutrons are being captured and fewer fission events taking place. These values are needed to accurately calculate fuel utilization efficiencies.

The IRML has been involved in preparing many samples such as $^{235}UO_2$, $^{239}PuO_2$, and $^{238}UO_2$ for use in neutron cross-section measurements. In the past ≤8-cm diameter deposits have been used for this purpose. The procedures used to prepare such targets have been described in the literature and now have been adapted for use in preparing large-area $^{237}NpO_2$ targets. The large $^{237}NpO_2$ deposits were used to assemble a fission chamber for measurements of the ^{237}Np neutron fission cross section. This data will be used as a nuclear cross section standard and will lead to more accurate cross sections for other materials employed in nuclear reactors.

A total of five $^{237}NpO_2$ targets having a coated area of 226 cm^2 (17.8 cm x 12.7 cm) were prepared by the vacuum evaporation-condensation of $^{237}NpO_2$ using an electron beam heat source previously described in Fig. 1. Schematically, the deposition assembly used for preparing these targets is shown in Fig. 9. As is shown, the large substrate was located 30.5 cm from the source and was rotated to achieve good deposition uniformity.

The system used is shown in Fig. 10. A vacuum of $<2 \times 10^{-5}$ torr was obtained by using a 0.4 m^3/cm roughing pump and a 15-cm diameter oil diffusion pump. The NpO_2, in powder form, was pressed into a pellet and placed in the electron beam gun crucible. After the system was evacuated to $<2 \times 10^{-5}$ torr, the rotating aluminum substrate was heated to approximately 200°C and the evaporation initiated. Actual NpO_2 thickness and uniformity was determined by weighing tared satellite targets after deposition was complete. An areal density of approximately 100 $\mu g/cm^2$ was obtained on both sides of the five 0.025-mm thick aluminum substrates. Deposit uniformity was ≤8 percent and the vapor collection efficiency was approximately 4 percent.

SUMMARY

Very large area deposits of actinide oxides can be prepared by physical vapor deposition. Normally, the only limitation in achieving the required uniformity of such deposits are the expense of the material and its availability. In most instances, uniformities of ≤5 percent can be achieved by employing single or multiple evaporation sources and adjusting the source-to-substrate distance.

REFERENCES

1. H. L. Adair, Nuclear Inst. and Methods 113, pp. 545-548, (1973).
2. Ibid. 1, p. 545.
3. Nuclepore Corporation, Nuclepore Membranes and Hardware for the Laboratory, Catalog LAB 20, p. 2.
4. Ibid. 3.
5. L. Holland, Vacuum Deposition of Thin Films, John Wilex and Sons, New York, p. 145, 1958.
6. Airco Temescal, Physical Vapor Deposition, pp. 80-83, 1976.
7. Ibid. 6.

FIGURE CAPTIONS

Fig. 1. Electron beam evaporation source.

Fig. 2. Schematic showing terms used in calculating the film thickness profile from two electron beam sources.

Fig. 3. Curves showing the uniformity variation for different distances from the two electron beam sources.

Fig. 4. Schematic of the system used for the $^{235}UO_2$ evaporations.

Fig. 5. Close-up view of the rotary substrate mechanism, quartz iodide heater lamps, quartz crystal monitor, and test plates used in film-thickness determination.

Fig. 6. Interior view of the $^{235}UO_2$ evaporation system.

Fig. 7. Schematic showing arrangement of $^{235}UO_2$ deposits on final substrate.

Fig. 8. Uniformity of the $^{235}UO_2$ deposits for 0.8 mg/cm^2 and 1.0 mg/cm^2 thicknesses.

Fig. 9. Schematic of $^{237}NpO_2$ system.

Fig. 10. Glove box system used for $^{237}NpO_2$ evaporations.

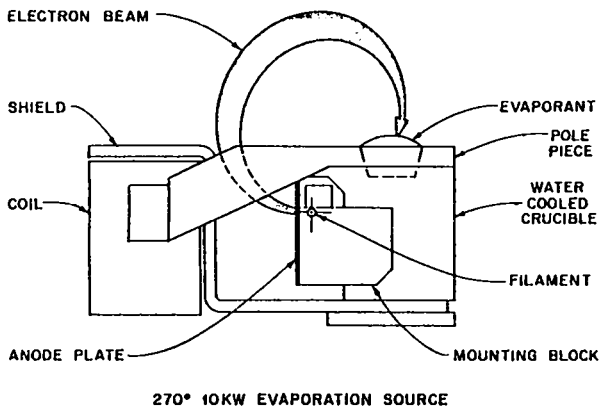

Fig. 1

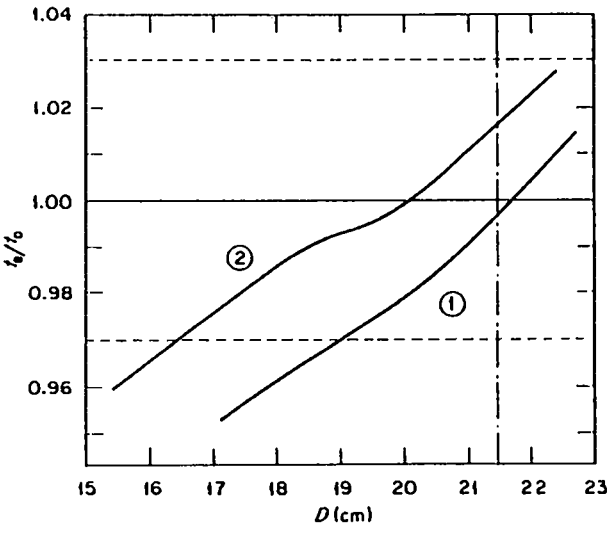

Fig. 3

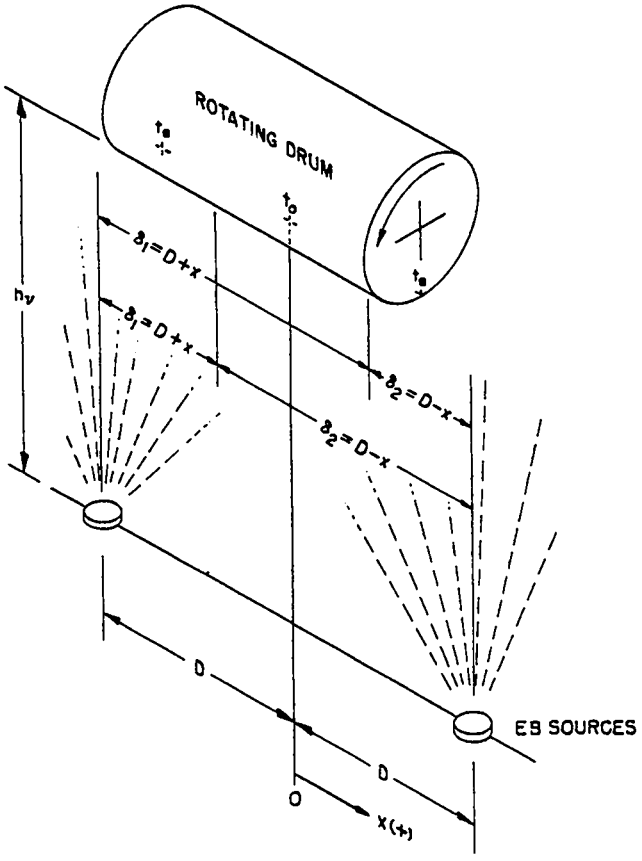

Fig. 2

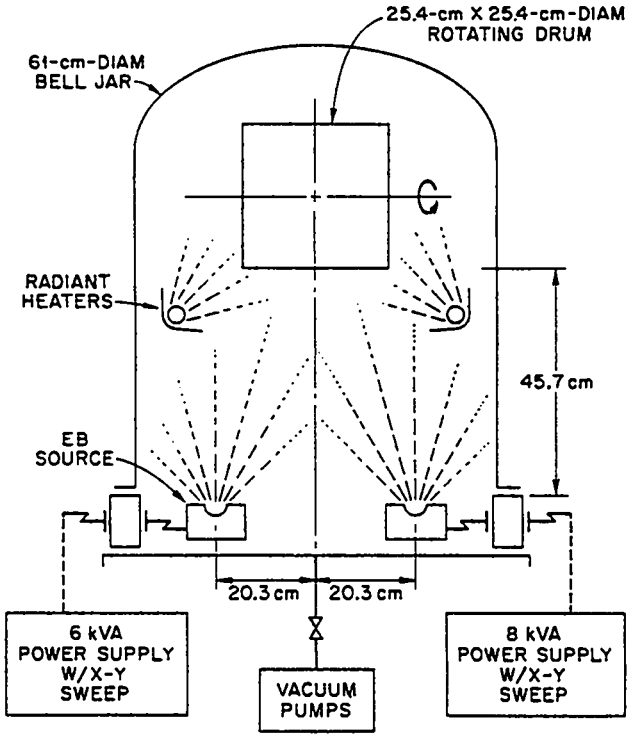

Fig. 4

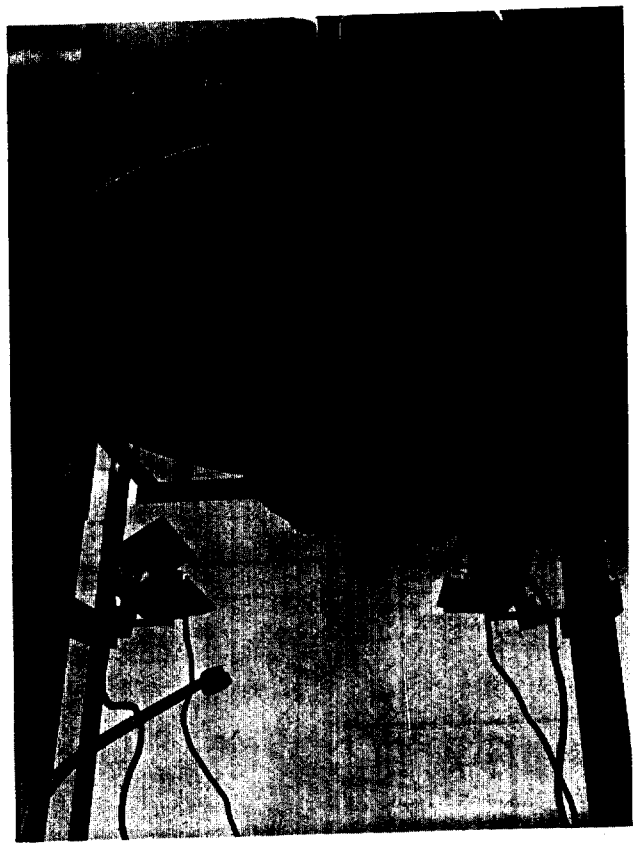

Fig. 5

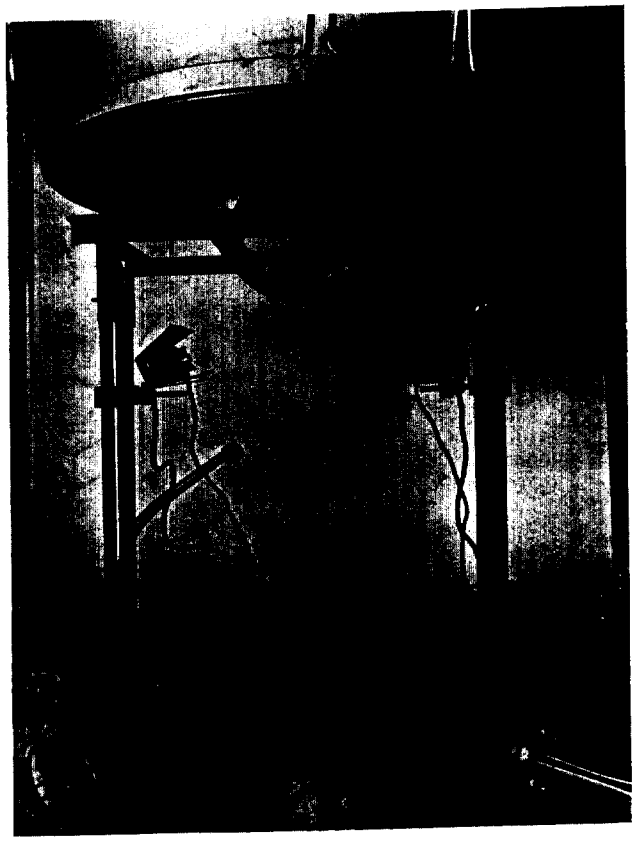

Fig. 6

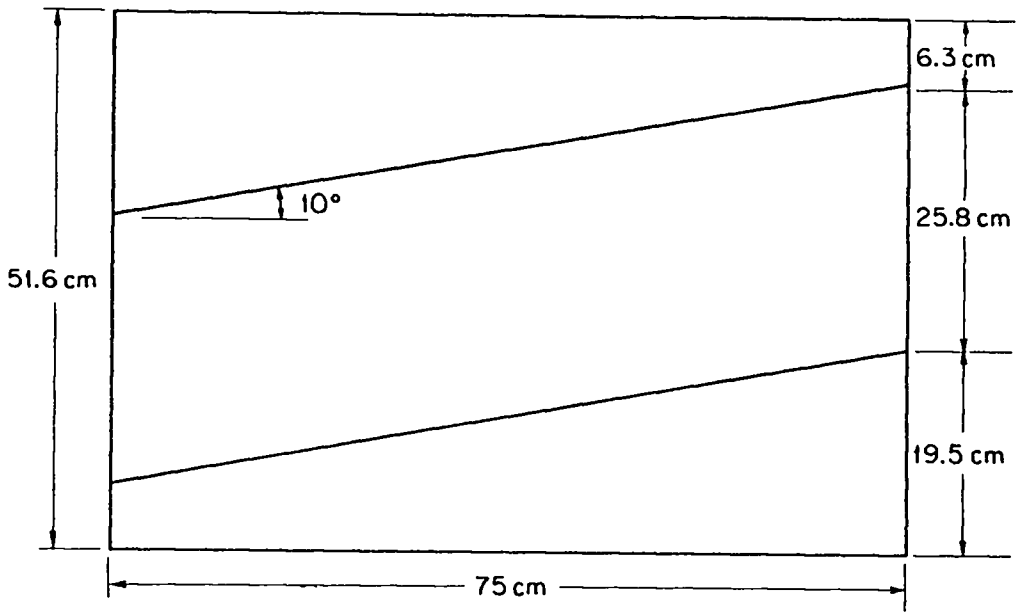

Fig. 7

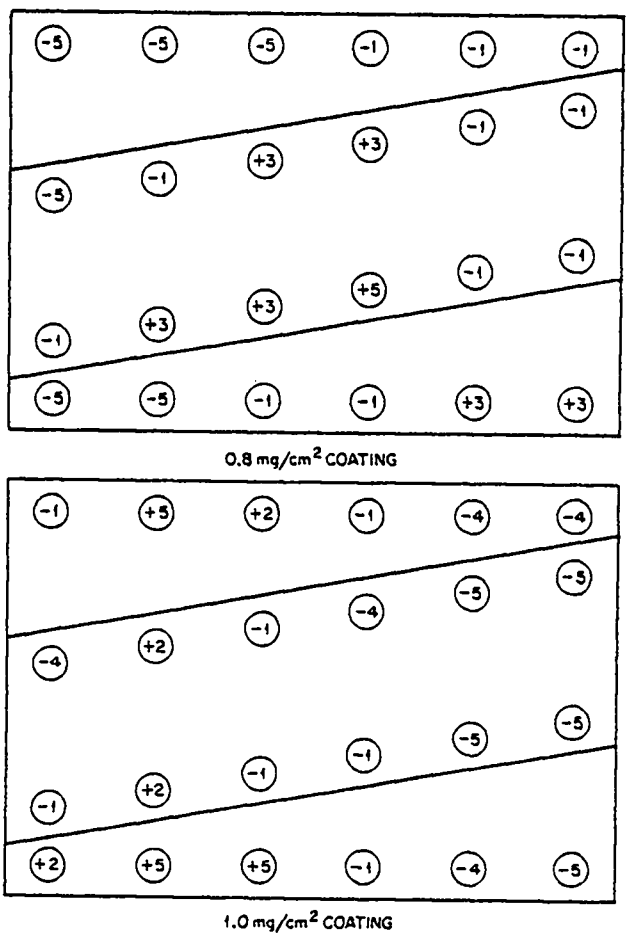

Fig. 8

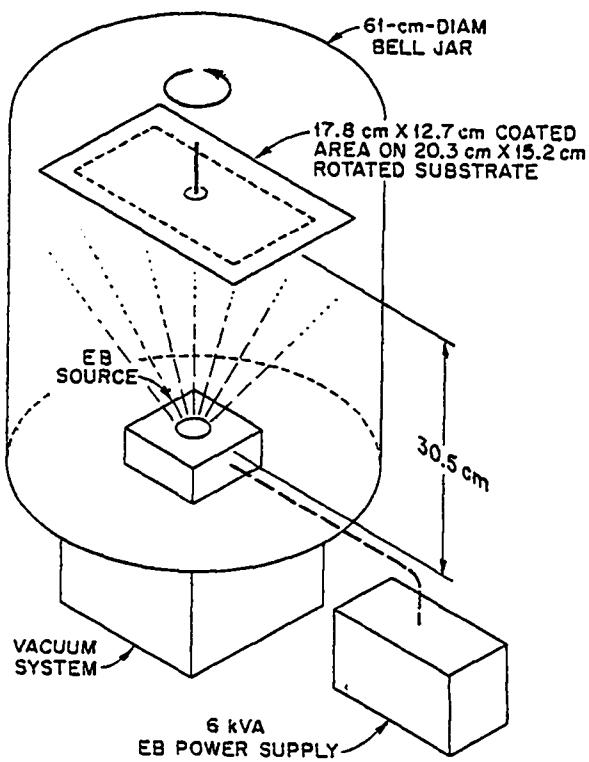

Fig. 9

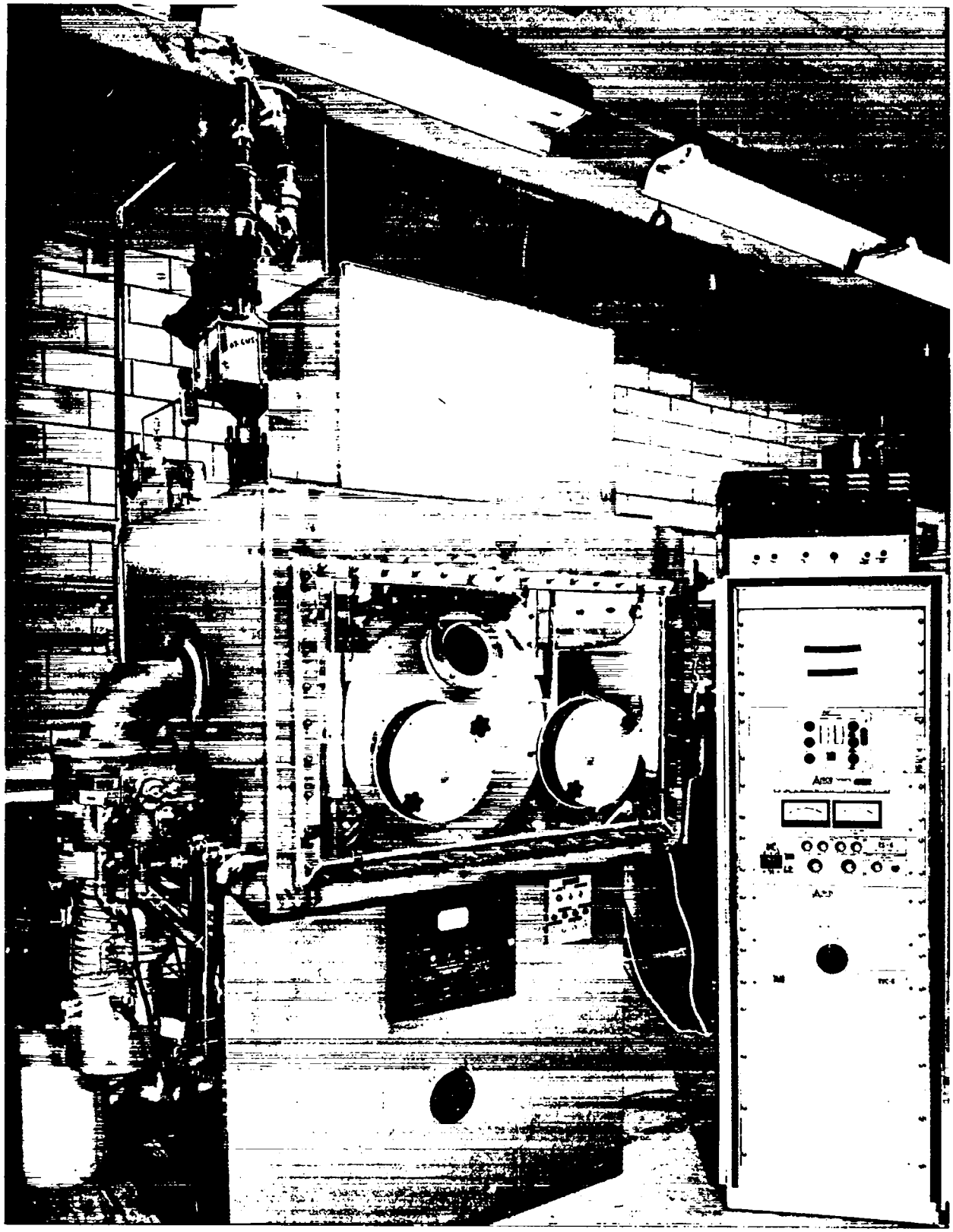

Fig. 10

Alternatives to Thin Film Carbon Foils for Use in Stripping Heavy Ion Beams

D. Ramsay

Department of Physics, Stanford University, Stanford, California 94305*

In reviewing papers published concerning stripper foil behavior, several questions arise. Why is it that so much work has been done on prolonging the life of carbon films and so little work done on looking for a substitute? What good does it do to bake, rotate and oscillate foils when there is no clear cut explanation of why they break in the first place? Well, as a target maker I have a sneaking suspicion that I am partly responsible for the bulk of the research being confined to carbon foils. Like people climb mountains, because they are there, physicists use carbon foils because we can make them.

In an attempt to atone for this negligence, I gathered up a cluster of surplus targets and ran them in the Van de Graaff accelerator at Stanford. Using an O^{+6} beam I destroyed thin films of B, Al, V, C and SiO_2. This paper would end right here except that two of the targets did not break. The first was a 2 $\mu gm/cm^2$ carbon foil backed with 10 $\mu gm/cm^2$ gold. (Figure 1a). This was exposed to the beam about the same length of time as a 2 $\mu gm/cm^2$ carbon target without any gold backing, which tore at the beam spot. Here you can see the familiar dark area in the center which could be due to carbon build-up by the cracking of hydrocarbons.[1] In an attempt to find out if this carbon layer varied depending on the target material, we ran a HfO film which was glass transparent under similar conditions.

The HfO target did not break and when examined two features were readily apparent. First it did not have as discernible a dark spot and the film now was wrinkled. (Figure 1b). The creases radiate out from the edge of the beam spot which remained perfectly flat and they stretch to the edge of the film which is 1.25 cm in diameter. There is evidence that the thickening of the beam spot foil area is not due to carbon build-up.[2]

Could the obvious strain present in the HfO foil be due simply to this thickening effect? We next evaporated an Al foil which had a center circular area (6 mm diameter), twice as thick as the rest of the film (2 cm diameter). (Figure 1c). This foil is 50 $\mu gm/cm^2$ and 25 $\mu gm/cm^2$ respectively. Thinner films, 10 and 20 $\mu gm/cm^2$ were tried but the center sections tore while drying. In the Al foil the thickened area is perfectly round, but if you look closely you can see that the tension between the wrinkles has distorted the edges of the circle into almost straight lines. Now our beam spot at Stanford is oval so the stresses are not as uniform. When we examined the broken carbon-only foil (Fig. 1d) and matched up the torn flaps we could see that tear was across the thick area. It has always bothered me that a film should ever break at its thickest part but if we visualize a mechanical dimensional distortion under radial stress, starting to rip at a point on the edge of the beam spot, we can see how it could tear across the center in one or possibly two directions and then stop abruptly, because the strain is relieved. This kind of tearing was the case in most of our foils and is typical of carbon greater than 1 cm in diameter. Thornton[3] reports that some foils after breaking flap in the beam and continue to strip electrons intermittently. It certainly seems possible that the rupture of a stripper foil could be due to purely mechanical strains

built up by a uniform flat foil becoming non-uniform, specifically thicker in the beam spot and thinner all around. The next question was, what mechanism could be responsible for thickening the film?

Early in the development of the semi-conductor industry there was a great deal of trouble caused by thin film devices failing due to what came to be called a mass transport effect.[4] (Figure 2). This is an aluminum film 1500 Å thick which has been carrying a direct current density of 10^6 A/cm^2. Both grain boundary and surface transport have left voids in the film. (Figure 3). Here we have a gold film, 6000 Å thick before and after passage of $2 \cdot 10^6$ A/cm^2 at 350°C for 2 hours. You can see the voids at the cathode on the right and hillocks at the anode on the left. In electromigration, aluminum and gold atoms move in the direction of the electron flow, i.e. toward the anode. For alternating current no mass transport has been observed. We know that when an ion beam passes through a foil it scatters off electrons (Figure 4a). In a carbon foil then, we have in essence a direct current flow from the outer rim of the foil toward the beam spot.[5] There is also a temperature gradient both of these conditions favor electrotransport[6] (Fig. 4b). Here we show schematically what could result if this phenomena is actually taking place. The perimeter of the beam spot would be depleted of material as it is transported toward the center; the beam spot area thickens; energy transmission decreases; the film tightens; radial stress lines appear from the strain of non-uniformity; and the foil tears. All these observed facts fall nicely into place, but is it theoretically possible?

Significant mass transport of Al and Au thin films occurs at current densities of 1 to $2 \cdot 10^6$ A/cm^2 in films 1500 to 6000 Å thick. Most carbon

stripper foils are on the order of 100 to 300 Å thick. (Figure 4c). To calculate the area we use πdt where d is the diameter of the beam spot and t the thickness of the film. For a 4 mm d spot the area is about $2.5 \cdot 10^{-6}$ cm^2. In order to get beam densities of 10^6 A/cm^2 in the stripper foil we would require a current of around 1 Amp. The actual current through the stripper foil[7] is approximately the same as the beam current incident on the foil estimated at 10 to 100 μA. This gives rise to a current density of 10 to 100 A/cm^2. This is too low by a factor of 10,000.

In reviewing the literature available on electromigration we were unable to find enough information to calculate the current densities needed for a thin carbon film to exhibit mass transport. Most of the work has been done with metals and surface areas were on the order of 10^{-5} cm^2.[8] Although there is a correlation between self-diffusion coefficients and electrotransport, the other factors entering into the equation are unknown for carbon. We decided to duplicate some of the earlier experiments[9] and substitute carbon for aluminum.

Carbon films 1 to 10 mm wide and 1 to 2.5 10^{-6} cm thick were deposited on glass slides. The ends were coated with aluminum for electrical contact and the length of the carbon strips varied from 1 mm to 5 mm. All of the samples failed. (Figure 5a). Resistence varied between 5 and 22 Meg ohms. The lifetimes in a vacuum of 10^{-5} Torr were from 8 hours at a current density of 2.7 A/cm^2 to 60 minutes at 10 A/cm^2. This is not the best illustration of what happened but it shows quite well that the carbon film is ruined. In other cases it was more apparent that there was a depletion of the film at the cathode. When viewed through a microscope there were some interesting features. Before total failure often there were streaks running

the length of the carbon film between anode and cathode. In one case there was a slight but definite decrease in resistance before failure. Possibly some of the aluminum atoms diffused across. Structural changes did not occur linearally with time. In every case destruction seemed to accelerate noticeably the last few minutes.

There was at least one more piece of information that we felt was needed. Since one of the original targets was a thin aluminum foil and it was destroyed in the beam, could there be a failure in an aluminum film at these low current densities? We evaporated a 4 $\mu gm/cm^2$ aluminum strip, 6 mm wide and 7 mm long on a glass slide and covered the ends with a thick coating of aluminum for electrical contacts. A 22 Meg ohm resistor was put in the circuit and a direct current of 100 μAmps was run through it for 90 minutes. The resistance slowly increased (a total of 65%) then the film failed. (Figure 5b). When examined the open channel at the cathode end was wider than the open area at the anode end. The channel was devoid of debris at the cathode side but there were islands of Al grains in the anode channel. This is not conclusive evidence of electrotransport but it is in keeping with the findings of other researchers except for the lower current density by a factor of 1000 and the considerably larger surface area, 0.42 cm^2 compared to $3.5 \cdot 10^{-5}$ cm^2.

To sum up then, we find that electromigration cannot be ruled out as at least one of the possible mechanisms for causing carbon stripper foil failure. If mass surface transport of carbon atoms in the direction of the electron flow is the primary factor then we can use this information to design a longer-lasting solid stripper. Beryllium for instance, has a self-diffusion factor of only 0.5, while for carbon it is 5.0. Instead of

a material which flows with the electrons why not a mixture of say carbon and platinum. It has been suggested that platinum migrates against the electron flow. Certainly it would increase the life of present stripper foils to start with as large a beam spot as possible and slowly focus it smaller. Also the larger the diameter of the foil the greater the lifetime. The smaller the area of the beam spot the shorter the lifetime. Heating it evenly reduces the temperature gradient and probably makes the foil more elastic. Making the supporting plastic thicker should help by furnishing a stronger mechanical support. Dielectrics like boron nitride are a possibility. At any rate the need for a solution is growing. Perhaps, a single crystal carbon foil is the answer; in that case, diamonds will be a target-makers best friend. There are five low Z elements that theoretically could serve as solid stripper foils; Be, B, Mg, Al and Si. If we add to that just low Z compounds like BeO, BN, and SiC we get over 20 possibilities, not to mention mixtures like Si with a dash of phosphorous or alloys like Be/Al. Then there are variations like grain size and crystal structure, thickness and diameter. Maybe one foil the size of a large pizza could be rotated like a phonograph record and would last 3 years.

Are there any more suggestions?

References

* Supported in part by the National Science Foundation.

1 J. L. Yntema, Nucl. Instr. and Meth. 98 (1972) 379.

2 P. Dobberstein, L. Henke, Nucl. Inst. and Meth. 119 (1974) 611.

3 S. T. Thornton, R. H. McKnight and R. C. Rittner, Nucl. Instr. and Meth. 101 (1972) 607.

4 Maissel and Glang, "Handbook of Thin Film Technology" (McGraw-Hill, 1970).

5 J. L. Yntema, IEEE Trans. on Nucl. Sci., Vol. NS-23, No. 2 (April 1976).

6 M. Etzion, I. A. Blech and Y. Komen, J. Appl. Phys., to be published.

7 J. L. Yntema, Nucl. Instr. and Meth. 113 (1973) 605.

8 I. A. Blech, Bell Labs., Murray Hill, N.J., private communication.

9 P. B. Ghate, Appl. Phys. Lett., Vol. 11, No. 1 (1 July 1967).

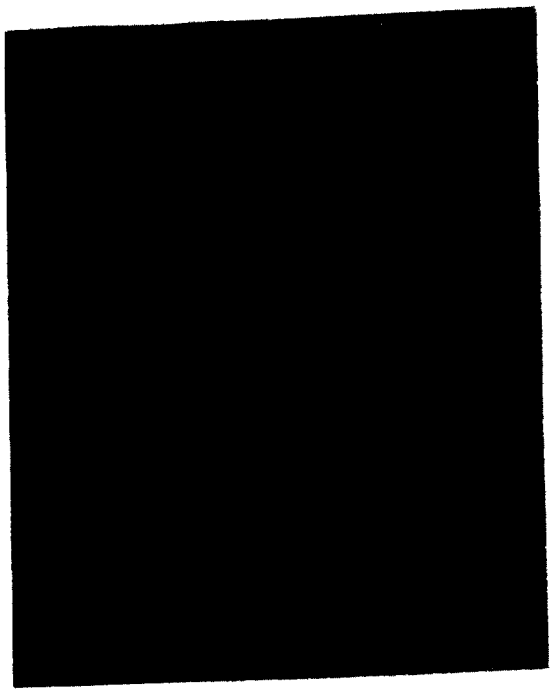

a.

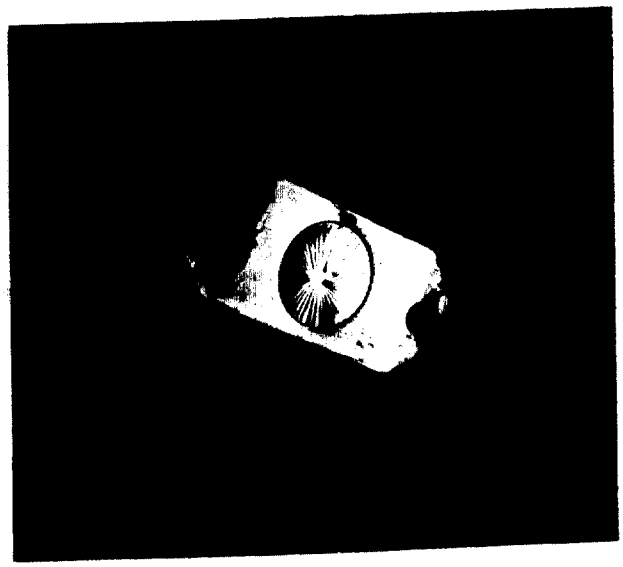

b.

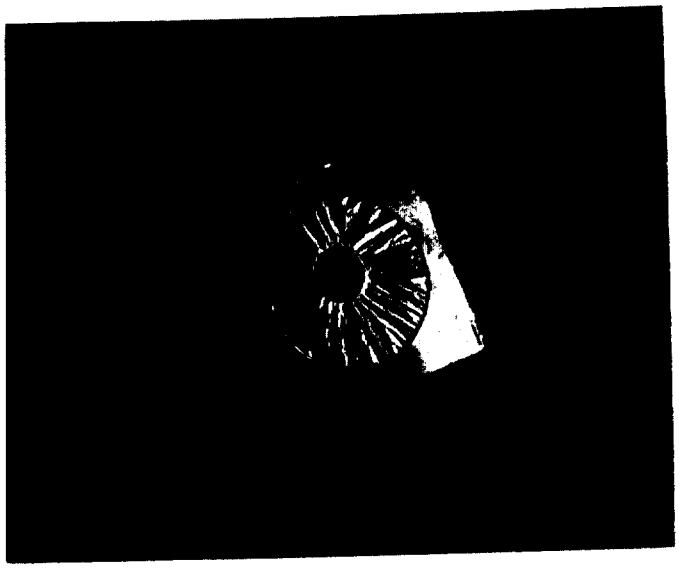

c.

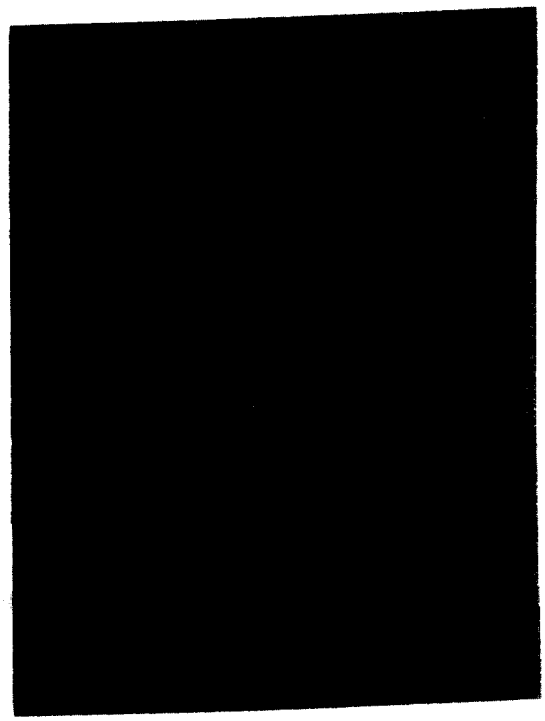

d.

Fig. 1

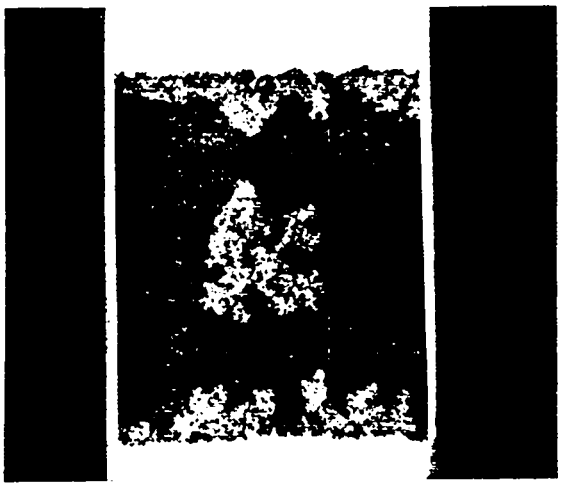

Fig. 2

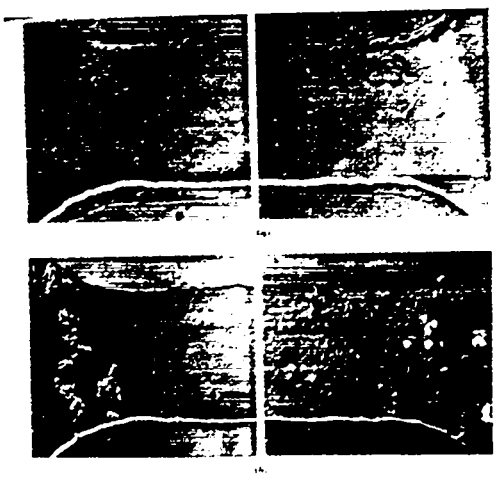

Fig. 3

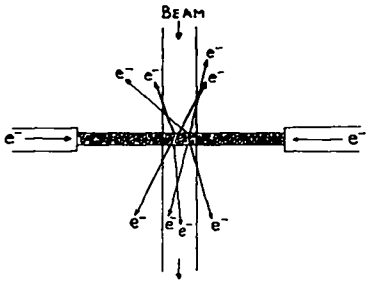
BEAM
e⁻

a.

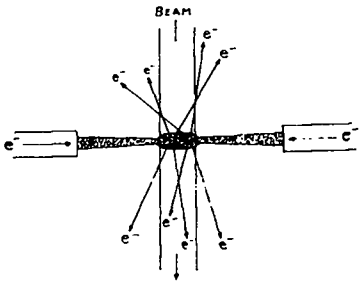
BEAM
e⁻

b.

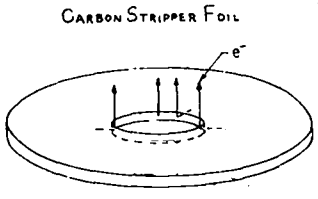
CARBON STRIPPER FOIL
e⁻
CURRENT DENSITY = Amps / πdt
d = diameter of beam spot
t = thickness of film

c.

Fig. 4

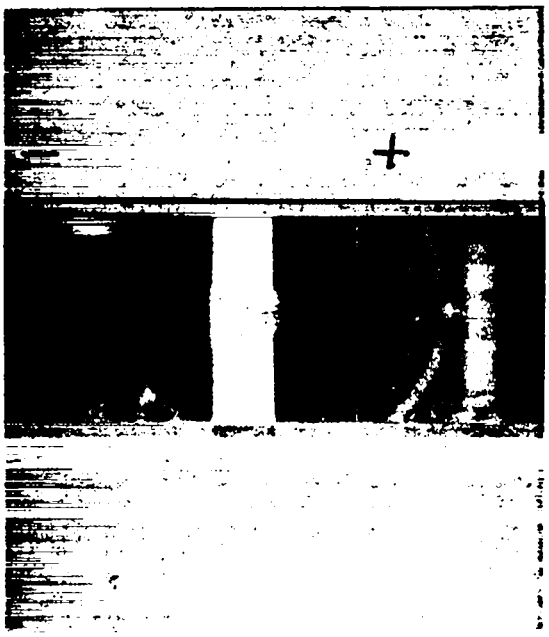

a.

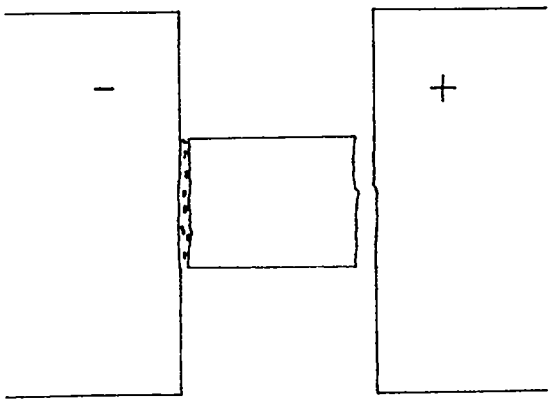

b.

Fig. 5

THE PREPARATION OF NITROGEN-15 TARGETS

by

J.D. Stinson

Division of Physics, National Research Council
Ottawa, Canada

A technique for the preparation of nitrogen-15 targets using titanium as a reactant is described. Targets in the range of 5 μg/cm² to 75 μg/cm² have been routinely produced. Evaporation and nitriding temperatures, chemical cleaning of substrates and vacuum system requirements are given.

Introduction:

Over the past eight years a technique has been used for the production of nitrogen-15 targets. Though the method of producing nitrogen targets is well known,[1] the technique described has been developed to provide better quality targets on a routine basis. Special attention has been paid to vacuum system requirements, deposition temperature and nitriding procedure to obtain some degree of purity. These targets have been used for αγ studies at the Van de Graaff accelerator installation at the National Research Council of Canada.

Vacuum System:

A commercial vacuum system with a 30 cm bell jar and a 10 cm oil diffusion pump has been modified to reduce oil back-streaming. A water cooled chevron baffle and a liquid nitrogen baffle have been added to provide the trapping for the work chamber. Oil back-streaming is further reduced by the addition of a zeolite trap between the fore-pump and diffusion pump. Roughing of the work chamber is accomplished with a separate zeolite trapped pump. The vacuum obtained with this system is better than 10^{-7} Torr after six hours of pumping and permits the evaporation process to proceed at better than 10^{-6} Torr.

Evaporation Source Preparation:

A tungsten source with a 1 cm dimple and a 0.25 mm thickness is used to evaporate the target titanium. A 20 cm distance from the evaporation source to the target substrate has been selected. This distance permits an acceptable uniformity of target thickness and allows easy calculation of source charge. A 1 mg charge of titanium evaporated to completion will give a 1 $\mu g/cm^2$ coating of nitrided titanium.

A three strand tungsten helix source 4.5 cm long x 1 cm diameter is used to evaporate 0.25 g of titanium for getter pumping.

A pre-firing of both evaporation sources at 1500°C in vacuum is carried out to minimize target contamination.

Substrate Preparation:

Metallurgical grade tantalum sheet in a strip 15.25 cm x 2.5 cm x 0.025 cm is used as a target backing. After deposition each strip

supplies four targets, 2.5 cm x 2.5 cm in size, from the centre section. To provide a clean surface for the titanium deposition the tantalum strip is chemically polished according to a recipe by Tegart.[2] The tantalum is immersed for 3 to 5 seconds in the following solution: 5:2:1.5 or 2 by volume of 98% H_2SO_4, 70% HNO_3, 49% HF. The tantalum is immediately rinsed in de-mineralized water and then dried in a nitrogen jet. The substrate surface after this treatment appears shiny and may have some orange peal effect under low magnification. The tantalum substrate is weighed on a semi-microbalance for eventual target thickness determination.

Chamber Fixturing:

Three pairs of water cooled electrodes feed power for target processing and are shown on the accompanying drawing. One pair of electrodes is required for each of the following functions: the evaporation of target titanium at A, outgassing of the substrate and nitriding the deposited titanium at B, and the evaporation of titanium for getter pumping at C. Titanium evaporated for gettering is shielded from the target substrate as illustrated.

The power required to perform the steps in the process at A and B is supplied by one power supply and is switched from one pair of electrodes to the other during the procedure. A second supply provides power for getter pumping at C. Both supplies are capable of providing 2 KVA of power.

A pyrex flask containing ^{15}N with a break seal and stopcock at D is attached to the chamber. A bleed valve provides control for leaking in the required quantity of gas.

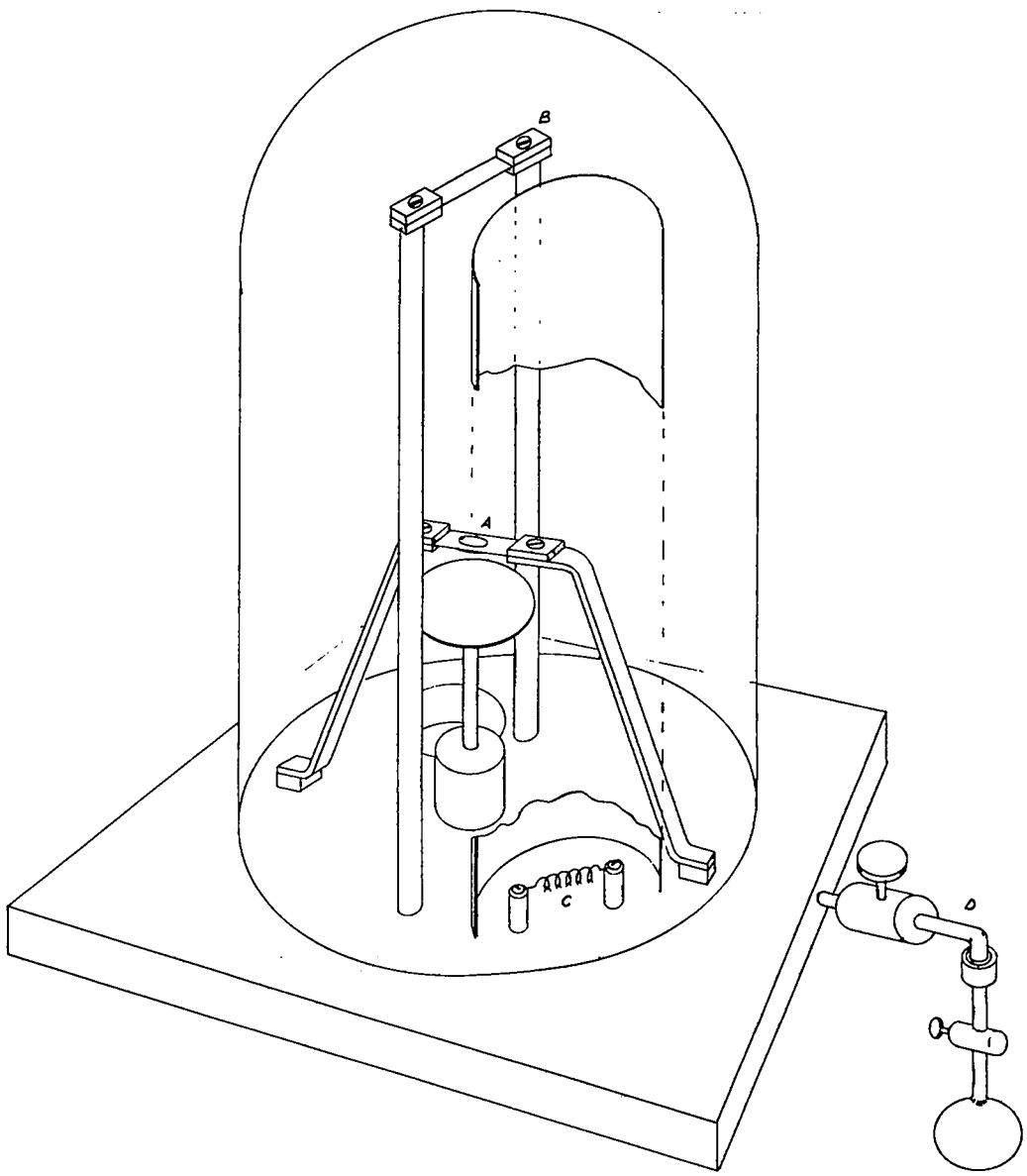
B
A
C
D

Processing Procedure:

A base vacuum of better than 10^{-6} Torr is required before proceding with the deposition process. Filling the trap with liquid nitrogen improves the vacuum on our system to better than 10^{-7} Torr.

Target processing is started by first outgassing the tantalum substrate by heating to 800°C for one or two minutes or until outgassing has ceased. The system pressure is allowed to recover before continuing further with the process. This usually takes no longer than three or four minutes.

The titanium getter source and the evaporation source are powered to simultaneously raise their temperatures to 1000°C, with an accompanying rise in vacuum pressure being observed. The getter source temperature is further increased to about 1700°C or until the titanium melts and begins to evaporate. The pumping action of the evaporating titanium rapidly reduces the chamber pressure lower than 10^{-7} Torr. The evaporation source temperature is now increased to completely evaporate the target titanium and takes about one minute to do so. After switching off the power to both evaporation sources, the vacuum chamber is isolated by closing the main valve.

Nitrogen-15 gas is bled into the vacuum chamber to a pressure of 300 millitorr. Nitriding is accomplished by heating the titanium coated tantalum in situ to an observed temperature of 750 to 800°C and maintaining this temperature for five minutes. The target is allowed to cool in the ^{15}N environment for one half hour before removal from the chamber. Weighing of the target and calculating the thickness completes the procedure.

The temperature figures quoted for the nitriding process are readings taken with an optical pyrometer and have not been corrected for emissivity.

General Comments:

Experience has shown that the nitriding temperature range previously stated is important. An incomplete nitriding reaction is the result of the temperature being too low; whereas, too high a temperature can cause nitrogen diffusion into the tantalum substrate resulting in a target with a poorly defined thickness.

The important contaminants in $\alpha\gamma$ studies are the low Z elements. These give a high background because of large cross sections for α reactions. Carbon and, to a lesser degree, oxygen are present in the targets produced. Researchers[3] have included in a publication, the results of an investigation of the purity and stoichiometry of target #148. It is not within the scope of this paper to report their complete findings; briefly stated, they found the following:

$TiN_{0.79}$ was representative of the nitriding efficiency.

The carbon, titanium atom ratio was equal to 0.11.

The oxygen, titanium atom ratio was less than 0.09.

It is not known if these results are valid for all the targets produced.

Some experimental work with reactants other than titanium has been done. Zirconium and niobium did not give as good results as titanium and considerably less development time was expended on these elements.

Improvements on this technique can be made; for example, titanium of higher purity could be used and an oil free vacuum system would undoubtedly reduce carbon contamination.

More than 160 targets have been produced by the method outlined here and improvements in technique and equipment are being evaluated.

The author gratefully acknowledges the advice and encouragement of Drs. R.S. Storey and W.R. Dixon.

(1) Aitken, J.H., University of Toronto, Private communication.

(2) Tegart, W.J. McG., *The Electrolytic and Chemical Polishing of Metals*, Pergamon, New York, 1959.

(3) Dixon, W.R. and Storey, R.S., 1971, Can. J. Phys. 49, 13.

REDUCTION TECHNIQUES FOR ISOTOPIC MATERIALS

Joanne M. Heagney and Joseph S. Heagney

MicroMatter Co., Seattle, WA.

INTRODUCTION

The inventory form of many of the isotopes of the elements provided by O.R.N.L., Isotope Sales is other than metal. The reason being in most cases that the metal is not the most stable form of the element. While most of these isotopes can be obtained from O.R.N.L. as metal, it is clearly advantageous in the case of the more reactive elements for the target-maker to perform the reductions simultaneous with or just prior to fabricating the target.

Table 1 lists those elements whose inventory form at O.R.N.L. is other than metal and which can be easily reduced using equipment and materials readily available to most target making facilities. Three basic reduction methods are indicated; furnace reduction with hydrogen gas, reduction-distillation with active metals or carbon and electrolytic reduction. These three methods will be discussed separately with attention to variations between different metals using the same reduction method.

HYDROGEN REDUCTIONS

Hydrogen reductions are by far the simplest and most straight forward of all the reduction techniques. Using a common tube furnace, reductions of isotopically enriched Cr_2O_3, CuO, GeO_2, In_2O_3, Fe_2O_3, $Pb(NO_3)_2$, Tl_2O_3 and WO_3 can be accomplished. The oxide is placed in a combustion boat and the boat inserted into the tube furnace. The combustion boat must be carefully selected so as not to contaminate the resultant metal (e.g. Iron forms a carbide if a graphite boat is used). Care must also be taken to select a combustion tube which is serviceable up to the maximum temperature at which the reduction will be carried out. Vycor tubes may be used up to 1000°C, Quartz to 1300°C and Silliminite (which is opaque) up to 1700°C. However, for most reductions, a Vycor tube is sufficient. A hinged type tube furnace is extremely advantageous in that it allows one to view the material when "jiggling" the combustion tube to consolidate a lower melting metal. It

also allows for more rapid cool down after reduction. Hydrogen from a tank is passed through a catalytic cartridge to remove oxygen and then through a trap of either phosphorus pentoxide or liquid nitrogen to remove water vapor. After thoroughly flushing the system with hydrogen, the gas may either be ignited and burned at the outlet of the combustion tube or vented in a fume hood. If the excess hydrogen gas is ignited, a small oil trap should be used to prevent "flashback explosions" in the tube which could be dangerous and costly in terms of loss of material. Table 1 lists the proper temperature range and type of combustion boat to use for each element.

Lead isotopes are provided by O.R.N.L., Isotope Sales as the nitrate. One can convert the nitrate to oxide by dissolving it in deionized water, adding an excess of ammonium hydroxide to precipitate lead hydroxide and finally by adding hydrogen peroxide to precipitate lead oxide. Wash the oxide thoroughly, centrifuge, decant, dry and then reduce with hydrogen. One can reduce lead nitrate directly by using a covered combustion boat with a couple of small holes in the cover to allow hydrogen flow. The cover prevents the nitrate from "spitting out" of the boat when it decomposes to the oxide.

REDUCTION - DISTILLATION

This method in general utilizes an active reductant like Aluminum, Calcium, Lanthanum, Zirconium, Thorium, etc. or Carbon, whose oxides are volatile. Usually the process takes place in a vacuum evaporator using any one of the many heating methods to achieve the reaction temperature. In most cases, the reduced metal evaporates near the reaction temperature, while the reductant and its oxides have very low evaporation rates at this temperature. In these cases, one can often evaporate a target foil directly onto the substrate. Usually, however, the reaction goes at a high enough temperature to cause some contamination of the deposit and a re-evaporation or re-distillation step is required.

The powdered oxide of the material to be reduced is mixed with the finely divided reductant and the mixture is pressed into a pellet to assure good physical contact and to exclude as much gas as possible. One and one-half to two times the stochiometric ratio of reductant to oxide is used to allow for oxidized reductant and non-uniform mixing. It is important to use finely divided reductant, but since active metal powders oxidize rapidly, they are most effective is freshly prepared from the bulk material just prior to each reduction. Filings from a lump are usually used, but there is some concern about

contamination from the file; therefore, a separate, unoxidized, high quality file is recommended for each reductant used. The pellets are loaded into a tight-geometry source and heated to the reaction temperature. For Ca, Mg, Sr, Sm and Yb oxides a resistance-heated tantalum pinhole or tube-type source is used (See Figure 1). For the higher temperature oxides like Dy, Er, Gd, Nd and Lu an electron heated tantalum crucible set-up is used. The rate of heating should be slow and care taken to avoid "runaway" as rapid out-gassing may eject pellets from the more open sources or deposit small "spits" of material on the substrate. The substrate is placed close to the source opening and in the case of large quantities is often movable to allow for the increase in thickness of the deposit. Substrates are chosen for non-interaction with and easy removal of the deposit. Polished tungsten sheet is often used. Some very carefully designed sources for use with induction heating have been made and reported by O.R.N.L.[1,2] A more detailed discussion of the reduction of the rare earth oxides may be found in the literature.[3,4]

In the case of the carbon reduction of Chromium and Iron, a graphite crucible in an electron heated crucible set-up is preferred; while for Cadmium and Zinc a resistance heated tantalum pinhole-type source is used. The reaction is monitored by the increase in pressure due to the evolution of CO_2 and CO. Little contamination occurs due to the high purity of carbon available and the extremely low vapor pressure of carbon. For large quantities the pumping load may be so large as to require extremely long times in the usual vacuum system. Also carbide formation may cause low yield or poor final metal.

ELECTROLYTIC REDUCTION

Electrodeposition is the most conservative method for the reduction of isotopic oxides of Zinc and Cadmium to obtain metal for rolling or vacuum evaporation. Usually better than 90% of the metal can be deposited on the cathode and what remains in solution can be recovered chemically. Figure 2 illustrates a simple electroplating cell used for plating small quantities of material. Construction details were designed for easy assembly and disassembly. The volume of plating solution is kept to a minimum in order to maximize the concentration for better plating efficiency and higher quality deposits. A plating cell with an internal diameter as small as 1/4" and a

solution volume of one to two milliliters might be used when plating limited quantities of isotopes of Zinc and Cadmium. It is also important to keep the plating baths free from unnecessary additives in order to obtain metals of as high a purity as possible. Some plating baths resulting in high yields and good quality deposits are as follows:

Cadmium - Dissolve CdO in NaCN solution. Add NaOH. Ratio of constituents should be about 2:6:1 (Cd, NaCN, NaOH). Keep the volume of solution to 1-5 ml. depending on the quantity of isotope available. Plate onto polished stainless steel or platinum. Use a platinum anode. Current density should be 5-10 ma/cm^2.

Zinc - Dissolve ZnO in NaCN solution. Add NaOH. The ratio of constituents should be 1.5-2:3:3 (ZnO, NaCN, NaOH). Use a platinum anode and either a platinum or stainless steel cathode. Current density should be 8-10 ma/cm^2.

Dissolve ZnO in dilute H_2SO_4. Add just enough NaOH to precipitate basic zinc oxide. Then barely redissolve the precipitate with dilute H_2SO_4. The pH should be no less than 3.5. Dilute NaOH must be added dropwise as the deposition progresses to maintain the pH above 3.5. A platinum anode and polished stainless steel cathode are used. The current density should be 2-10 ma/cm^2.

Deposits may be either flexed free from the cathode in the case of the less adherent ones or they may be scraped free using a razor blade. If the resulting metal deposit is to be used for rolling, it should be as free of oxides as possible. Clean metal beads may be obtained by melting under ammonium chloride.[5] This is a rather risky procedure when small quantities of material are involved, as the procedure is apt to cause significant losses. Press the metal into a single pellet and place it at the bottom of a small pyrex, conical-bottomed centrifuge tube. Add just enough ammonium chloride to cover the pellet. Carefully heat the bottom of the tube over a bunsen burner until the Zinc or Cadmium metal just melts and swirls slightly in the molten ammonium chloride. Cool quickly and remove the bead of metal. Wash it thoroughly in deionized water and dry in acetone. If significant loss of material does occur, one can recover the material chemically from the ammonium chloride. This cleaning technique may also be used for lead metal.

TABLE 1. REDUCTION DATA

MATERIAL	REDUCTANT AND METHOD	TEMP.(°C)	BOAT TYPE	COMMENTS
$Ba(NO_3)_2$	Lanthanum Red.-Dist.	900-1200	Ta Pinhole or Tube	Convert nitrate to carbonate with $(NH_4)_2CO_3$. Reduce to oxide by heating in Ta boat.
CdO	H_2 in Tube Furnace	350-425	Vitreous C	Low yield due to volatility of Cd metal.
CdO	Carbon Red.-Dist.	600-800	Ta Pinhole	CO_2 evolution limits power input and indicates rate of reduction.
CdO	Electrolytic	-	-	See section on electrolytic red. for details.
$CaCO_3$	Lanthanum Red.-Dist.	900-1200	Ta Pinhole or Tube	Heat $CaCO_3$ in Ta boat to about 850°C to reduce to CaO.
Cr_2O_3	H_2 in Tube Furnace	1300-1500	Porcelain	Use liquid nitrogen water trap
Cr_2O_3	Carbon Red.-Dist.	1000-1500	Graphite or Ta Crucible	CO_2 evolution limits power input and indicates rate of reduction.
Cr_2O_3	Electrolytic	-	-	See Reference 6 for details.
CuO	H_2 in Tube Furnace	200-600	Vitreous C	-
Dy_2O_3	Zr or Th Red.-Dist.	1600-1800	Ta Crucible	See section on Red.-Dist. for details.
Er_2O_3	" " "	1700-1900	" "	" " "
Eu_2O_3	Lanthanum Red.-Dist.	900-1200	Ta Pinhole or Tube	" " "
Ga_2O_3	H_2 in Tube Furnace	About 500	Vitreous C or Quartz	-
Gd_2O_3	Zr or Th Red.-Dist.	1800-1950	Ta Crucible	See section on Red.-Dist. for details
GeO_2	H_2 in Tube Furnace	600-700	Vitreous C or Quartz	-
In_2O_3	" " "	About 500	Vitreous C or Quartz	-

TABLE 1. REDUCTION DATA

MATERIAL	REDUCTANT AND METHOD	TEMP.(°C)	BOAT TYPE	COMMENTS
Fe_2O_3	H_2 in Tube Furnace	600- 900	Quartz or Porcelain	-
Fe_2O_3	Carbon Red.-Dist.	1000-1500	Graphite or Ta Crucible	CO_2 evolution limits power input and indicated rate of reduction.
$Pb(NO_3)_2$	H_2 in Tube Furnace	400- 600	Vitreous C	Convert nitrate to oxide and reduce or use covered combustion boat when reducing nitrate to prevent losses.
Lu_2O_3	Zr or Th Red.-Dist.	1850-1950	Ta Crucible	See section on Red.-Dist. for details.
MgO	Lanthanum Red.-Dist.	800-1200	Ta Pinhole or Tube	" " "
Nd_2O_3	Zr or Th Red.-Dist.	1650-1900	Ta Crucible	" " "
Sm_2O_3	Lanthanum Red.-Dist.	900-1200	Ta Pinhole or Tube	" " "
SiO_2	Tantalum Red.-Dist.	1800-2000	C Crucible	" " "
$Sr(NO_3)_2$	Lanthanum Red.-Dist.	900-1200	Ta Pinhole or Tube	Convert nitrate to carbonate with $(NH_4)_2CO_3$, then reduce to oxide at 850°C in Ta boat.
Tl_2O_3	H_2 in Tube Furnace	300- 325	Vitreous C	Oxide is volatile. Do not exceed 325°C. Use wet H_2 - bubble gas through water.[7]
SnO_2	" "	600-1000	Vitreous C	-
WO_3	" "	450- 800	Quartz	Heat at 450°C to reduce to metal. Then heat to 800°C for 1 hr. to prevent metal from becoming pyrophoric.[7]
Yb_2O_3	Lanthanum Red.-Dist.	900-1200	Ta Pinhole or Tube	See section on Red.-Dist. for details.
ZnO	Carbon Red.-Dist.	600- 800	Ta Pinhole	See section on electrolytic red. for details.
ZnO	Electrolytic	-	-	See section on electrolytic red. for details.

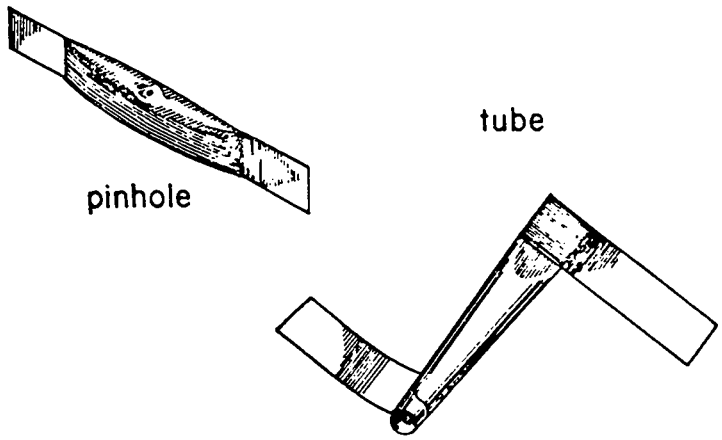

Fig. 1. Resistance-Heated Evaporation Sources.

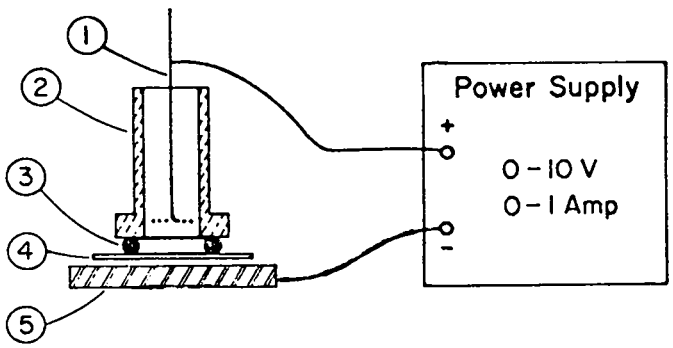

Fig. 2. Electroplating Cell Used for Small Quantities of Material.

1 - platinum spiral or wire; 2 - 1/4-1/2-in.-ID Lucite plating cell; 3 - O-ring seal; 4 - backing to be plated (cathode); 5 - metal base

REFERENCES

1. E. H. Kobisk, Isotop. Radiat. Technol. 7 (1), 1-3 (1969.

2. E. H. Kobisk and W. B. Grisham, Mat. Res. Bull. 4, 651-62 (1969).

3. L. Westgaard and S. Bjornholm, Nucl. Instr. and Meth. 42, 77-80 (1969).

4. F. H. Spedding and A. H. Daane, Metals 6, 504 (1957).

5. F. Karasek, Argonne National Laboratory, private communication.

6. P. R. Kuen, F. R. O'Donnell and E. H. Kobisk, Nucl. Instr. and Meth. 102 (1972).

7. E. McDaniels, Oak Ridge National Laboratory, private communication.

8. C. A. Hampel (ed.). Rare Metals Handbook, 2nd ed., Reinhold Publishing Corp., London, 1961.

9. R. E. Honig, RCA Rev. 23, 567 (1962).

10. Fredrick Lowenheim (ed.). Modern Electroplating, 2nd ed., Wiley Publ. Co., New York, 1963.

DEUTERATED TITANIUM TARGETS ON THIN BACKINGS

A. Méens

Centre de Recherches Nucléaires, Laboratoire PNPA
67037 Strasbourg-Cédex, France

Abstract

Stretched deuterated titanium targets on different thin metallic substrates have been prepared by evaporating titanium onto backings in a deuterium atmosphere.

I. - INTRODUCTION

Deuterated titanium targets on thin substrates have been prepared and stretched on special target holders for recoil distance lifetime and magnetic moment measurements. Deuterated polyethylene could not be used because of its rapid deterioration under bombardment. Neither was the method proposed by Gallant [1] applicable because of difficulties incurred in stretching the annealed and brittle thin targets.

The method used here consisted in the evaporation of titanium in a tenuous atmosphere of D_2. The titanium gets the deuterium to form in the best conditions $Ti \cdot D_{1.6}$ [Ref. 2] which is stable to 500°C.

II. - PROCEDURE

A diagram of the apparatus is shown in Fig. 1. One gram of titanium was placed in the crucible of the electron gun. The backings were fixed on a substrate heater, 15 cm above the crucible. The system was evacuated with an oil diffusion pump, to a vacuum of 5.10^{-6} Torr. When this vacuum was attained, liquid nitrogen was forced through a circuit located above the trap of the pump. This accessory was necessary

to condense backstreaming oil vapors that would occur at the D_2 working pressure. At the beginning of the titanium evaporation, the backings, heated to 200°C, were protected by a shield. When steady evaporation of titanium was reached, a needle valve was opened to introduce D_2 at a pressure of 5.10^{-3} Torr. After a few minutes the shield was removed and the material proceeded to deposit on the backings. The rate of evaporation and the film thickness were monitored with a quartz oscillator. The evaporation was performed over a period of 2-3 h so as to permit the titanium to absorb a maximum of D_2. It was found by trial and error that the parameters mentioned above were fairly critical for the successful preparation of the films.

Targets of 250 to 300 $\mu g/cm^2$ of deuterated titanium have been made on the following backings :

- 1 mg/cm^2 of gold evaporated on mirror surfaced plates [3],
- 250 $\mu g/cm^2$ and 450 $\mu g/cm^2$ of nickel supplied by the Chromium Corporation. The nickel surfaces were cleaned in an argon glow discharge. The copper substrates of the nickel foils were later removed with Richard's solution,
- 800 $\mu g/cm^2$ of copper evaporated on glass slides with barium chloride as release agent. For some of the latter the copper substrates were removed in order to obtain self-supporting targets of deuterated titanium. These targets, however, could not be stretched.

Target preparations are planned using other metals such as rare earths since their deuterated forms are purported to possess a temperature stability superior to that of deuterated titanium [4].

III. - TARGET THICKNESS MEASUREMENTS

To determine the quantity of deuterium occluded, use was made of the D (p, p_o) nuclear reaction for which the cross section at $\theta_{lab} = 165°$ has been measured by Sherr et al. [5]. Figure 2 shows typical spectra of

scattered protons for an incident energy of 2.5 MeV. Spectrum 2a was obtained by bombarding the deuterated side of the target and furnished the ratio of deuterium to titanium plus copper. Spectrum 2b is the spectrum obtained by bombarding the non-deuterated side of the target and permitted evaluation of the quantities of titanium and copper which then appeared in resolved peaks. Taking into account the Rutherford scattering cross section for titanium, we found that the quantity of occluded deuterium corresponded to approximately 2 $\mu g/cm^2$.

Although the proportion of deuterium turned out to be less than that sometimes found in thick targets, these thin targets were well adapted to a plunger system. With them, measurements have been made on magnetic moments of the first excited states in the mirror nuclei ^{21}Ne and ^{21}Na [Ref. 6].

Acknowledgements

The author would like to thank G. Costa for performing the elastic scattering experiments to determine the target compositions, and A. Pape for aid especially during the manuscript preparation.

References

1) J. L. Gallant
Nucl. Inst. and Meth. 102 (1972) 477.

2) P. Pascal
Nouveau Traité de Chimie Minérale
(Masson and Co., Paris, 1965) - Tome IX, p. 176.

3) J. L. Gallant
International Conference of the Nuclear Target Developement Society, Argonne National Laboratory, 1975.

4) Brochure of "Nukem GmbH", D-6450 Hanau 1, Postfach 110080, West Germany.

5) R. Sherr, J. M. Blair, H. R. Kratz, C. L. Bailey and R. F. Taschek, Phys. Rev. 72 (1974) 662.

6) F. A. Beck, T. Byrski, G. J. Costa, J. P. Vivien
International Meeting on Hyperfine Interactions, Louvain 1975.

Figure Captions

Fig. 1 Schematic diagram of the apparatus used to prepare deuterated titanium targets.

Fig. 2 Spectra of elastically scattered protons from a deuterated titanium target, on a copper backing.

a) Beam impinging on the deuterated side. Peaks of titanium and copper are unresolved.

b) Beam impinging on the non-deuterated side. Titanium and copper peaks resolved.

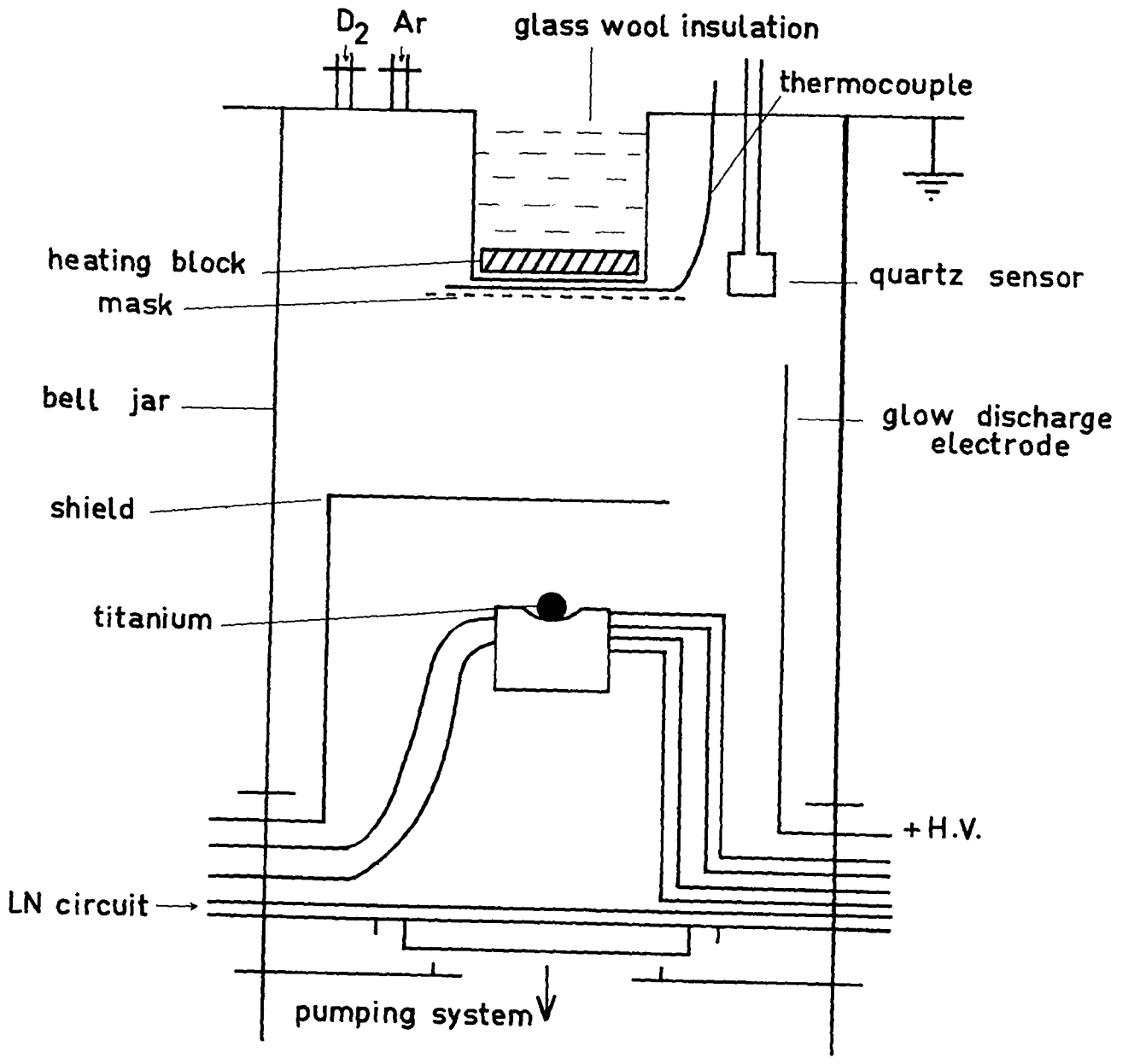
D_2 Ar
glass wool insulation
thermocouple
heating block
mask
quartz sensor
bell jar
glow discharge electrode
shield
titanium
+H.V.
LN circuit
pumping system

figure 1

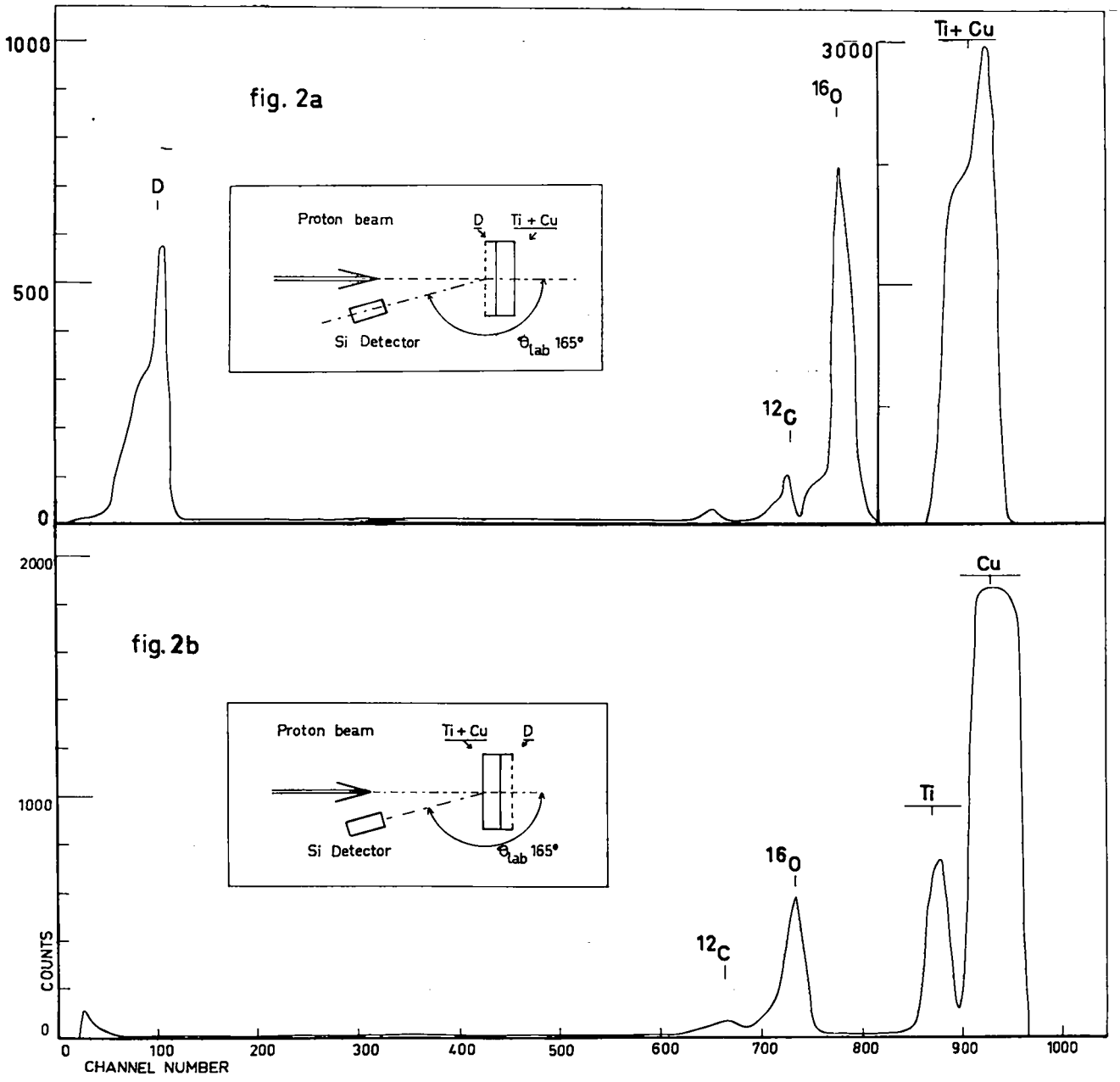
fig. 2a
1000
500
0
D
Proton beam
D
Ti + Cu
Si Detector
θlab 165°
12C
16O
3000
Ti+ Cu
fig. 2b
2000
1000
0
Proton beam
Ti+Cu
D
Si Detector
θlab 165°
12C
16O
Ti
Cu
COUNTS
0
100
200
300
400
500
600
700
800
900
1000
CHANNEL NUMBER

TARGETS OF SILICON OXIDE AND VANADIUM OXIDE ENRICHED IN ^{18}O ON VARIOUS BACKINGS

A. Méens

Centre de Recherches Nucléaires, Laboratoire PNPA
67037 Strasbourg-Cédex, France

Abstract

Enriched water has been electrolyzed and the resulting $^{18}O_2$ reacted with silane and vanadium to form silicon oxide and vanadium oxide. The product was then evaporated onto various backings.

I. - INTRODUCTION

Anodic oxidation is a well known technique for making oxygen targets, especially self-supporting ones or those on chemically non-reactive substrates [1-4]. This method is not applicable if the desired substrate, iron for example, is reactive. In such a case an oxide can be prepared and evaporated onto a backing. We have prepared tungsten oxide with enrichied ^{17}O as Muggleton [5-6] suggested, but for other experiments, a metal derived component of lower Z was required. For one series of experiments [7] silicon oxide was prepared. For another series [8], where silicon was too light, we prepared vanadium oxide. This report will describe the methods of preparation of silicon and vanadium oxides using ^{18}O enriched water.

II. - PREPARATION

A. Silicon Oxide

The silicon oxide preparation is based on two reactions :

1) Electrolysis of water to liberate $^{18}O_2$,

2) Reaction of O_2 with silane [9]

$$SiH_4 + 2O_2 \longrightarrow SiO_2 + 2H_2O.$$

A diagram of the apparatus is shown in Fig. 1. In essence, the apparatus has two functional components : Part 1, the vessel for the electrolysis and Part 2, the reaction chamber for the silicon oxide formation. Part 1 contains the enriched water and is cooled by a water-ice bath. This part could not be pumped and so was flushed for about an hour with argon before the electrolysis. Part 2 was evacuated with a rotary pump and then purged with argon. During the operation the $^{18}O_2$ was swept into Part 2 by the circuit 4→6 (see Fig. 1). The flow rate was monitored via the number of bubbles passing a mineral oil trap. A trial run with ordinary water was perfomed to determine the flow rate produced by the electrolysis. The silane flow rate was adjusted to exceed the stoichiometric proportions necessary to react with the flowing oxygen. The argon carrier gas flow rate was the same as that of the electrolysis products. The excess silane burned with a small flame at the oil trap upon contact with air. We have worked under the following conditions :

- A volume of 0.1 cm^3 of water to which a small quantity of metallic sodium was added to facilitate the electrolysis.
- An electrolyzing current of 200 mA. The electrolysis of the water was complete after approximately 150 min. The silane flow was then stopped and the argon flow continued until the excess SiH_4 was flushed out of the system.

A total of 70 mg of white powder presumed to be $Si^{18}O_2$ [Ref. 9] was obtained, representing a conversion efficiency for $^{18}O_2$ of 50 %.

B. - Vanadium oxide

This compound was prepared in two steps :

1) The production of $^{18}O_2$ by electrolysis of water,

2) The oxidation of vanadium metal by heating in $^{18}O_2$.

The electrolysis was performed in a glass system illustrated schematically in Fig. 2. During electrolysis, traps 2, 3, 4 and 5 were open and 1, 6 and 7 were closed. To prevent contamination by air, the system was outgassed by heating and flushed with argon. Prior the collection of the $^{18}O_2$ used for the reaction, a volume of $^{18}O_2$ approximately five times that of the components d + f (see Fig. 2) was electrolyzed away through the oil valve g . A syringe was used as a reservoir to collect the $^{18}O_2$ at constant pressure. The initially evacuated quartz reaction vessel, containing the vanadium metal, was pressurized to one atmosphere with $^{18}O_2$ from the syringe in several steps, closed off by valve 6 and disconnected from the system. The vessel was then brought to 800°C in a resistively heated stainless steel chamber.

With 75 cm^3 of $^{18}O_2$ at STP and 125 mg of vanadium powder, 240 mg of grayish-red product, presumed to be V_2O_5 [Ref. 10] was obtained. This represents a chemical yield of 96 %.

III. - TARGET PREPARATION

For silicon oxide targets, a pellet with a stoichiometric mixture of $Si^{18}O_2$ and Si corresponding to the reaction

$$SiO_2 + Si \longrightarrow 2\,SiO$$

was prepared. The pellet was evaporated with a Varian electron gun onto iron foils that had been precleaned in an ionic discharge in argon. With a 16 mg pellet, films of 100 $\mu g/cm^2$ of $Si^{18}O$ were obtained at a boat-foil distance of 7 cm.

The vanadium oxide was evaporated in the form in which it was formed using a procedure similar to that for $Si^{18}O$. Films of 150 $\mu g/cm^2$ were obtained from a 30 mg pellet.

The resulting targets were used in magnetic moment measurements [7-8] in which the ^{18}O enrichment was found to be about 90 % in all cases. The initial ^{18}O enrichment of the water was 98.5 %.

Acknowledgments

The author would like to thank M. Goldberg for his interest and aid, and A. Pape for his assistance with the manuscript preparation.

References

1) G. Amsel, Ann. Phys. (Paris) 9 (1964) 309.

2) A. Aladjen and D. G. Branden, Vac. Sci. and Tech. 6 (1969) 635.

3) D. Phillips, Nucl. Instr. and Meth. 116 (1974) 195.

4) M. A. Saettel, International Conference of the Nuclear Target Development Society, Argonne National Laboratory , 1975.

5) A. H. Muggleton and F. A. Hove, Nucl. Inst. and Meth. 12 (1961) 192.

6) A. H. Muggleton and C. T. Parsons, Nucl. Inst. and Meth. 27 (1964) 397.

7) M. Forterre, J. Gerber, M. B. Goldberg, J. P. Vivien and K. H. Speidel, Phys. Lett. 55B (1975) 56.

8) J. Gerber, M. B. Goldberg, K. H. Speidel, Phys. Lett. 60B (1976) 338.

9) P. Pascal, Nouveau Traité de Chimie Minérale (Masson and Co., Paris, 1965) Tome VIII, p. 331.

10) P. Pascal, ibid., Tome XII, p. 167.

Figure captions

Figure 1. - Schematic diagram of the apparatus used for preparing silicon dioxide.

Part 1 : Electrolysis vessel

Part 2 : Reaction chamber

The cross-hatched part is made of copper. The rest is in pyrex.

1-7) needle valves
a) argon bottle
b) silane bottle
c) manometer
d) to rotary pump
e) water-ice bath
f) mineral oil trap
g) flexible joint
h) fritted glass.

Figure 2. - Schematic diagram of the apparatus used for preparing vanadium oxide.

The system is made of pyrex except for the reaction vessel which is made of quartz.

1-7) valves
a, g) oil valves
b) electrolysis tube
c) water-ice bath
d, e) security traps
f) dessicant
h) removable syringe
i) reaction vessel
j) vanadium powder
k) glass-quartz connection.

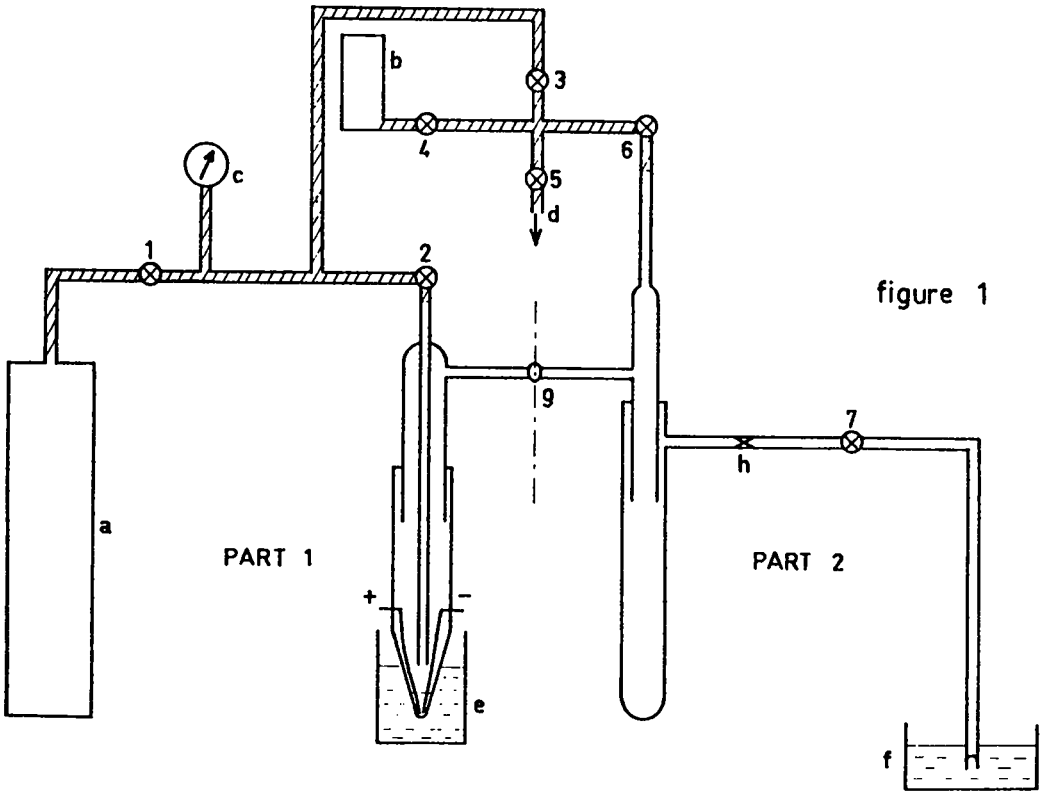

figure 1

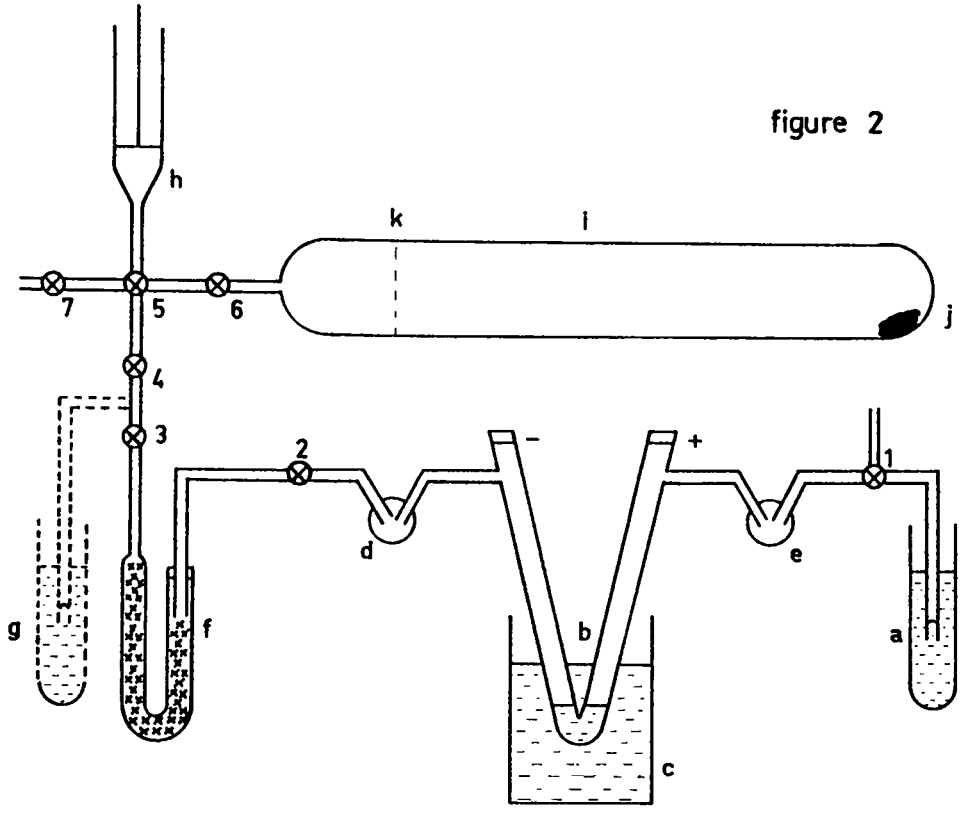

figure 2

PREPARATION OF ISOTOPICALLY ENRICHED MERCURY TARGETS

H. U. Friebel, Dagmar Frischke, R, Großmann, W. Hering,
H. J. Maier[+)] and H. Puchta

Sektion Physik der Universität München, Abteilung Kernphysik
8046 Garching bei München, W-Germany

ABSTRACT

Mercury targets have been prepared in form of HgS-films, consisting of isotopically enriched mercury and sulfur. The sulfide compound was chosen because of its comparatively high thermal stability. Starting up with HgO and elemental S, a three-step process was developed resulting in black HgS-films:

1. Metallothermic reduction of HgO to metallic Hg
2. Conversion of metallic Hg and powdered S to HgS using a ball mill
3. Vacuum sublimation of HgS on a LN_2-cooled metallic backing

The procedure was utilized for the routine production of HgS-targets in the thickness range between 5 $\mu g/cm^2$ and 3 mg/cm^2 on 80 $\mu g/cm^2$ up to 10 mg/cm^2 thick Al, Ni, Cu and Bi foils. The overall efficiency of the process is approximately 20 %.

[+)] presented the paper

1. INTRODUCTION

The primary difficulty in performing nuclear reactions on mercury is usually to obtain a suitable target. We have prepared isotopically enriched mercury targets in two different ways: first, by electrolytic deposition of mercury metal[1] and second by vacuum evaporation of HgS, a special selected mercury compound.

Electrolytic deposition of mercury metal requires a metallic backing which is able to form an amalgam as for example copper, gold or bismuth. A great number of bismuth-amalgam-targets has been produced and tested in our laboratory. It became apparent during the course of this development, that the homogeneity and the in-beam stability of these targets were unsatisfactory. On the other hand, vacuum condensed mercury sulfide films on metallic backings proved to be excellent targets for heavy ion transfer reactions.

This situation is illustrated by Fig. 1, which shows two spectra originating from ^{204}Hg. The spectrum on the left was taken with a ^{204}HgS target on a thin aluminum backing. It is a typical spectrum of a homogeneous target, with two gaussian shaped peaks indicating elastic scattering from the ground state and inelastic scattering from the first excited state, respectively. The spectrum on the right was taken with a metallic mercury target on a bismuth career foil. It features an elastic peak with a large low energy tail. This indicates strong energy straggling, caused by severe target inhomogeneities. In fact, the average thickness of this target is 1.5 mg/cm^2. The local effective thickness however fluctuates between 0 and

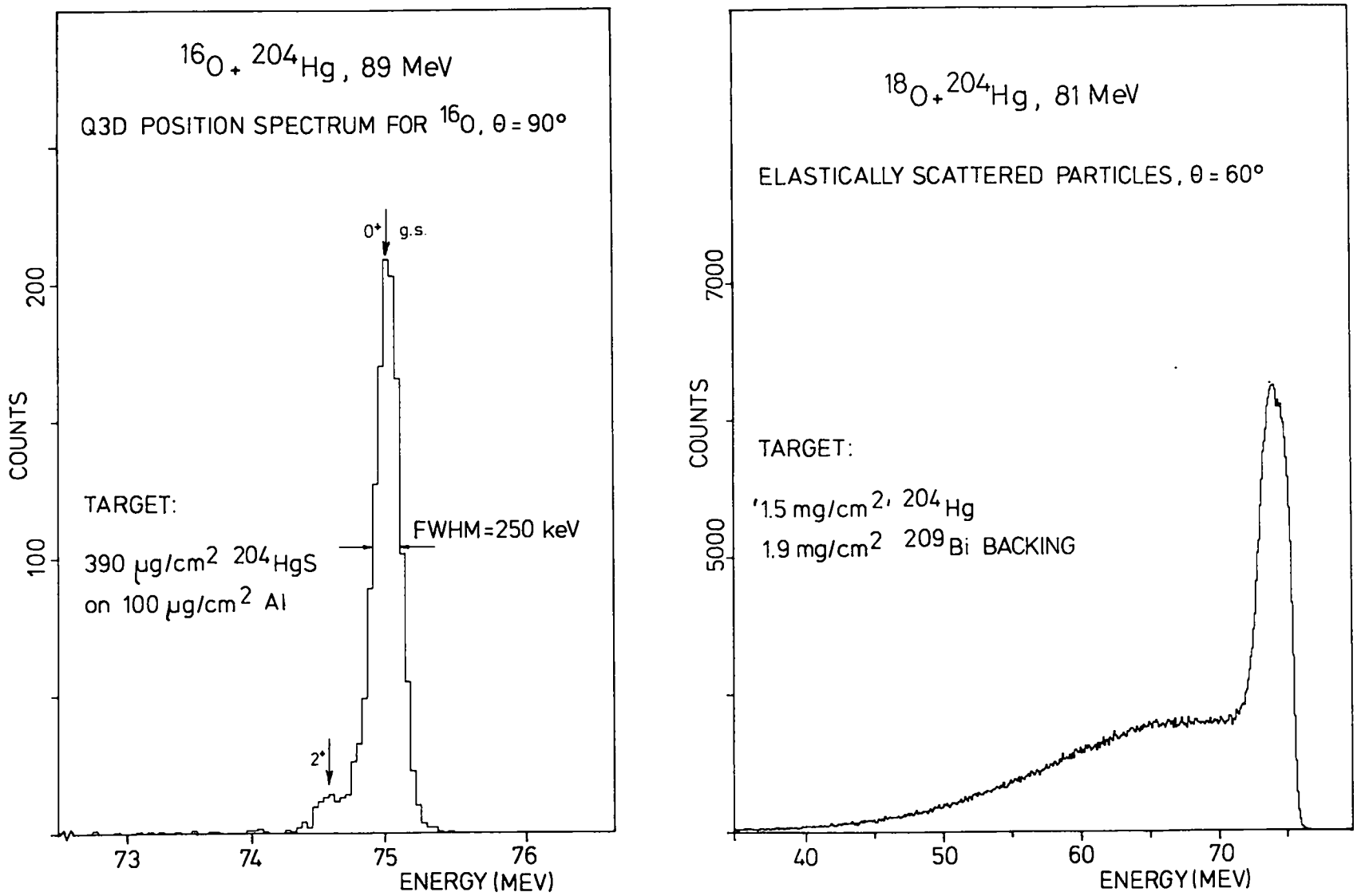

Fig. 1: Spectra from isotopically enriched ^{204}Hg-targets: ^{204}HgS on thin Al-backing (left) and ^{204}Hg in a Bi-matrix (right)

17 mg/cm^2 as may be estimated from the shape of the tail.

The maximum allowed beam current is about 20 particle nA for the HgS-target and about 1 particle nA for the amalgam target.

These facts demonstrate the superior quality of the sulfide target. In the following, a detailed description of the preparation of HgS-targets will be presented.

HgS was selected as the most suitable compound for mercury targets because of its chemical and thermal stability. In addition, at least one sulfur isotope could be tolerated as a target compound in all our experiments with mercury.

Two modifications of mercury sulfide are known: a red, hexagonal α-form, commonly known as cinnabar, and a black, cubic ß-form known as meta-cinnabar. Our preparation methods result in thin films of the black, meta cinnabar modification. This is of no importance for the nuclear experiments.

2. CONCISE PROCESS DESCRIPTION

The process of preparation depends upon the question whether both mercury and sulfur must be isotopically enriched or not. The scheme in Fig. 2 gives a summary of all possible modifications of the procedure. The most general case is the requirement of isotopic enrichment for both elements (column (1) in Fig.2). Since isotopically enriched mercury is supplied in form of HgO by the ORNL and enriched sulfur in the elemental form, the first problem is to prepare HgS starting up with these materials. This is done by a metallothermic

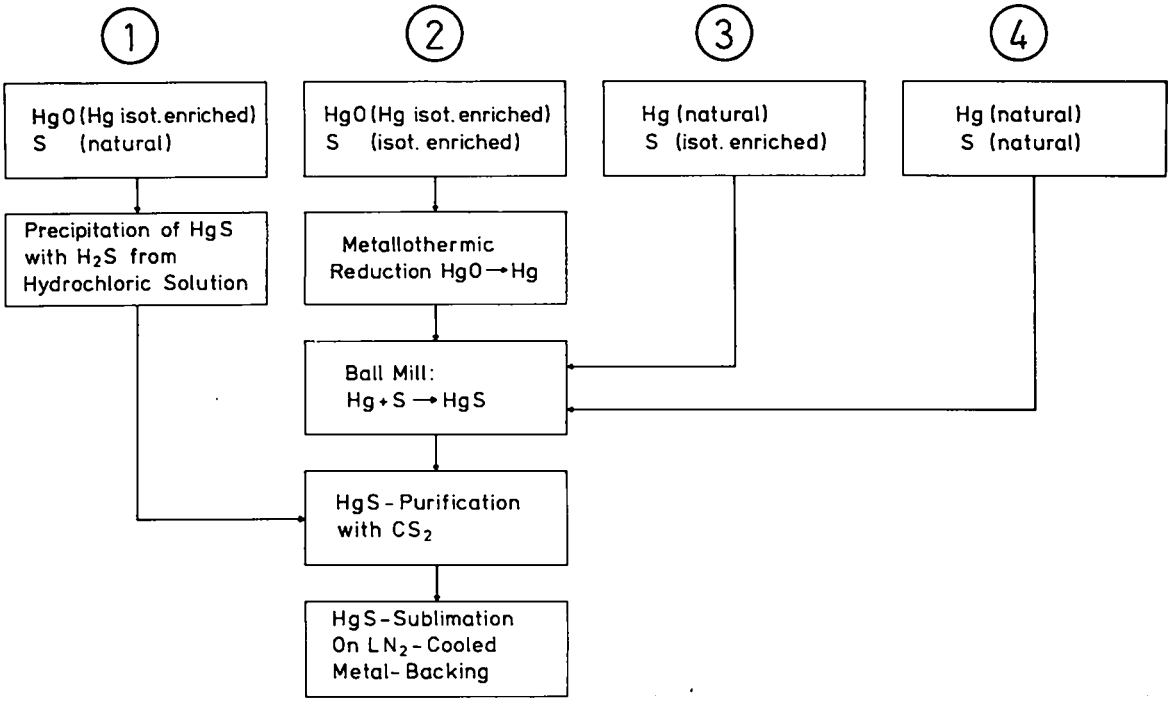

Fig. 2: Schematic view of procedures involved in HgS target production

reduction of mercury oxide to mercury metal followed by a treatment of the metal together with powdered sulfur in a ball mill whereby mercury sulfide is formed. An excess of free sulfur is removed by a purification process with CS_2. The second problem is the target preparation in its narrow sense. It is accomplished by vacuum condensation of HgS on a cooled metal backing.

If the natural isotopic mixture of sulfur can be tolerated but isotopically enriched mercury is required (column (2) in Fig. 2), the preparation of HgS is done in the usual standard way by dissolving HgO in hydrochloric acid and precipitating HgS from that solution with H_2S.

If the natural isotopic mixture of mercury is admitted but isotopically enriched sulfur is required - for instance for the preparation of a sulfur target - it is convenient to start up with metallic mercury and powdered sulfur (column (3) in Fig. 2). Likewise the trivial case - natural isotopic mixture of both mercury and sulfur - may be treated if mercury sulfide is not available from stock (column (4) in Fig. 2).

3. DETAILS OF THE PROCEDURE

3.1. Preparation of Mercury Metal

The conversion of mercury oxide to mercury metal is done by a special reduction distillation technique, utilizing the set-up outlined in Fig. 3. The substantial part of this set-up is a quartz vessel composed of a sphere and a U-shaped tube. The spherical part

$$HgO + R \longrightarrow Hg\uparrow + RO$$

Collection Efficiency: 70 %

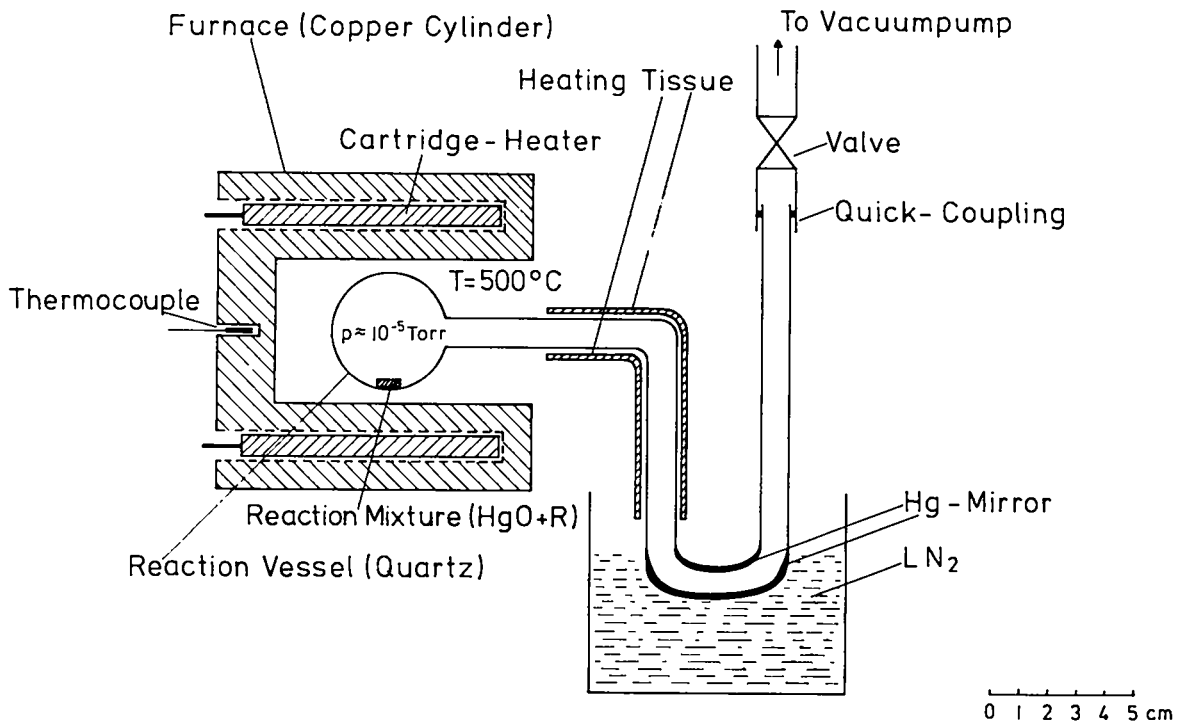

Fig. 3: Set-up for reduction of HgO

can be heated by means of a simple oven, which consists of a cylindrical copper block with four installed 250 W cartridge heaters. A pellet made of a mixture of HgO and a suitable reductant is placed in the spherical part of the vessel. The reduction is initiated by heating the pellet up to 500 ^{o}C in a vacuum of approximately 10^{-5} Torr. The mercury vapour produced at this temperature is forced to condense in the U-shaped region. This is accomplished by slightly heating the upper section of the tube with a heating tissue and cooling the "U" by liquid nutrogen. The result of this procedure is a metallic mirror which converts to a mercury droplet when the tube is allowed to warm up. The efficiency of this reduction is about 70 %.

The proper selection of the reductant is crucial for the success of the reaction.We have found tungsten powder to meet all requirements of the present problem.First, its vapour pressure and the vapour pressure of its oxide are low compared to the vapour pressure of mercury, which is a necessary condition for every reduction-distillation process. Second, tungsten enables a temperature-controlled completion of the reaction. This may be understood by a simple thermodynamic consideration. The diagram in Fig.4 shows the oxygen-affinities of some important elements by means of the dissociation pressures of their oxides. The dissociation pressure is the partial pressure of oxygen above the oxide in a thermodynamical equilibrium. The lower the dissociation pressure of an oxide at a distinct temperature, the higher the affinity for oxygen of the element in question. The strong reductants are located in the lower right region of this diagram, and vice versa the elements with

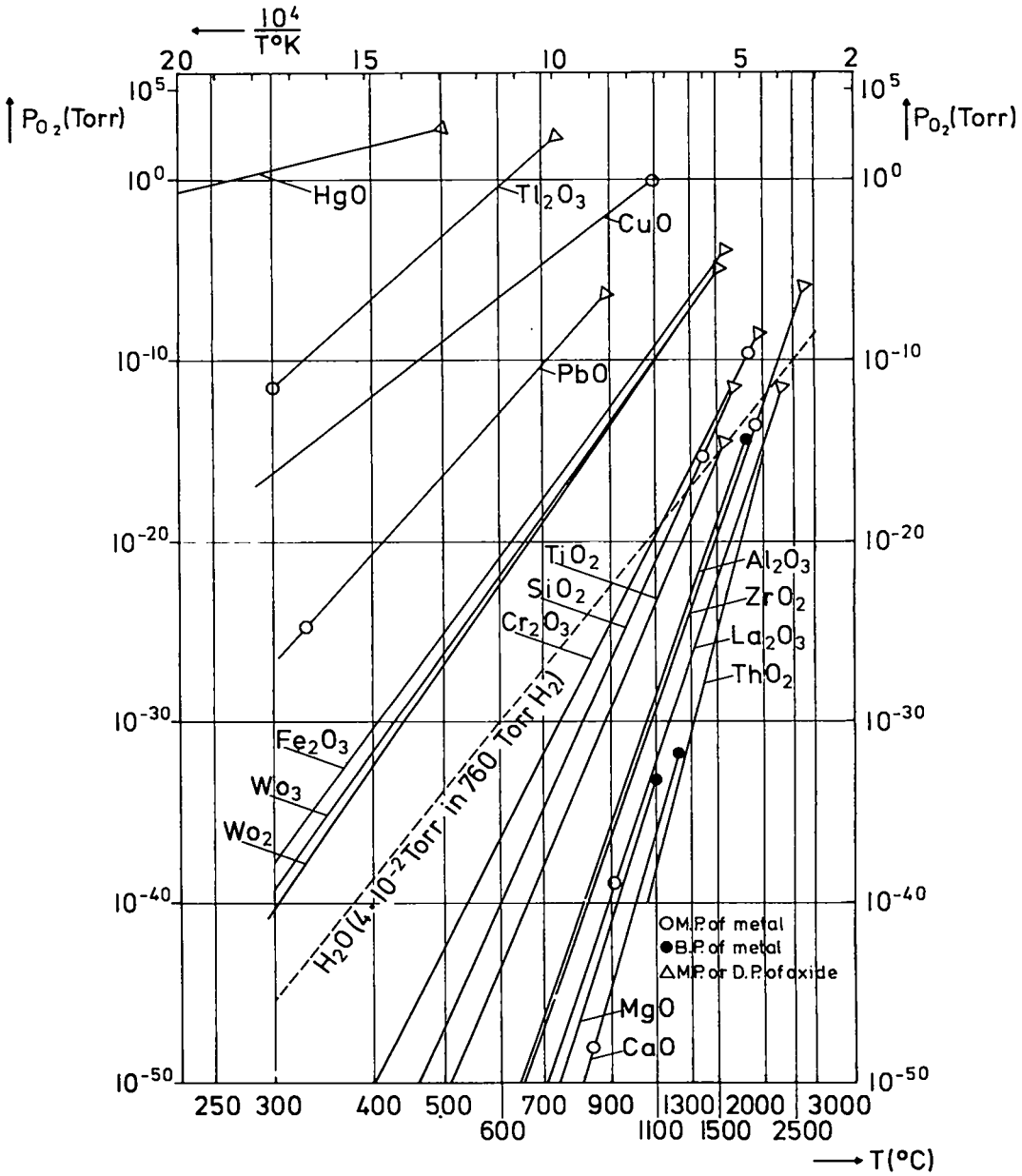

Fig. 4: Partial pressure of O_2(P_{O_2}) of some metal oxides as function of temperature

easy reducible oxides in the upper left region. From a thermodynamical point of view, a certain oxide may be reduced by any element whose oxide has a lower dissociation pressure. Hence mercury oxide is expected to be easily converted to metal by classical reductants as for instance zirconium and thorium. However, because of the extremely high oxygen-affinity of these two elements, the reaction with mercury oxide runs into an explosion, which causes the powdered mixture of metal and oxide to spread around the whole reaction vessel and thus leads to a contamination of the condensing mercury. If we now consider tungsten, its affinity for oxygen is considerable weaker. This allows a control of the reaction speed by variation of the furnace temperature, using tungsten as the reductant. At 500 ^{o}C, the reaction comes to a completion in about 10 minutes.

3.2. Preparation of mercury sulfide

HgS is prepared by the following procedure: mercury metal is carefully mixed with an excess of about 10 % of the stoichiometric amount of sulfur. The mixture is then treated in a ball mill for several hours. Thereby the two elements react and black mercury sulfide is formed according to the formula

$$Hg + S \quad HgS \ .$$

The ball mill (Fig. 5) is of the planetary type with milling cylinders spinning around their own axis and simultaneously rotating on a horizontal disk. A photo of a milling cylinder with the grinding balls and the reaction mixture inside is shown in Fig. 6. The construction material of cylinder and balls is agate. The centri-

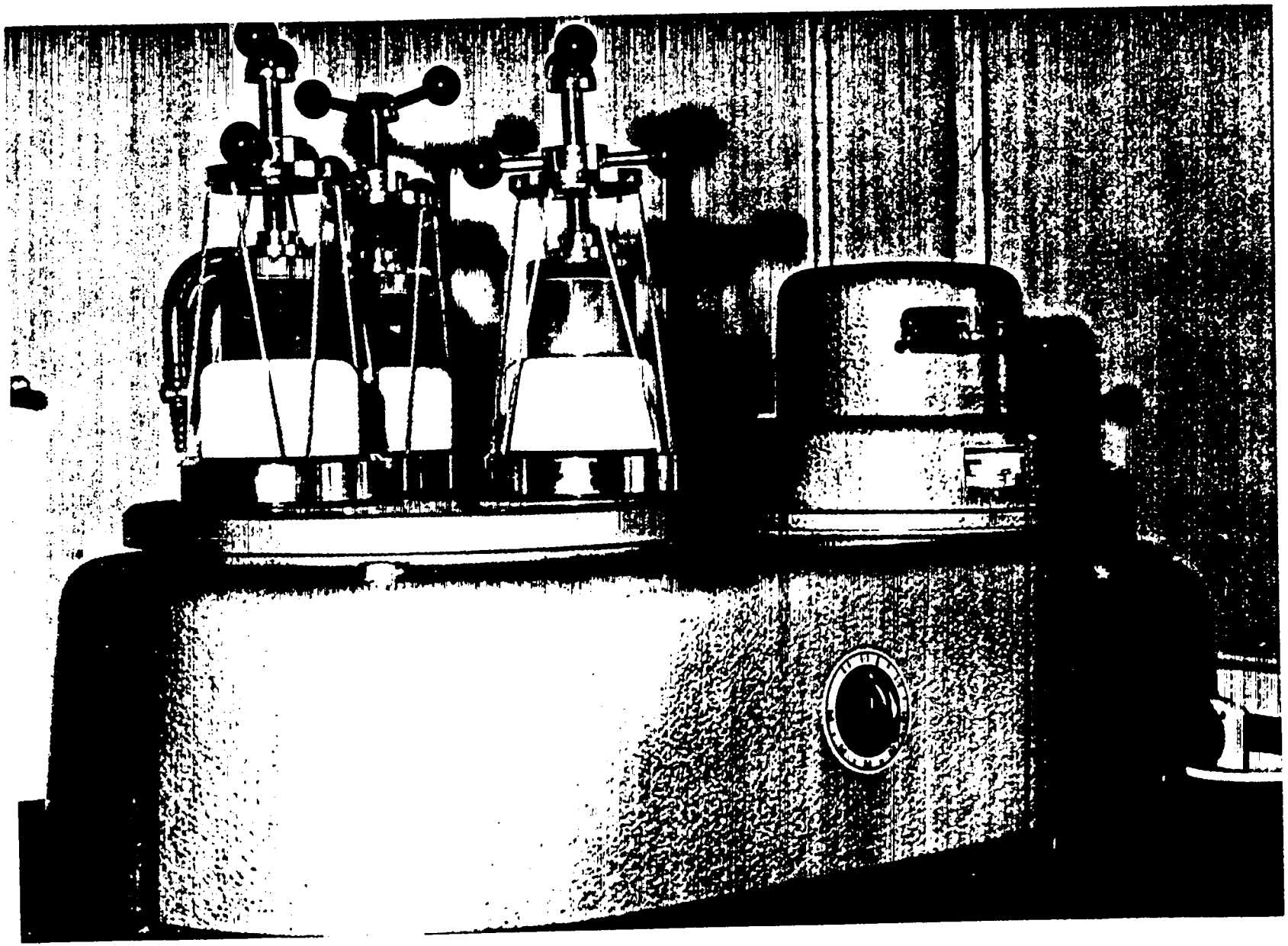

Fig. 5 : View of ball mill

Fig. 6: View of milling cylinder

fugal force reacting on the balls reaches up to 12 times the gravity. This guarantees a thorough contact of the two elements and a nearly complete conversion to HgS .

HgS prepared in this way usually contains a fraction of free sulfur. This is removed by treating the freshly prepared compound with CS_2 in an extraction apparatus of the Thielepape type.

The efficiency of this method of preparing HgS is about 90 %. The overall-efficiency up to this point - referred to the amount of mercury expended - is about 65 %.

3.3. Vacuum condensation of HgS

The growth of the HgS thin film is accomplished by vacuum sublimation of mercury sulfide on a cooled metal backing. A collimating tantalum boat is used to optimize the collection efficiency and average values of about 150 $\mu g/cm^2$ per mg of sublimed material are achieved. It is vital for the success of the procedure, that the temperature of both the evaporation source and the substrate are well controlled during operation. The temperature of the boat must be kept strictly below 300°C to prevent a dissociation of the weekly bound mercury sulfide molecules. Substrate cooling on the other hand is necessary to enforce a condensation of the volatile material. The optimum substrate temperature turned out to be -130 °C, which is a compromise between a satisfactory condensation efficiency and a tolerable amount of internal stress of the HgS film. At temperatures considerably lower than -130 °C large internal stresses are ob-

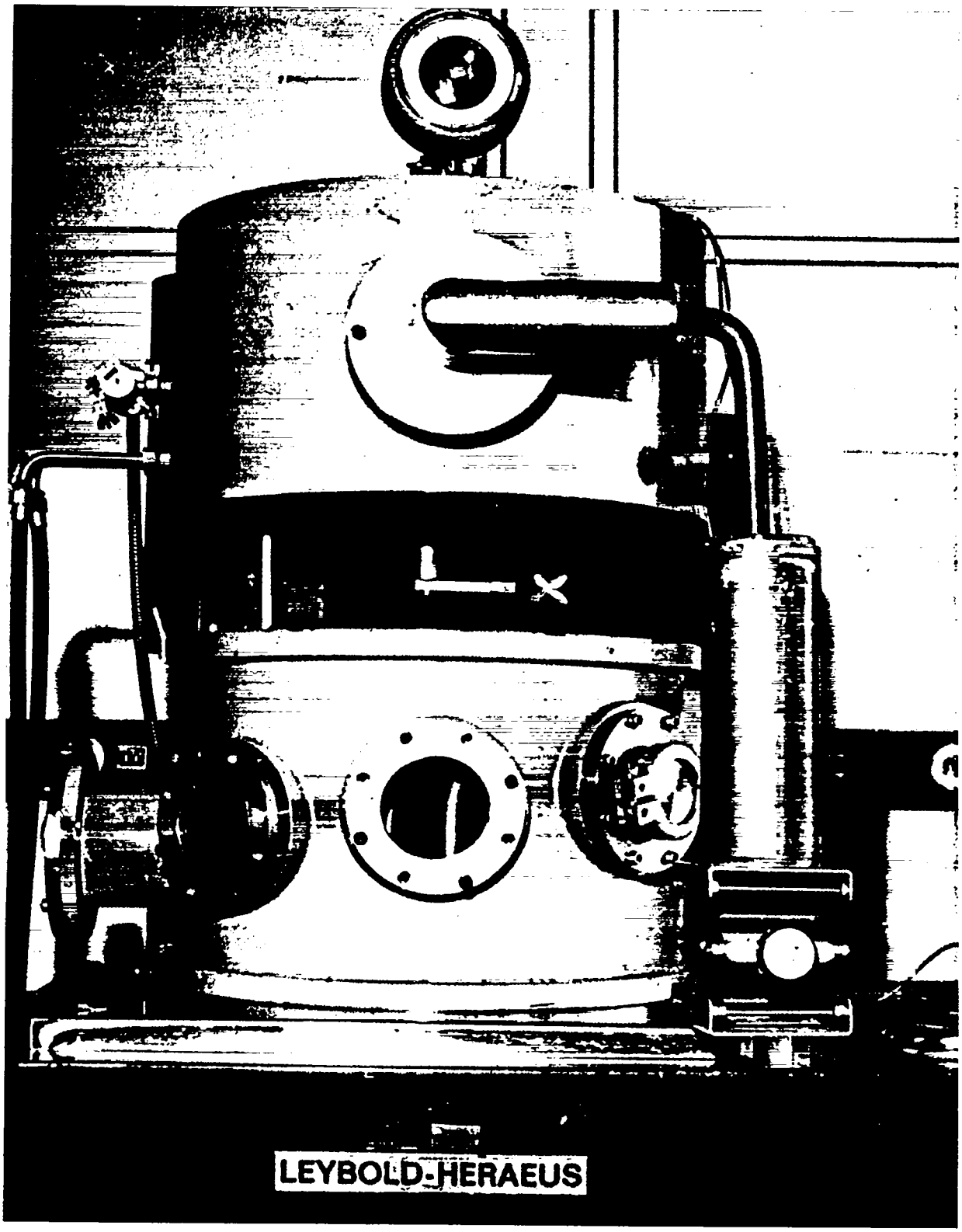

Fig. 7: Substrate holder (x) with cooling device

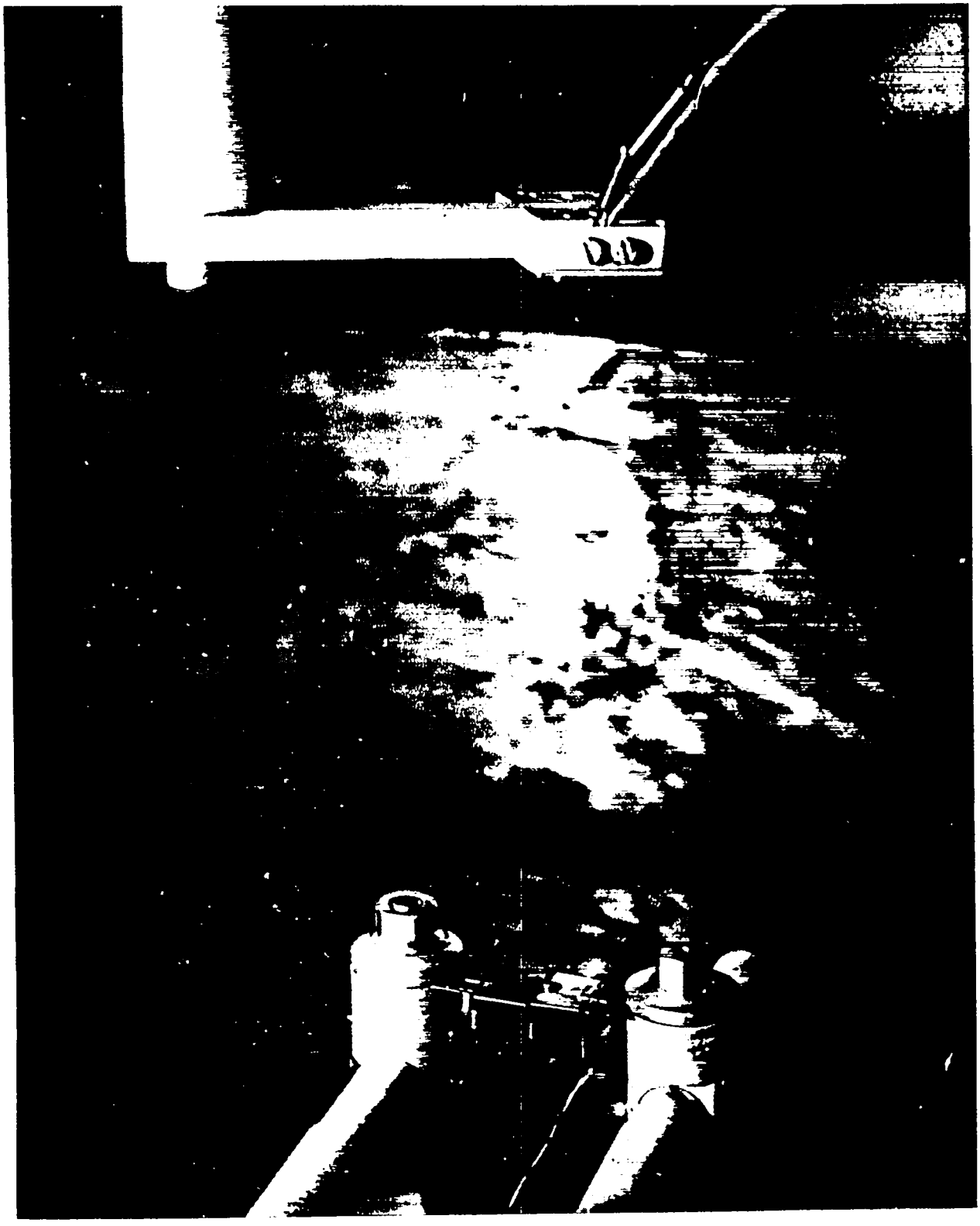

Fig. 8: Detailed view of evaporation source and substrate holder

served. They cause the thin film to split off the backing when this is warmed up. For reasons of thermal conductivity a metallic backing must be used. In Fig. 7 the practical realization of the evaporation arrangement is shown. The substrate holder (x) is mounted on one end of a copper rod, which is fed out of the vacuum chamber through a 0.5 mm thick sheet of stainless steel and cooled by liquid nitrogen on its other end outside the chamber. Thermal losses to the walls of the vacuum chamber are minimized by this construction. The desired substrate temperature is adapted about one hour after beginning of cooling and remains sufficiently constant during the 5 minute sublimation process. Fig. 8 shows the substrate holder and the evaporation source in more detail. When the vacuum chamber is closed, the substrate is automatically centered above the source in the correct distance of 2 cm.

4. FINAL DATA

Up to the present day, HgS-targets in the thickness range between 5 $\mu g/cm^2$ and 3 mg/cm^2 have been prepared. Various backings were used, i.e. Al 80 $\mu g/cm^2$, Ni 300 $\mu g/cm^2$, Cu 300 $\mu g/cm^2$ and Bi 500 $\mu g/cm^2$.

30 mg of mercury oxide and 3.5 mg of sulfur are necessary to produce 1 target of 3 mg/cm^2 thickness with a diameter of 15 mm. This corresponds to an overall efficiency of 20 %, referring to the expended amount of mercury.

References:

1) H.J. Maier et al.: Jahresbericht 1972 des Beschleunigerlaboratoriums der Universität und der Technischen Universität München

A METHOD FOR STRETCHING ULTRATHIN POLYPROPYLENE FILMS

by

D. M. Barrus and R. L. Blake

University of California, Los Alamos Scientific Laboratory

ABSTRACT

The method of stretching non-oriented polypropylene film over a heated, Teflon-covered, aluminum disk is used to prepare films of thickness ranging from 1500 Å to 15000 Å. Thickness variations of less than 20% over areas up to 100 cm^2 are relatively easy to achieve. Since polypropylene contains only carbon and hydrogen, it is an effective window for proportional counters in detecting ultrasoft X-rays. Such films have also been used as windows for gas absorption cells and energy-loss nuclear detectors, and as isolation windows for clean, high vacuum systems.

Published in Rev. Sci. Instr. 48 (1977) 116.

PREPARATION OF ULTRATHIN POLYETHYLENE FOILS BY FILM CASTING*

by

Betty Cranfill

University of California
Los Alamos Scientific Laboratory
Los Alamos, New Mexico 87545

ABSTRACT

A procedure for making polyethylene foils with a thickness of 0.02 μm to 2 μm by the film casting method is described. The thickness of the foils is determined by the concentration and temperature of the solution, and the quality is controlled by the uniformity of temperature and rate of solution drainage.

---

* Work performed under the auspices of the U. S. Energy Research and Development Administration.

Thin plastic films are often used in the fabrication of laser fusion targets. They are used for support films, as in the ball and disk type of target shown in Fig. 1. Here a deuterium and tritium filled glass microballoon is sandwiched between two 500 angstrom thick plastic films. A thicker plastic disk surrounds the microballoon, producing the interference rings shown.

Thin plastic films are also used for single foil and double foil flat targets which require a material with a high hydrogen content, and for ion-spectroscopy experiments which require a deuterated film. Polyethylene is an ideal material for these types of targets.

By using the film casting method, it is possible to produce polyethylene films over a wide range of thicknesses. Useful films down to 200 angstroms thick have been made and still thinner ones can be made, although they are very fragile and may not be useful.

The method described uses glass microscope slides as the casting surface. This limits the size of the film, but there is no reason to believe the apparatus couldn't be modified to produce larger films. The current method produces uniform areas of about 5 cm^2 with no more than 10% variation in thickness. The thickness is determined by the solution concentration and temperature.

The film casting apparatus is shown in Fig. 2. The solution is contained in the 500 ml. flask. It is forced up through the center tube into the vessel at the top by means of air pressure produced by the bulb attached to the flask. A glass microscope slide is placed in the solution and the vessel is then drained by releasing the pressure by means of a stopcock.

To provide uniform heat, a spherical heating mantle encloses the flask and a two foot heating tape is wrapped around the neck of the flask and the upper vessel. The temperature of both is regulated by a variable power supply. The upper heating reduces heat loss and it maintains a uniform temperature during drainage and evaporation which is important in producing uniform films. The flask and heating mantle are placed on a magnetic stirrer to mix the solution and to help maintain an even temperature distribution.

It is also necessary to heat the microscope slide to approximately the same temperature as the solution. This is easily done on a hot plate. Cold slides will result in cloudy, uneven films, and slides that are too hot will produce very thick films.

When the solution has drained from the upper vessel, the slide is removed and allowed to dry. It dries almost instantly and the film may be removed by flotation on water as soon as it has cooled to room temperature. It comes off quite easily and there is no need to coat the slide with a releasing agent.

When it is floating on water, bright interference colors may be seen and uniform areas selected. Figure 3 shows some films floating on water. The gold one is made from a 2% solution and is about 1000 angstroms thick. It appears to be quite uniform over almost its entire area. There is one which is almost invisible and has a gray appearance. It is about 600 angstroms thick and was made from a 1% solution. There are also two films made from a 3% solution which are about 2000 angstroms thick. When lighted from one angle they appear the same color. The lighting for the photography unfortunately made them appear different colors. These show more color variation and do not appear to be quite as uniform as the thinner ones, but they still have usable areas of uniformity.

Thicker films tend to be less uniform than the thinner ones, and the films tend to be thicker at the top of the slide and thinner towards the bottom. Also the edges tend to be thicker. There may be some variation from slide to slide if there is any temperature change, but they are generally quite consistent and the interference colors may be used to select areas of the desired thickness.

The graph in Fig. 4 shows the film thickness plotted as a function of solution concentration at a particular temperature. Curves A and B show the results of polyethylene dissolved in toluene at 102° C and 88° C, respectively. Higher temperatures than the boiling point of toluene, which is about 110° C, are required to dissolve concentrations higher than 6%, so xylene is used, which has a boiling point of about 140° C. Curves C and D show the results of polyethylene in xylene at 130° C and 100° C.

Films as thick as 2 micrometers have been made reproducibly by this method using an 8% solution in xylene at 130° C. The thinness of the films that can be made is limited only by their strength.

At first it appeared that more polyethylene went into solution at the higher temperatures to account for the increase in thickness, but upon further examination this does not appear to be the case. The solution appeared clear with no undissolved particles and no particles on the films. Rather, it is the rate of evaporation of the solvent which influences the thickness. Curves A and C are almost continuous. Both were done close to the boiling points of the solvents used. Curve D was done at a temperature considerably below the boiling point of xylene, but still higher than the temperature of curve B, yet thinner films were produced at an equal concentration.

This seems reasonable when the process involved in the deposition of the film is considered. Warm temperatures and vapors in the vessel and a slow rate of evaporation maintain a fluid state so the solution is able to drain

down the slide, leaving a thinner film. If the film dries too quickly, drainage down the slide is inhibited and a thicker film is deposited.

This also becomes apparent if a very hot slide is placed in the solution. As the solution is drained from the vessel, the heat from the slide evaporates the solvent very quickly and a very thick film is deposited. Films up to several micrometers thick have been made in this way from 5 to 6% solutions, but the reproducibility is very poor.

The rate of drainage is also an important factor, but the film caster provides a fairly uniform rate, although the higher concentrations drain slightly slower due to increased viscosity.

The type of polyethylene used also influences the results. Microthene FN 510 was used in this case. It is a low density, low molecular weight type. A higher density type was also tried. A 3% solution required temperatures over 100° C to dissolve and did not produce similar results.

The film thicknesses were measured by interferometry. Those under .5 micrometers were measured by the Senarmont method and those over .5 micrometers were measured by the Jamin-Lebedev method. These techniques measure the difference in optical path lengths through the sample and the background.

Thus, by using the film casting method it is possible to produce thin to ultra-thin polyethylene films of the desired thickness by simply choosing the proper concentration and temperature. The films have a usable area of uniformity and many may be produced easily in a short period of time.

FIGURE CAPTIONS

Figure 1. Ball and disk target.

Figure 2. Film casting apparatus.

Figure 3. Polyethylene films on water.

Figure 4. Polyethylene film thickness vs solution concentration.

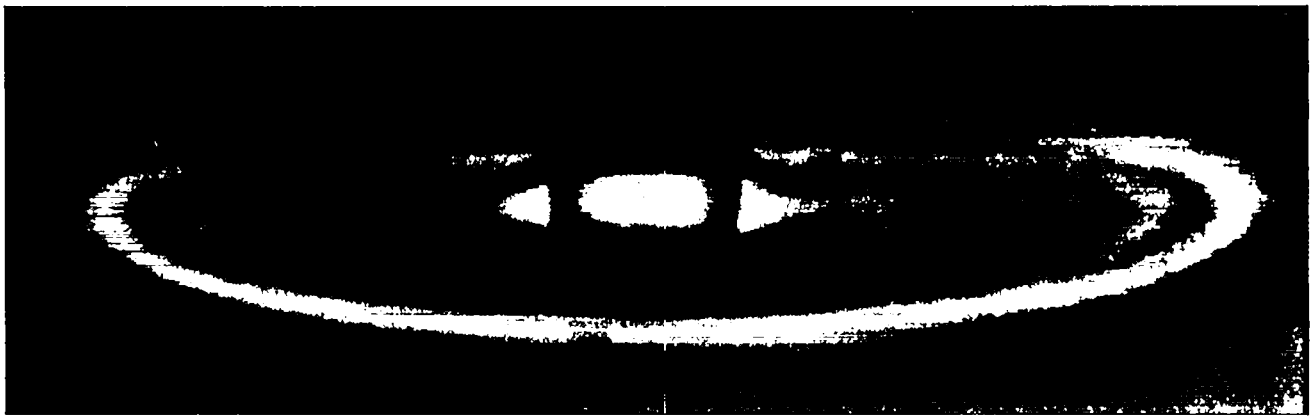

Fig. 1

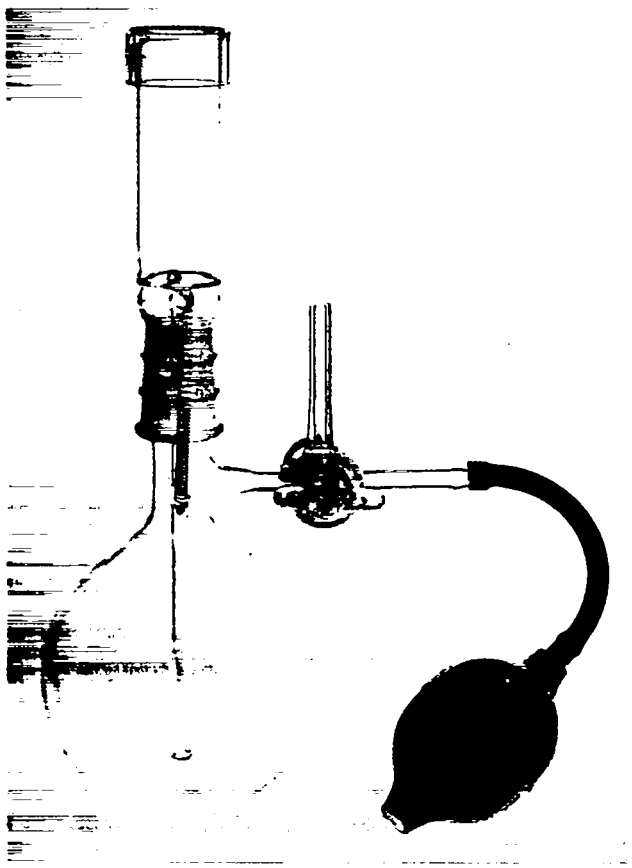

Fig. 2

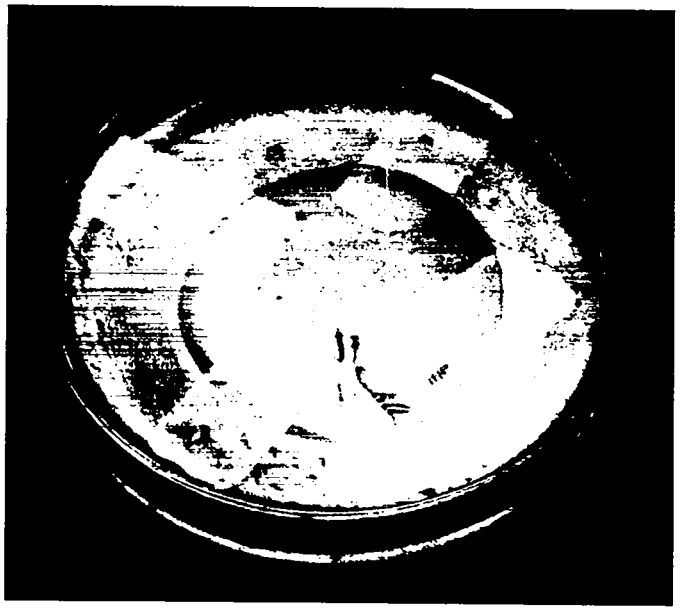

Fig. 3

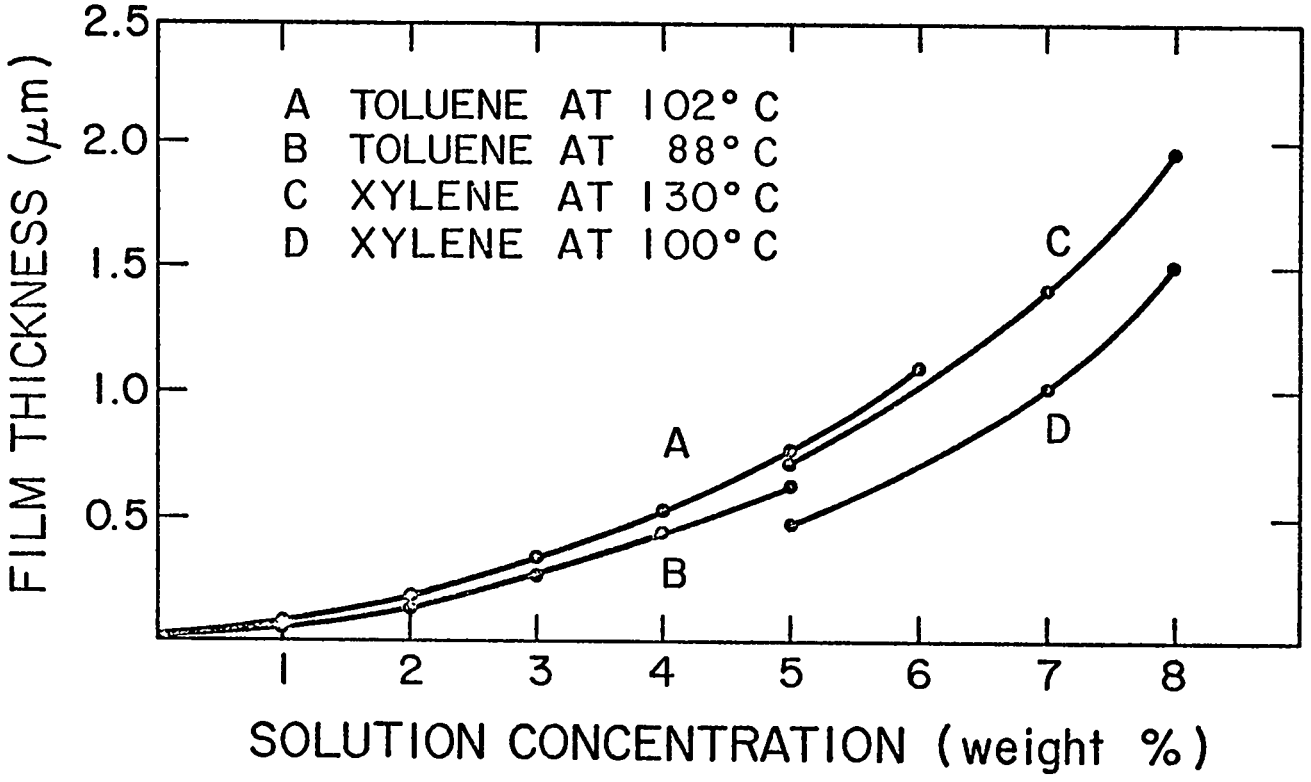
A TOLUENE AT 102° C
B TOLUENE AT 88° C
C XYLENE AT 130° C
D XYLENE AT 100° C
FILM THICKNESS (μm)
2.5
2.0
1.5
1.0
0.5
1
2
3
4
5
6
7
8
SOLUTION CONCENTRATION (weight %)
A
B
C
D

Fig. 4

PLASTIC-BONDED TARGETS OF CARBON-13 AND SILICON

R. K. Rohwer and M. J. Urizar
University of California, Los Alamos Scientific Laboratory,
Los Alamos, New Mexico 87545

INTRODUCTION AND BACKGROUND

This is an account of a successful effort to mold thin, large area (18 x 10.5 cm) targets of elemental carbon and silicon for pion scattering experiments. The carbon was enriched to 90% in the ^{13}C isotope. The silicon was natural. Both of these materials, as supplied, were in the form of very fine powders. This made the problem difficult. There were also restrictions on the binder. A minimum of binder should be present and ideally it should contain only carbon and hydrogen. Heavier elements such as oxygen and fluorine present in many plastics would have interfered with the scattering experiment.

Group WX-2 at LASL is a weapons group and part of our assignment is the fabrication of plastic-bonded explosives. These are very highly filled (binder lean) systems of fine particle size materials. We have developed techniques for applying plastic coatings to these materials to form a molding powder and then pressing this molding powder into finished parts. Thus the target program was not so foreign to our background as one might think.

We were fortunate to have a binder on hand that met the chemical requirements and was a much better binder than polyethylene, an obvious

candidate. This material is Kraton 1101. It may not have been the best possible binder but it had two outstanding virtues for this program. It was available and we knew how it behaved.

Kraton 1101 is one of a group of thermoplastic rubbers made by Shell Chemical Co. It is a block copolymer of styrene and butadiene in a 30/70 ratio. It is soluble in toluene, chlorinated solvents and some other solvents, and insoluble in water, acetone and alcohols. It has a distinct softening point at about 100°C and becomes progressively more fluid at higher temperatures.

DETAILS AND PREPARATION

Carbon Molding Powder

The ^{13}C-enriched material was furnished to us as an extremely fine powder. The small particle size made it necessary for us to modify our standard slurry technique. In this preparation we first prepared a lacquer of Kraton in toluene. The carbon powder was then added to the lacquer and the resultant paste stirred and aged for about one hour. The paste was then poured slowly into a container of well agitated water at 60°C. Stirring was continued and the mixture was heated to 76°C where the toluene started to distill. All the toluene was removed by about 85°C. At this temperature the batch was cooled and the solids recovered by filtration. The resulting molding powder was dried overnight in a forced draft oven at 65°C.

Quantities used for a 67-g batch of molding powder at a 92/8 - carbon/-Kraton weight ratio were:

Kraton 1101	5.36 g made into lacquer in 100 cm^3 of toluene
Carbon	61.64 g

The paste of the two materials mentioned above was poured into 400 cm^3 of water in an 800-cm^3 beaker.

Silicon Molding Powder

The silicon powder was not as fine a particle size as the carbon but it had a different surface chemistry which would not allow us to use the hot-water slurry process. To prepare this molding powder we took advantage of the fact that Kraton is not soluble in acetone. A Kraton lacquer was prepared and the silicon powder was stirred into it just as in the carbon preparation. This paste was then poured into a large quantity of well-stirred acetone. The acetone extracted the toluene from the paste particles to give firm molding powder agglomerates. This powder was allowed to settle, most the acetone and some fines were decanted, and the solids were then recovered by filtration. The filter cake was washed twice with acetone to remove more toluene and then once with water to remove the acetone. The finished powder was dried overnight at 65°C in a forced draft oven.

Quantities used for a 65-g batch of 92/8 - silicon/Kraton were:

Kraton 1101	5.217 g in 60 cm^3 of toluene.
Silicon	60.0 g

The paste of these materials was poured into 600 cm^3 of acetone in a 1-liter beaker.

Pressing

Each of the above molding powders was ground to pass through a 20 mesh seive. The proper amount of the screened powder was poured into

the die and very carefully leveled. This step is important because at these high loadings the material will not flow when it is pressed, it merely consolidates in place. Thus uneven powder distribution will yield a final part with large density variations. After the powder was leveled, the top punch was lowered onto the powder and the entire die was placed in a 140°C oven to heat. When the die temperature reached 130°C, it was transfered to the press. Pressure was applied in several steps with the pressure being reduced to zero after each step. When the final pressure of 5400 psi was reached, it was maintained until the die had cooled to about 50°C. At this temperature the Kraton is no longer mobile and the die was disassembled and the part removed.

The die was a heavy, bolted picture frame resting on a bottom punch. The top punch was a rectangular plug. All the interior surfaces were polished to a 16 micro-inch finish and none of the parts stuck despite the fact that no mold release was used.

CONCLUSION

This is not presented as an optimum preparation, rather it is a description of a process that yielded usable parts for a program that had to be completed in a very short time.

THICK TARGETS FOR IN-BEAM HYPERFINE STUCTURE STUDY*

T. Minamisono† and D. Ramsay
Department of Physics, Stanford University
Stanford, California 94305

Production of nuclear polarization is the first step in the study of hyperfine structure (H.F.S.) detecting nuclear radiations. This is possible by employing nuclear reactions initiated with polarized[1] and unpolarized beams[2]. Once the polarization is produced, our concern is its preservation during the nuclear lifetime of the specific state we are interested in and to keep the effect given from the electromagnetic perturbation fields.

Our specific interest was in the β-emitting nuclei with lifetimes of a few seconds, which were produced by the (p,n), (p,α), (d,p) and (d,n) reactions initiated with fast polarized beams accelerated by the tandem Van de Graaff at Stanford University. The typical beam energy was 5 - 15 MeV with a beam intensity of ≈ 10 na.

The polarization of the incident beam was transferred to the product nuclei. the polarization was detected by measuring the β-decay up-down asymmetry along the polarization produced (Fig. 1). The energy of the β-rays was higher than several MeV. A typical counting rate of 10^3 - 10^4 c.p.s. with 10% β-asymmetry was observed using a thick target.

In order to take advantage of the above experimental conditions, the targets must satisfy several conditions. They must be thick enough to stop every product nuclei and also stop the beam to utilize all available energy. They must be of high purity to retain product polarization since there is a spin-lattice relaxation process by which polarization is destroyed. It is known that paramagnetic impurities shorten the relaxation time. Thus there should not be many paramagnetic

ions, or if produced, they should not remain long enough to shorten the relaxation time.

They must be well annealed in order to take advantage of the crystalline internal field. They should be kept at a specific temperature when in use to protect the polarized element against the static and dynamic depolarization mechanisms caused by radiation damage. This damage should either be healed quickly or frozen in a certain crystal site by choosing a suitable temperature. The final site of the recoil implanted nuclei in the ionic sample should be a substitution of the same isotope or other elements where the electronic configuration is diamagnetic and stable. For this purpose, it is appropriate to choose a sample in which an element with similar mass-weight recoil nuclei is included. Metallic samples are known to be suitable as implantation media for a short-lived state. This type of target has been well investigated and is used to keep the nuclear polarization of the nuclear states with milli-second to a few seconds, by combining with low temperature techniques[3].

The targets we used were metallic plate, pressed or fused polycrystals and single crystals.

^{7}Lithium metal: A slice was cut from an enriched block 10 mm x 10 mm x 2 mm or $\approx$ 150 mg/cm^2 and kept in dry kerosene until ready to use. The surface was then thoroughly etched in ethyl alcohol to remove residual oils and oxide. As mentioned above, the depolarization mechanisms are well known for the lighter element metals and it is very useful for the polarization phenomena study to determine the absolute polarization transfer in the present ^{7}Li(d,p)^{8}Li reaction (Fig. 2). Other examples are polycrystalline ZrB_2 and single crystal Si and ZrB_2.

Ionic polycrystals: The general procedure where one or both compounds were water soluble, e.g., Calcium bromide-Potassium bromide, was to dry them thoroughly in air at $\approx$ 100°C. The materials were then suitably mixed and melted under an

Argon atmosphere in an Aluminum oxide crucible to form a chemical compound. Reducing the temperature very slowly through the crystallization zone, a few degrees per minute, was effective in preserving greater polarization in the sample. If practical, the resultant sample may be sliced to target thickness. Another method was to grind the crystals with mortar and pestle. Then, three to four hundred milligrams of the powder was pressed between two stainless steel plates (Premier Brand Ferrotype) at about three tons per square inch[3]. The resulting two cm diameter disc was trimmed at the edges to one and a half cms and mounted with Zipbond contact cement on a Tantalum split-ring holder (Fig. 4 a, b). The typical final target thickness was 100 - 150 mg/cm^2.

In cases where the compounds were not water soluble, the fine powders were thoroughly mixed and dried by heating in vacuum before melting or fusing. When the pressed discs were too fragile to mount, as with Magnesium oxide-Aluminum oxide, the mixture of the power of 1 μm diameter grain was heated to ≈ 100°C on a hot plate and treated with two to five drops per side of a polyethylene-xylene solution (1 mg to 1 ml) and allowed to dry under a fifty ml beaker. This made them mechanically strong enough to handle. When the compound was reactive to either oxygen or water, the target was prepared in a glove box under dry Argon. The powder was sandwiched between two Tantalum foils .0025 mm thick, separated by a glass ring spacer 1.2 mm in diameter by 1 mm thick, and sealed vacuum tight with fast-setting epoxy (Zynolyte brand) (Fig. 4 c). The energy of the incident beam of particles and the β-rays were ≈ 10 MeV and > 2 MeV respectively and can penetrate the window.

Single crystal targets $LiIO_3$[4], Si,$KCaBr_3$[4], KBR,CaF, and MgF_2 were prepared for the hyperfine structure study of the associated elements. Slices 0.5 to 1.0 mm were made with a diamond saw using light mineral oil as the lubricant. The crystalline axes were selected to match the specific hyperfine study.

We have shown several examples of choosing a suitable target and preparing it carefully, in which recoil implantation was possible and nuclear polarization was kept for $\approx$ 10 seconds (Figs. 2, 3 and Table 1). Since we are able to produce various polarized elements by imitating nuclear reactions with polarized beams, there may be other ways to prepare targets which are suitable for specific hyperfine studies.

* Work supported in part by the National Science Foundation

† On leave from the Department of Physics, Osaka University, Toyonaka, Osaka 560, Japan

---

REFERENCES

[1] T. Minamisono, et al. "Measurement of the Quadrupole Moment of ^{8}Li by Use of a Polarized Deutron Beam and N.M.R. Detection," Physical Review Letters 34, 1465 (1975).

[2] E. Matthias and D. A. Shirley. "Hyperfine Structure and Nuclear Radiations," North Holland Publ. Co., Amsterdam (1968).

[3] K. Sugimoto, H. Horie. Journal Phys. Soc. Japan 34, supplement (1973).

[4] M. Kusuhara. "A method for the Preparation of Dueterated Polyethylene Targets," Nucl. Inst. and Methods 83, 328 (1970).

[4] Synthesized by Dr. R. Feigelson, Materials Research Center, Stanford University.

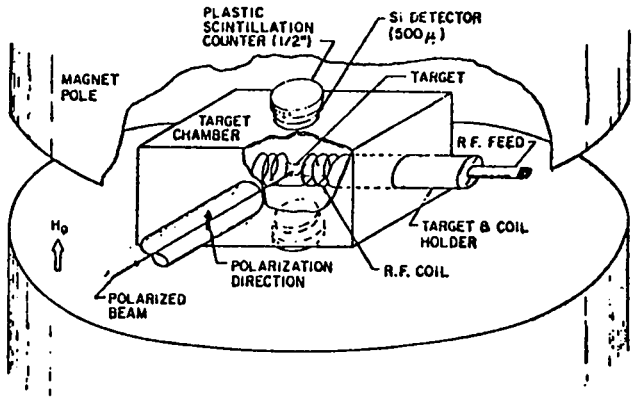

Fig. 1

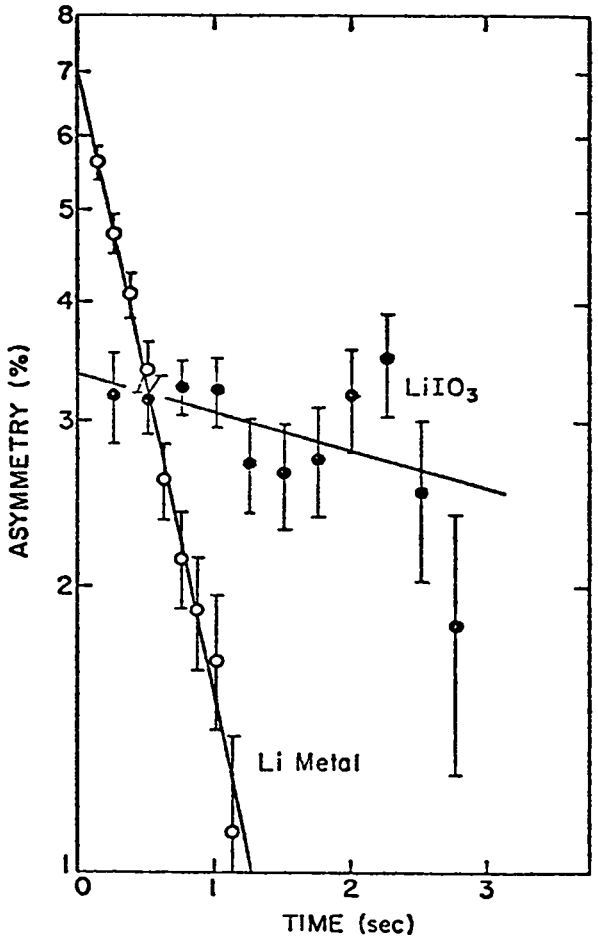

Fig. 2

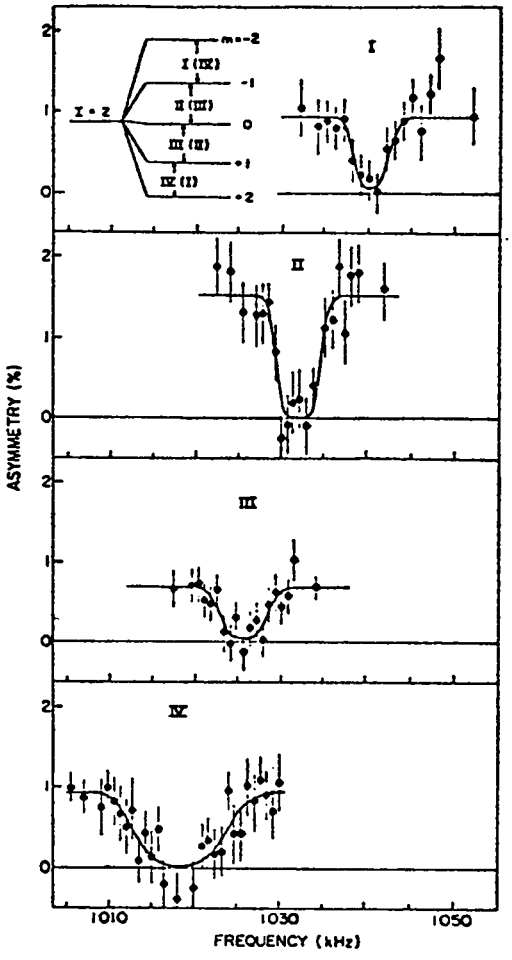

Fig. 3

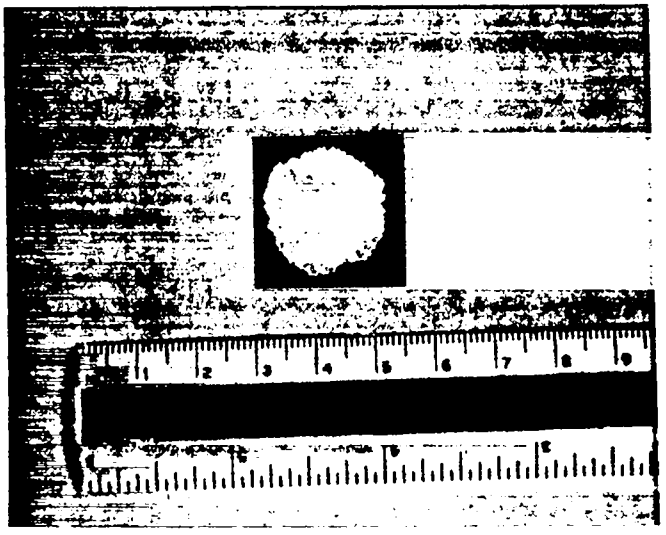

a

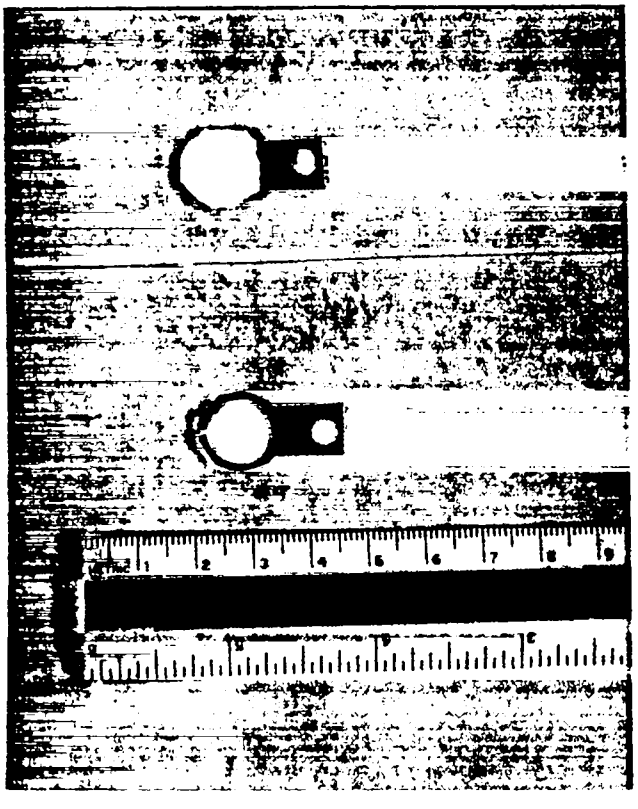

b

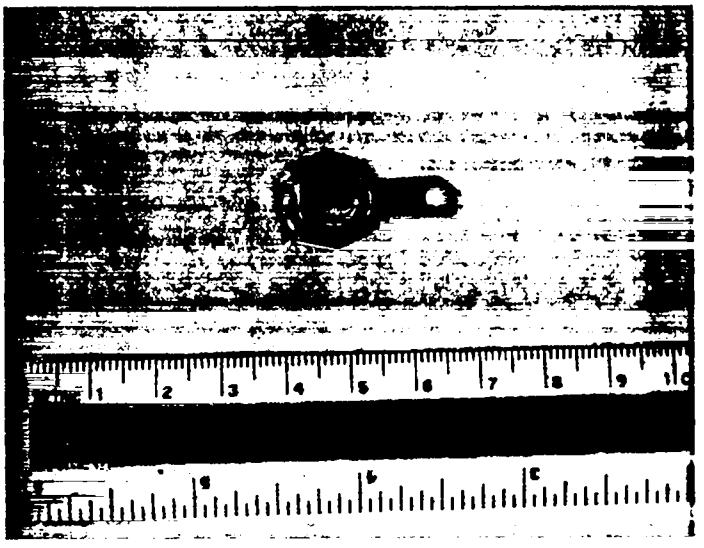

c

Figure 4

Table 1 Polarization Transfer

Product Nucl. $(I^{\pi}, T_{\frac{1}{2}})$	Target	Nuclear Reaction	β-decay Asymmetry $(R(\downarrow)/R(0)-1)$
$^{8}Li(2^{+}, 0.84S)$	Li metal $LiIO_3$	$^{7}Li(d,p)^{8}Li$	+ 9%
$^{12}B(1^{+}, 20\ ms)$	ZrB_2	$^{11}B9d,P)^{12}B$	+ 9
$^{29}P(\frac{1}{2}^{+}, 4.2\ s)$	Si(crystal)	$^{28}Si(d,n)^{29}P$	- 3.5
$^{29}P(\frac{1}{2}^{+}, 4.2\ s)$	Si(crystal)	$^{29}Si(p,n)^{29}P$	- 1.5
$^{31}S(\frac{1}{2}^{+}, 2.6\ s)$	Red P	$^{31}P(p,n)^{31}S$	- 1.
$^{39}Ca(3/2^{+}, 0.87)$	$KCaBr_3$ KBr	$^{39}K(p,n)^{39}Ca$ "	- 3 - 1
$^{25}Al(5/2^{+}, 7.2\ s)$	Si(crystal)	$^{28}Si(p,\alpha)^{25}Al$	- 0.5
$^{29}P(\frac{1}{2}^{+}, 4.2S)$	P or S	$^{32}S(p,\alpha)^{29}P$	- 2.

* Deuteron polarization $P_z = 0.6$ $E_d = 5 \sim 12$ MeV

** Proton polarization $P_z = 0.65$ $E_p = 5 - 12$ MeV

A RAPID AND ACCURATE METHOD FOR MEASURING THE THICKNESS OF EXTREMELY THIN TARGETS

Peter Maier-Komor

Physik-Department, Techn. Universität München, Germany

ABSTRACT

With carbon as an example the possible accuracy of the thickness measurement of light transparent foils is demonstrated. With a quartz prism-spectrophotometer the transmission characteristics of carbon foils in the energy range of 200 - 2500 nm was investigated. The transmittance as a function of carbon foil thickness was measured at different wavelengths. With these data the absorption coefficients and the reflectivities of carbon foils were calculated.
Knowing these optical constants for one wavelength it is easy to calculate the absolute thickness of a carbon foil by measuring only its transmittance for this monochromatic light. With this method carbon foils were investigated grown on different parting agents, to see if there might be an epitaxial effect, giving different crystalline clusters in the almost amorphous carbon foils.

INTRODUCTION

The necessity of precise thickness measurements of thin carbon stripper foils is shown on the example of a Lamb shift experiment with hydrogen like S-ions. The current of the hydrogen like S-ions should be very stable compared to the current of the most probable charge-state. The problem is that the charge-state distribution varies rapidly with the

stripper thickness at the extreme charge states. S-ions cause high migration in the stripper foils which requires to exchange frequently the stripper foils of nearly the identical thickness. The required carbon thicknesses are 3 - 6 $\mu g/cm^2$.

To estimate the thickness gravimetricly we have a Mettler ME 21 electronic vacuum microbalance. If you cut the target out of the frame, the error of the total surface area will be about 10 % for very thin foils, and if you weigh the frame without and with the foil, the error will be about 0.5 $\mu g/cm^2$ because of adsorption and desorption effects. So, both methods have an error of about 10 % for a 5 $\mu g/cm^2$ foil and are very tedious and time consuming.

X-ray, α - or β - absorption are all ruled out due to their very low absorption. There is at present no theory, which well describes the energy loss distribution of light ions in extreme thin foils, because the effect of resonance collisions with bound atomic electrons cannot be calculated with good accuracy.

Heavy ions cant be used due to the charge-state distribution shift.

Rutherford scattering of light ions is a good method to determine the areal density of such thin foils. But you need a small accelerator, and this method is also very time consuming.

We investigated a very old method which is mostly used for only semi - quantitative measurements [1].

The diagram in these papers shows that light absorption is very sensitive for carbon foils in a thickness range from 5 - 50 $\mu g/cm^2$. But this diagram itself is not useful for quantitative information, because the light meter is not calibrated and the wavelength range of the light is unknown. And last not least the thickness calibration might be just report how the carbon foils of Oak Ridge behave.

Absorption of monoenergetic light in matter is described by Beer's law. The transmitted intensity I_T is equal to the incoming monoenergetic intensity I_o multiplied with the exponential function of the absorption coefficient μ and the foil thickness x (fig. 1).

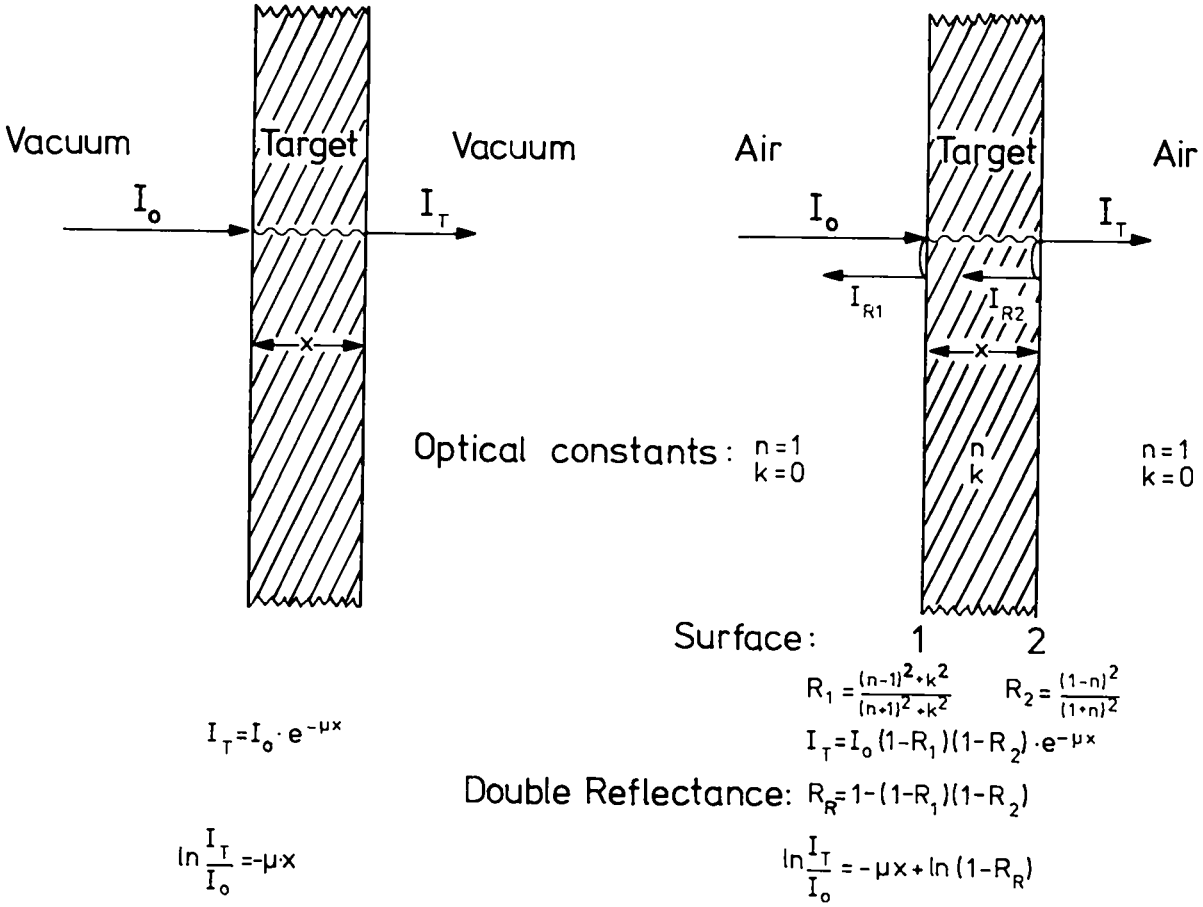

Fig. 1: Calculations of transmittance and double reflectance.

Using this law for the transmittance of monochromatic light through a thin foil you cant neglect the reflectivity at the foil. The reflectance can be calculated using the optical constants: refractive index n and absorption coefficient k. At both bounderies occurs reflection.

At the first surface the reflectance is $R_1 = \frac{(n-1)^2 + k^2}{(n+1)^2 + k^2}$.

At the second boundery the reflectance is $R_2 = \frac{(1-n)^2}{(1+n)^2}$.

Of course there is also a reflection component of the reflected intensity I_{R2} at the first surface but for high absorption coefficients k one can neglect this contribution to the transmitted intensity I_T. All light scattering in the foil is neglected, which is a good approximation for nearly all thin foils measured with a commercially available spectrophotometer with its big acceptance angle of the collecting mirror.

The transmitted intensity through a thin foil is $I_T = I_o \cdot (1-R_1) \cdot (1-R_2) \cdot e^{-\mu x}$. μ and k are both the absorption coefficient but only with different dimensions, we will use for μ the dimension $\left[\frac{cm2}{\mu g}\right]$.

Later we will notice, that the transmittance as a function of foil thickness yields a term of reflectance at both surfaces. This double reflectance is $R_R = 1-(1-R_1) \cdot (1-R_2)$. The finite equation is now $\ln \frac{I_T}{I_o} = - \mu \cdot x + \ln (1-R_R)$.
With this equation it should be easy to measure the thickness of a target foil: one just need a spectrophotometer and data on n and k out of the literature. But the literature is very poor on optical constants for carbon.

A. Cosslett and V. E. Cosslett [2]) measured the variation of optical absorption with thickness of evaporated carbon films, 1 - 30 $\mu g/cm^2$ thick.

They saw no constant absorption coefficient for the different thick carbon films. One reason for the results of Cosslett could be, that the surface of the carbon has a different physical behaviour due to adsorption. This would be surprising for me. Carbon is such an active material that foils of target

thicknesses up to 100 or 200 $\mu g/cm^2$ should completely adsorb through the whole thickness. The main reason seems to be that the optical constants depend on the electronic structure of the carbon or graphite crystals. The crystalline structure of carbon films might depend on thickness.

Taff and Phillip [3]) have investigated the optical properties of carbon in a natural graphite crystal, a pyrolytic graphite sample and mechanically polished glassy carbon sheet.

Fig. 2 shows their two limits of possible reflectivity of a carbon surface. The curve for natural graphite and pyrolytic graphite is nearly identical. The reflectivity of glassy carbon is generally lower. Glassy carbon exhibits no distinct crystal structure, it is almost amorphous.

Di Nardo and Goland [4]) investigated the optical properties of a 6 to 7 $\mu g/cm^2$ carbon foil prepared on potassium hydroxide as parting agent in the wavelength range 2200 Å - 5800 Å. They compared their results with the data of Taft and Philipp.

I calculated the double reflectance and the absorption coefficient from their data (fig. 3). The absorption coefficient is shown in fig. 3 only with the dimension $\left[\frac{1}{Å}\right]$ for there was no information about the specific gravity of the materials.

The optical constants of their carbon foil-investigated-lie between the data of graphite and glassy carbon.

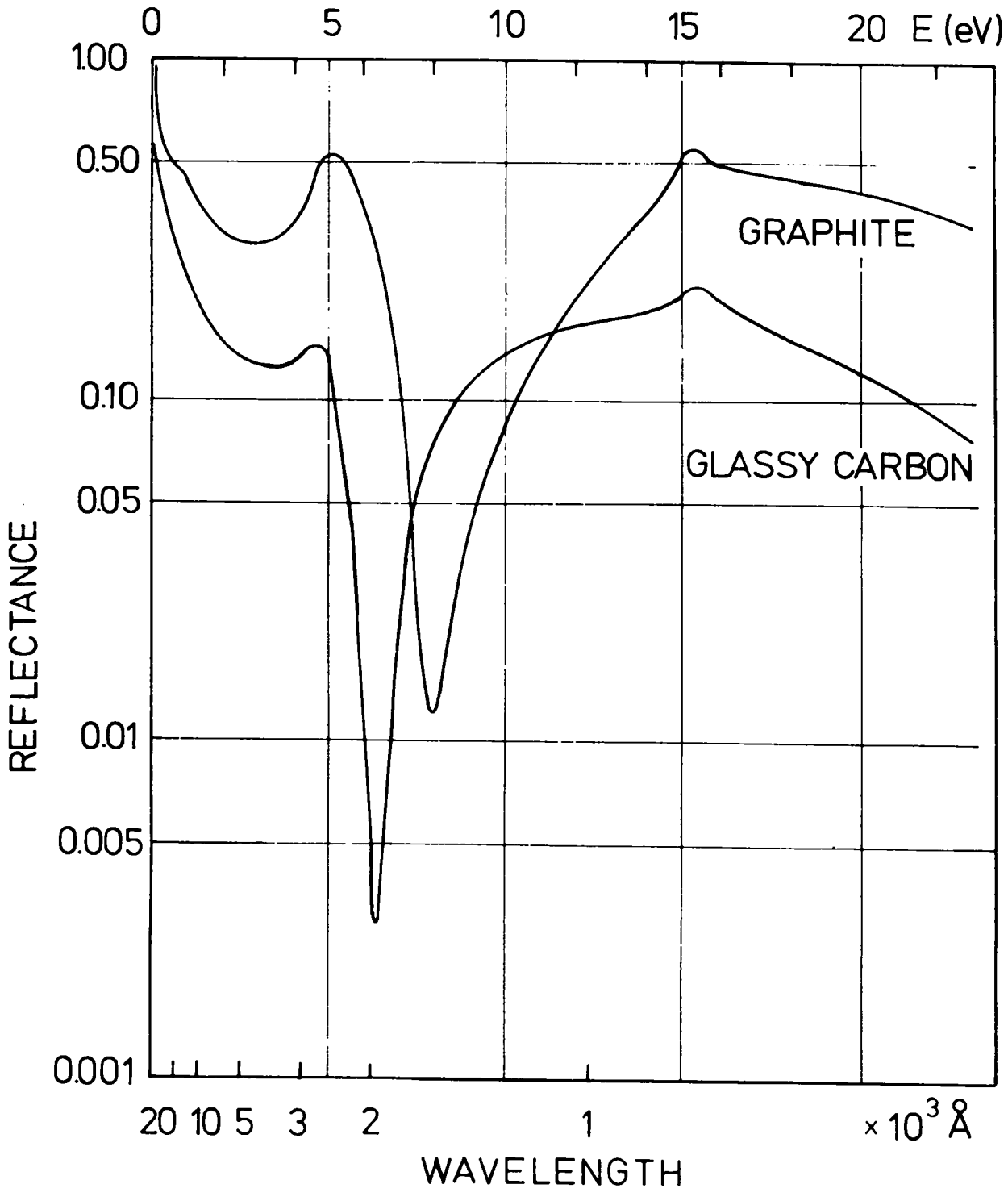

Fig. 2: Spectral dependence of the reflectance of graphite and glassy carbon.

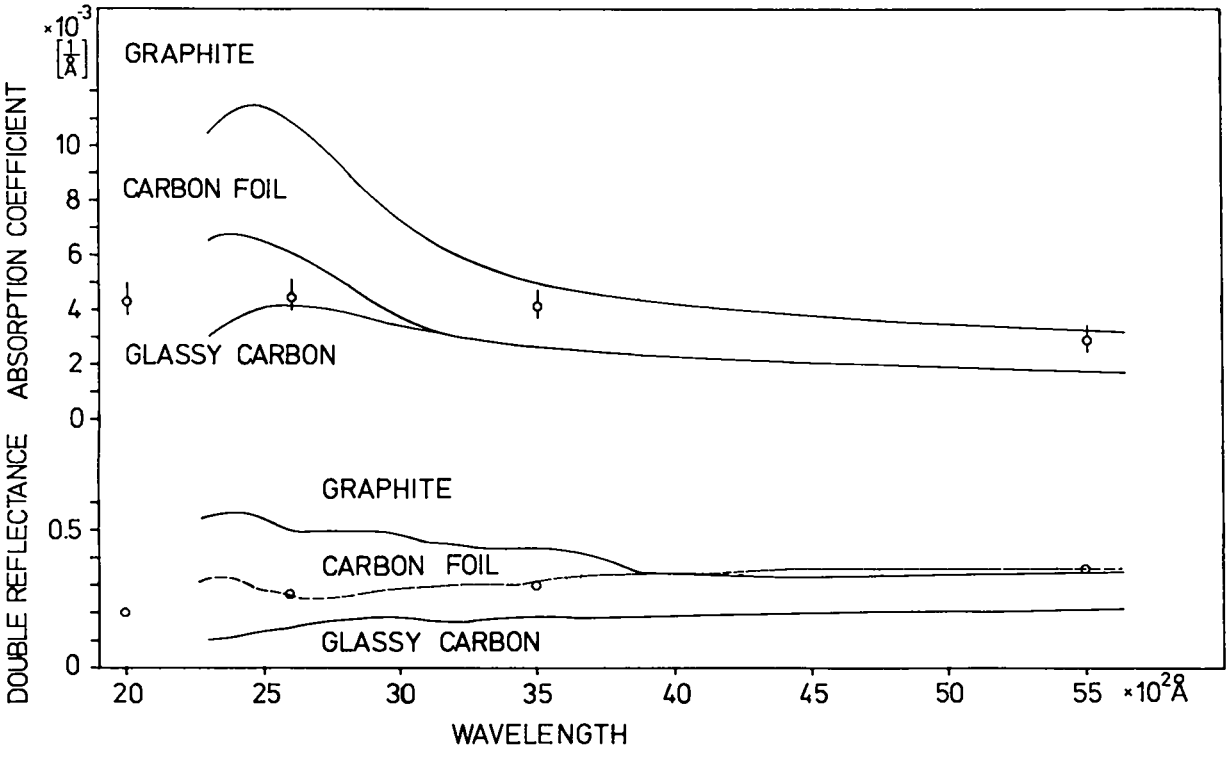

Fig. 3: Double reflectance and absorption coefficient as a function of wavelength.

You may recall the approximation about the effect of substrate temperature on the condensation process: When the substrate temperature is less than 10 - 20 % of the absolute melting point the deposited material is nearly amorphous, the first crystal growth starts with about 30 % of the absolute melting point. At about 60 % the film will be as dense and as ductile as the bulk material. With this point of view all carbon evaporated on normal parting agents must be amorphous, because the melting point of carbon is at about 3820° K. This simple approximation seems to be not quite true for carbon.

There are indications that carbon foils made with a Betaine - Sucrose solution [5]) as parting agent show a more graphitic structure than carbon targets prepared with other parting agents.

EXPERIMENTAL AND RESULTS

With an electron gun evaporator we produced carbon foils of various thicknesses up to 150 $\mu g/cm^2$ on two different parting agents. One parting agent was Betaine-Sucrose, the other was Na F , which was evaporated just before the carbon evaporation on microscope slides in a thickness of about 50 $\mu g/cm^2$. The carbon source substrate distance was 50 cm. The thickness measurements were done with a well calibrated Kronos quartz thickness monitor. The carbon foil thickness calculations were done with the approximation of a carbon point source (about 3 mm in diameter) and equal sticking coefficients for the not cooled quartz and the substrate surface.

With a Zeiss quartz prism-spectrophotometer PMQ3 we measured the transmittance as a function of wavelength from 2000 Å - 25000 Å shown in fig. 4.

a) is the curve for a carbon foil 10.6 $\mu g/cm^2$ thick grown on Betaine - Sucrose as parting agent

b) is the curve for a carbon foil 11.2 $\mu g/cm^2$ thick grown on NaF.

c) is the curve for a carbon foil bought at Commercial Products of Atomic Energy of Canada Limited. The thickness of this foil should be 10 $\mu g/cm^2 \pm 20$ %. If this foil does not behave too different from our foils the thickness was about 14 $\mu g/cm^2$.

In general you see, if you want to measure the thickness of thin carbon foils you should do this at short wavelengths. But one can measure the thickness of thick carbon foils at long wavelengths where the foil would be opaque for short wavelengths.

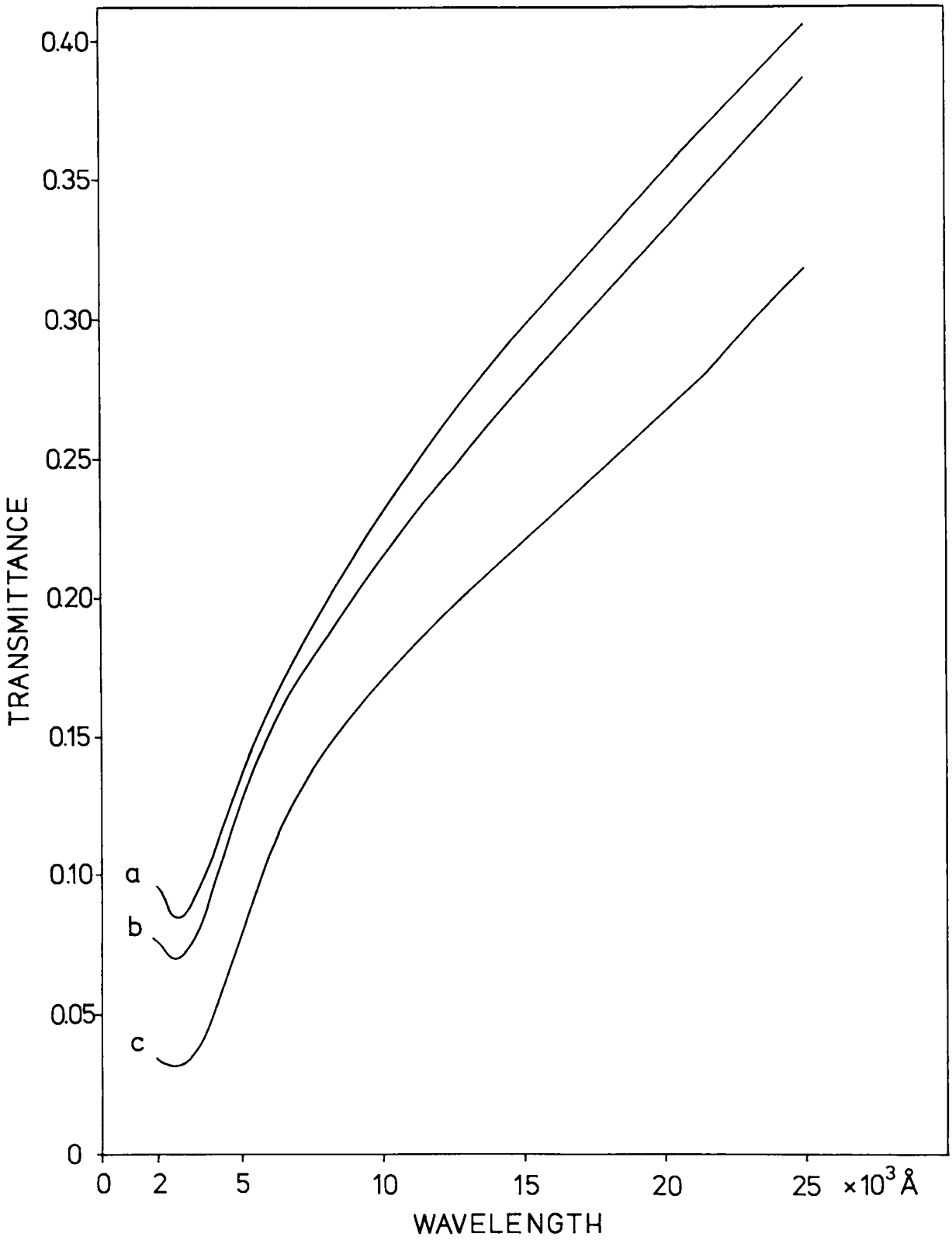

Fig. 4: Spectral dependence of the transmittance for three different carbon foils in the 10 $\mu g/cm^2$ range.

In fig. 5 is shown the transmittance as a function of carbon foil thickness for 4 wavelengths. The full circles are for carbon foils made on Betaine - Sucrose. The open circles are for foils made on NaF. The lines are fitted through the points for the Betaine made carbon foils.

The points for the NaF made carbon foils would give their own line with nearly the same gradient, but with less double reflectance, which can be seen at the extension of the line to zero thickness. The dashed lines with the higher gradient show the tunnel effect for light. This effect starts approximately at a thickness $X\left[\frac{\mu g}{cm^2}\right] = \frac{\lambda\,[\text{Å}]}{138}$, which suggests that one should not measure carbon foil thicknesses in this range.

For the longer wavelengths, the measured points do not lie perfectly on the fitted line. This means that different crystalline structure shows more effect at this long wavelengths.

If the crystalline structure is dependent on evaporation rate we can explain the deviations at the long wavelengths, because we did not try to get the same evaporation rate for every carbon foil.

Fig. 6 shows the same functions for shorter wavelengths. The tunnel effect cannot be seen, because we did not produce such thin foils. Here the full circles are nearest to the fitted lines at 3500 Å and 5500 Å. From 2000 Å to 3500 Å there is nearly no difference between the open and full circles, which suggests that the optical constants are not sensitive to a different crystalline structure, which seems to be in no good agreement with the data of Di Nardo and Goland (fig. 3). The circles in this diagram are our calculated data in this region for carbon foils on Betaine - Sucrose. To get the absorption coefficient in the dimension $\left[\frac{1}{Å}\right]$ we used a value of 2 for the specivic gravity.

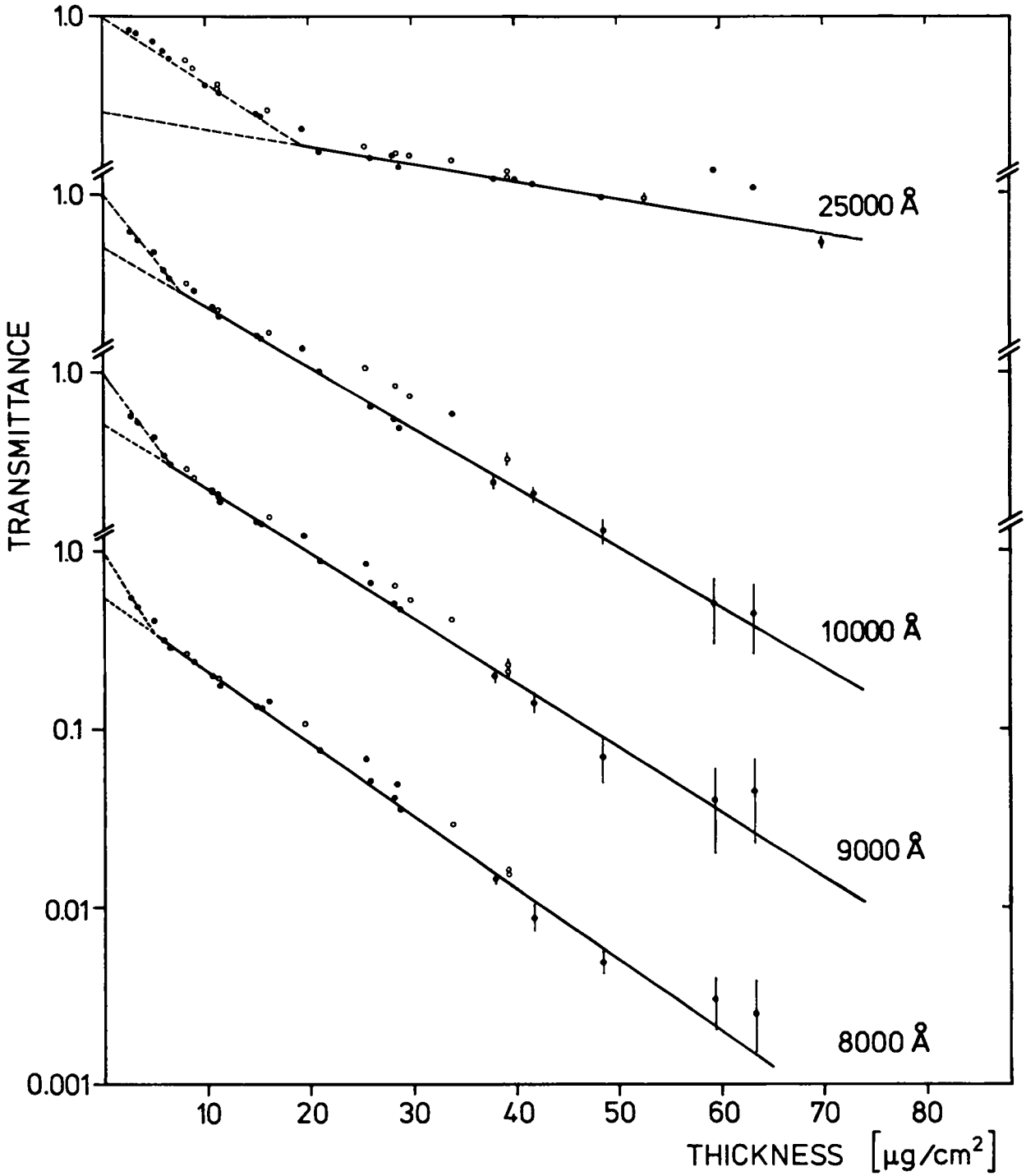

Fig. 5: Transmittance as a function of carbon foil thickness for 4 wavelengths.

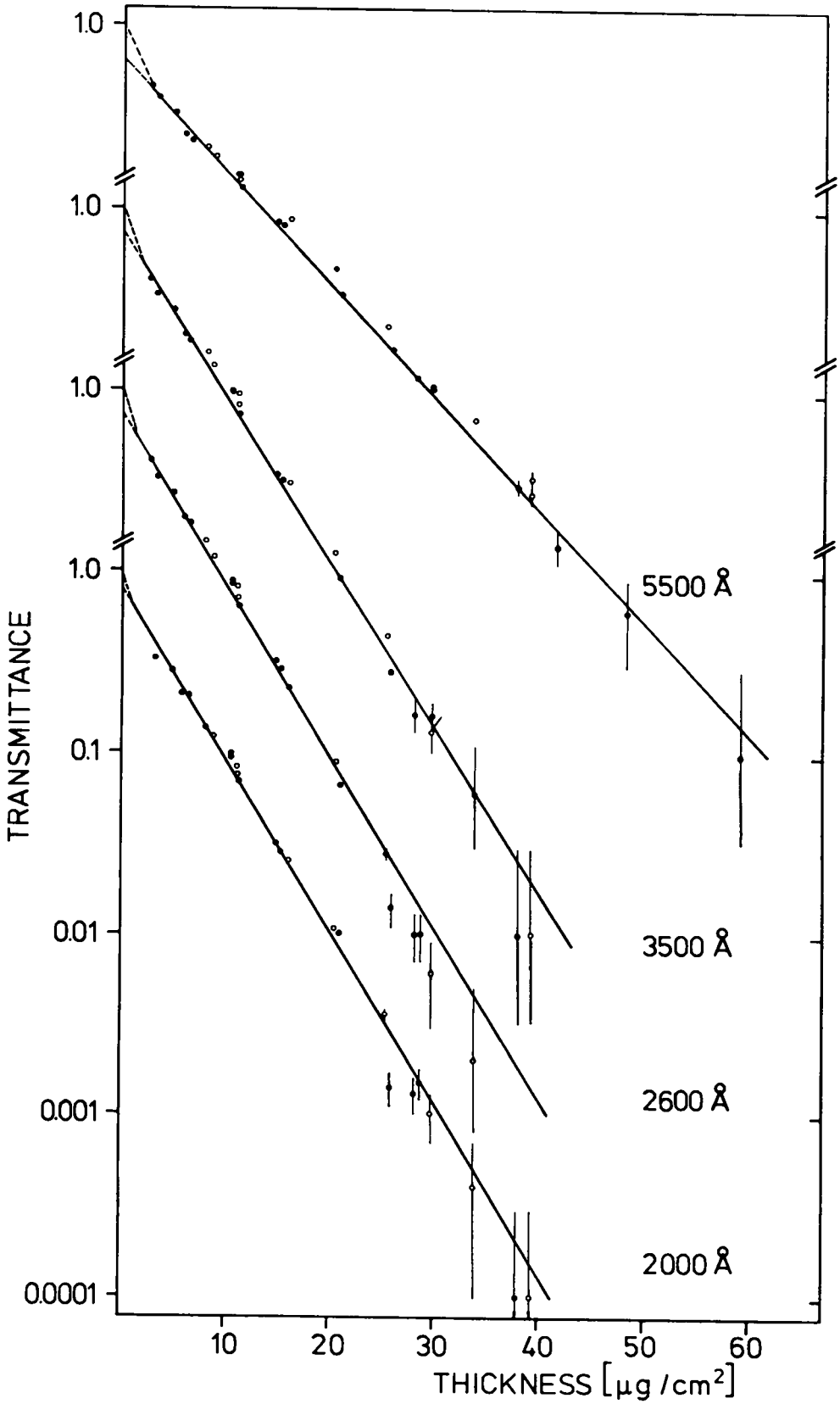

Fig. 6: Transmittance as a function of carbon foil thickness

If we use the specivic gravity of 2.25 for graphite and a specivic gravity of 1.3 $\pm$ 0.1 for the carbon foil, which is a value of amorphous carbon the curves for the absorption coefficients of graphite and carbon foil are nearly identical. This means that the cyrstalline structure is of nearly no consequence for the absorption coefficient in this wavelength range. Now the measurements of Di Nardo and Goland give within the errors the same results than our data.

For our carbon foils the data are most precise in the wavelength region from 3500 Å - 8000 Å. The absolute thickness is correct within 5 %, but the main advantage of this method is that the relative thickness is correct within 0.5 %, which means for example one can distinguish between a 5 $\mu g/cm^2$ and a 4.98 $\mu g/cm^2$ carbon foil.

What one can learn for carbon foil production is: The parting agent may influence the crystal growth in the carbon layer. The carbon foil should be more stable if it is more like graphite, this means let us surch for parting agents which give more double reflectance.

R E F E R E N C E S

1) Adair H.L. and Kobisk E.H.,
P. 29 in Proceedings of the conference of the Nuclear Target Development Society, Argonne 1975.

2) Cosslett A. and Cosslett V.E.,
Brit. J. Appl. Phys. 8, 374 (1957).

3) Taft E.A. and Philipp H.R.,
Phys. Rev. 138, A 197 (1965).

4) Di Nardo R.P. and Goland A.N.,
J. Opt. Soc. Am. 61, 1321 (1964).

5) Maier-Komor P.,
Nucl. Instr. and Meth. 102, 485 (1972).

PRODUCTION OF FRACTIONAL ATOMIC LAYER STANDARDS OF NIOBIUM AND VANADIUM*

G. E. Thomas and P. J. Dusza

Argonne National Laboratory, Argonne, Illinois 60439

ABSTRACT

In controlled-fusion research, one method of determining surface effects is to measure the sputter yields of high-energy ions and neutrons for various solids. Due to the low-atom-displacement cross sections for these processes at high particle energies, only fractional atomic-layer deposits can be collected in reasonable irradiation times. Quantitative analysis of these collectors is best done by comparison with standards of comparable thickness. To produce such standards a modified Pierce-type electron-beam-gun evaporation system with a thickness monitor was used. An "accurate" Nb standard of 0.1-monolayer deposit thickness was prepared by evaporation under controlled conditions. Nb standards of 1.1 , 0.11, and 0.011 monolayers were produced in a single evaporation. These standards were then calibrated to the "accurate" standard. The errors quoted do not include those associated with the monitor itself. The relative accuracy of the standards was verified by Rutherford backscattering and ion micro-probe measurements. Standards of Nb and V on single-crystal Si substrates were produced.

*Work performed under the auspices of the USERDA, Division of Physical Research.

Most of the targets which are produced at the Physics Division target-fabrication facility at Argonne National Laboratory are used in basic research experiments. The very thin fractional-atomic-layer targets described in this paper were used in an experiment which yielded valuable information for the fusion power program. We will first briefly describe this experiment, then present the method of fabrication of the targets, and finally discuss the techniques used to determine the target thicknesses.

Experimental Arrangement

At Argonne National Laboratory Kaminsky, Das, and Dusza are performing experiments in which they are studying surface effects related to controlled thermonuclear devices.[1] One aspect of this research deals with measurements of sputter yields of high-energy ions and neutrons for various materials, such as niobium, which might be used for the plasma-containment vessel or other fusion-reactor components. The experimental arrangement for neutron-sputtering measurements is shown in Fig. 1. Neutrons with energies of 14.1 MeV from the Lawrence Livermore Laboratory Rotating-Target Neutron Source[2] strike the target, cause the release of atoms from the target which in turn are collected on silicon discs placed on either side of the target. Because of the low neutron fluence and of the low cross section for the displacement of atoms by 14.1-MeV neutrons, only fractional atomic layers of material can be collected in a reasonable irradiation time and since sputter yields are determined by measuring the amount of target material collected on the silicon discs, the analytical techniques used had to be calibrated with fractional-atomic-layers standards.

Three "relative" standards were first produced using the configuration shown in Fig. 2 in which the silicon substrates were respectively 7.0 cm, 22.1 cm, and 70.0 cm from the niobium evaporation source. The Kronos[3] quartz thickness monitor was also 7.0 cm from the source. Using this geometry with a Pierce-type electron-beam-gun evaporator,[4] a thickness monitor deposit of 0.23 $\mu g/cm^2$ produced a self-consistent set of substrates with niobium deposits of 1.1, 0.11 and 0.011 monolayer standards in one evaporation. As a result, there was excellent intercalibration between these three standards; the thickness of the deposits relative to each other are known with an accuracy of 5%.

A more accurate 0.1 monolayer niobium standard was then produced with the thickness monitor 10 cm, and the target substrate 70 cm distance from the evaporation source. At these distances the evaporation produced both a 0.1-monolayer thick deposit on the target and a deposit thickness on the monitor of 0.97 $\mu g/cm^2$, sufficient for good statistical accuracy. This "accurate" standard was then used to calibrate the thickest "relative" standard and in turn it was used to calibrate the other two "relative" standards.

Deposit Thickness Determination

We set out to quantitatively calibrate three techniques (schematically shown in Fig. 3) used for deposit thickness measurements. The most successful technique was Rutherford backscattering, shown schematically in Fig. 4. A collimated beam of 1.5-MeV $^4He^+$ particles from a 2-MeV Van de Graaff[5] struck the standard, and the particles which were scattered at 90° were detected by a silicon-barrier device. A typical energy spectrum as recorded on a multi-channel analyzer is shown in Fig. 5. As can be seen in

the figure, the helium atoms which were scattered from the niobium had much more recoil energy than those from the lighter silicon atoms. The good resolution of the niobium peak indicates there was very little straggling while the broad continuum results from considerable straggling and multiple scattering of particles off of the silicon substrate. The background intensity in the area under and near the niobium peak is largely due to pulse pileup from the silicon substrate which, in part, limits the sensitivity for detecting niobium.

Most of the niobium-standard values plotted on the thickness-versus-intensity graph of Fig. 6 fall within error for a good line fit. Note the position on the graph of the "accurate" standard.

The second method tried was that using an Auger Electron Spectrometer (AES). Although this method has sufficient sensitivity to measure these standards, it was not relied on for quantitative data because the few monolayers of carbon and oxygen surface contamination attenuated the niobium signal. Sputter cleaning, which is usually used to remove such contamination, would probably have also removed some of the niobium.

The third method was that using the Ion Microprobe Mass Analyzer (IMMA) and is shown in Fig. 7. With this method a 10-μm-diameter ion beam (e.g. 20-keV O^-) was rastered over a target surface area of 200 μm × 160 μm. Some of the sputtered target material was then mass analyzed, producing the niobium spectrum in Fig. 8. The iron contaminant was probably picked up during vapor deposition. Next, a depth profile of one mass was obtained by setting the analyzer at the mass of interest (93 for Nb) and noting the intensity as a function of time, while sputtering. Figure 9 shows intensity curves for several niobium standards.

Errors

The errors associated with the various standards are shown in Table I. The distance error includes the position of both the standard and monitor in relation to the evaporation source. The monitor thickness error of one Angstrom is used only when determining the "accurate" standard accumulative error. In Fig. 6, the vertical error bars are those associated with systematic errors and the horizontal error bars are those associated with statistical errors.

Summary

Fractional atomic layers of both niobium and vanadium have been produced using the e-gun system. By determining the thickness of the "accurate" standard with greater statistical accuracy and by reducing the "pile-up" background, it would be possible to produce more accurate and also possibly thinner standards.

Acknowledgments

We would like to thank Dr. M. S. Kaminsky for his continued interest in this project. We would also like to express our appreciation to Dr. G. T. Garvey for his support of the target-fabrication facility.

References

[1] Manfred Kaminsky, CRC Critical Reviews in Solid State Sciences, 6, (4), 433—457 (Aug. 1976).

[2] R. Booth and H. H. Barshall, Nucl. Instr. and Methods, 99, (1972).

[3] Kronos film thickness monitor model QM 321, Kronos, Inc. represented by Veeco Instruments, Inc., Arlington Heights, Illinois.

[4] Electron beam gun system, model VeB-6, Veeco Instruments, Inc., Arlington Heights, Ill.

[5] High Voltage Engineering type JN.

Figure Captions

1. Configuration for sputtering niobium or silicon substrates.
2. Set-up for evaporating materials on silicon substrates.
3. Systems for measuring target thicknesses.
4. Rutherford backscattering schematic.
5. Niobium energy spectrum from Rutherford-backscattered alpha particles.
6. Intensity curves for various thickness niobium targets.
7. Ion microprobe used for measuring target thicknesses.
8. Mass spectrum of niobium standard target using ion microprobe.
9. Curve of intensity versus thickness using the ion microprobe for various standards.

Table

1. Niobium standards showing error sources.

TABLE I

Niobium Standards

Thickness (monolayers)	Errors (%) Distance,	Thickness,[a] (Monitor)	Accurate Std.	Estimated Accumulative Error (%)
Accurate Std.				
0.1	2.0	10		12
Relative Stds.				
1.1	4.0	40	12	15
0.11	3.0	40	12	15
0.011	3.0	40	12	15
0.0022	3.0	100	12	15

[a]Monitor thickness error used for accurate std. error calculation only.

NEUTRON SPUTTERING CONFIGURATION

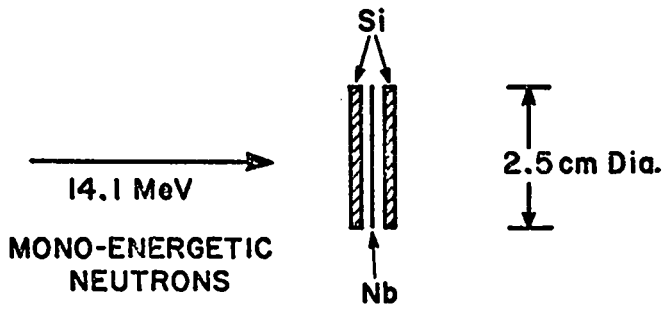

Fig. 1

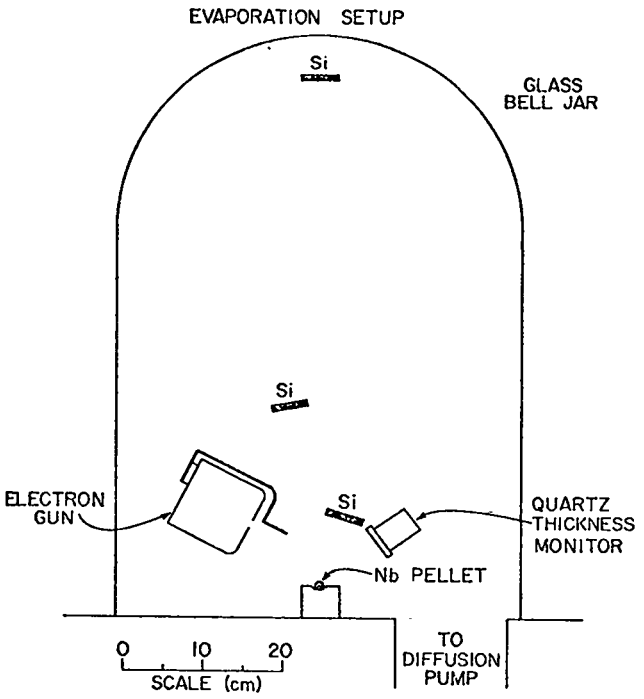

Fig. 2

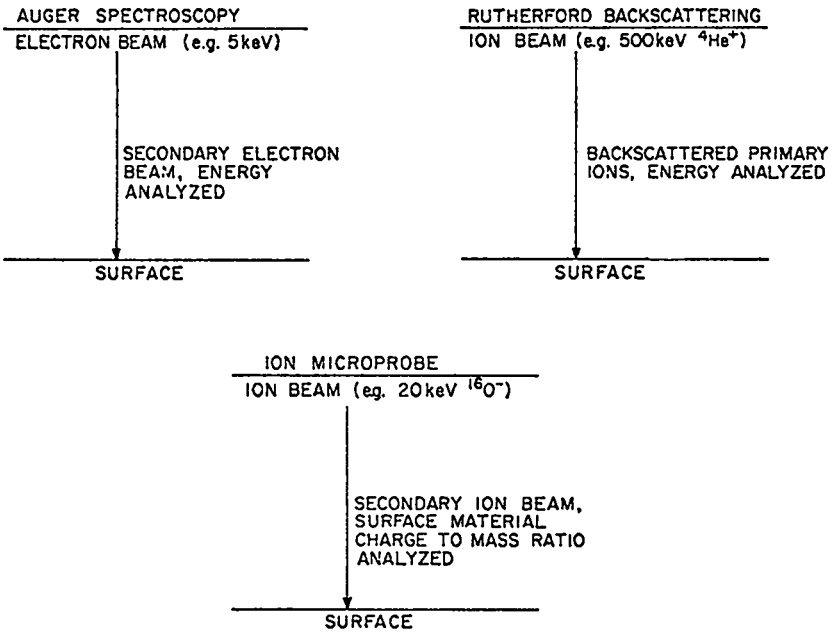
AUGER SPECTROSCOPY
ELECTRON BEAM (e.g. 5keV)
SECONDARY ELECTRON BEAM, ENERGY ANALYZED
SURFACE
RUTHERFORD BACKSCATTERING
ION BEAM (e.g. 500keV $^4He^+$)
BACKSCATTERED PRIMARY IONS, ENERGY ANALYZED
SURFACE
ION MICROPROBE
ION BEAM (eg. 20keV $^{16}O^-$)
SECONDARY ION BEAM, SURFACE MATERIAL CHARGE TO MASS RATIO ANALYZED
SURFACE

Fig. 3

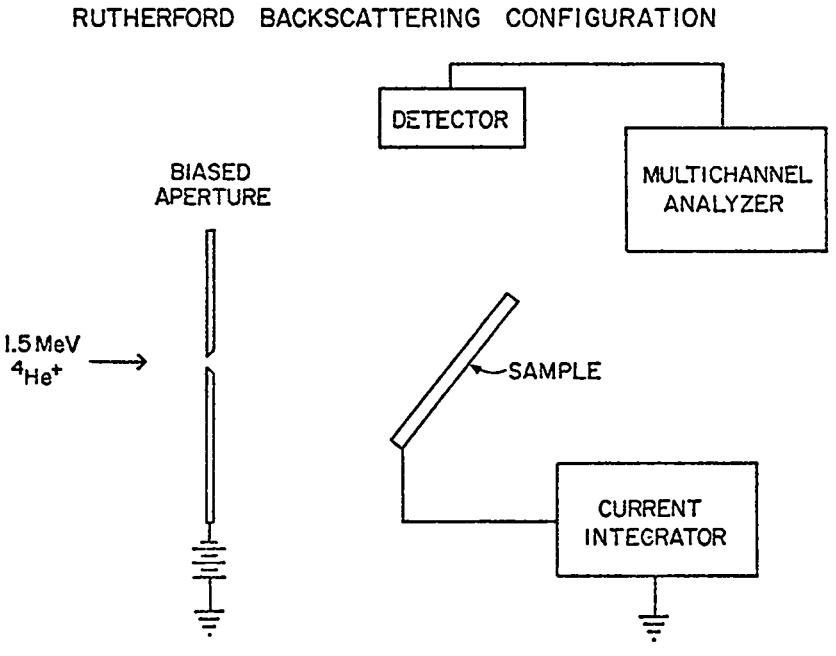
RUTHERFORD BACKSCATTERING CONFIGURATION
DETECTOR
MULTICHANNEL ANALYZER
BIASED APERTURE
1.5 MeV $^4He^+$
SAMPLE
CURRENT INTEGRATOR

Fig. 4

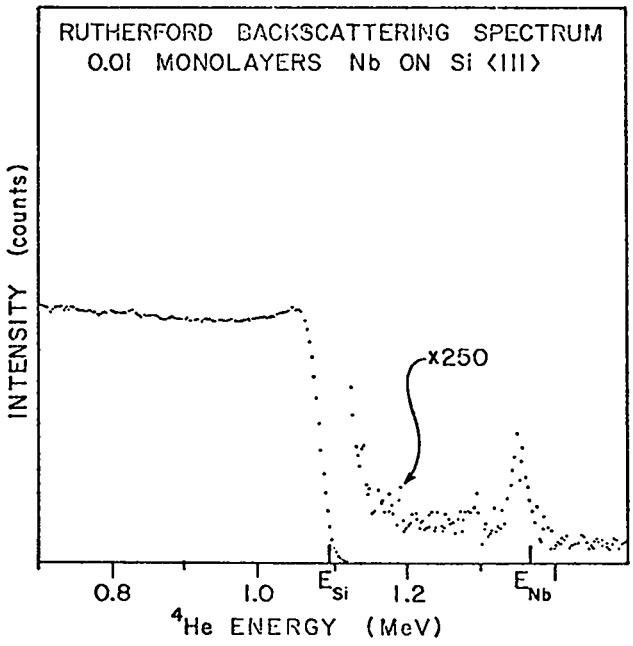
RUTHERFORD BACKSCATTERING SPECTRUM
0.01 MONOLAYERS Nb ON Si ⟨111⟩
INTENSITY (counts)
x250
0.8
1.0
E_Si
1.2
E_Nb
⁴He ENERGY (MeV)

Fig. 5

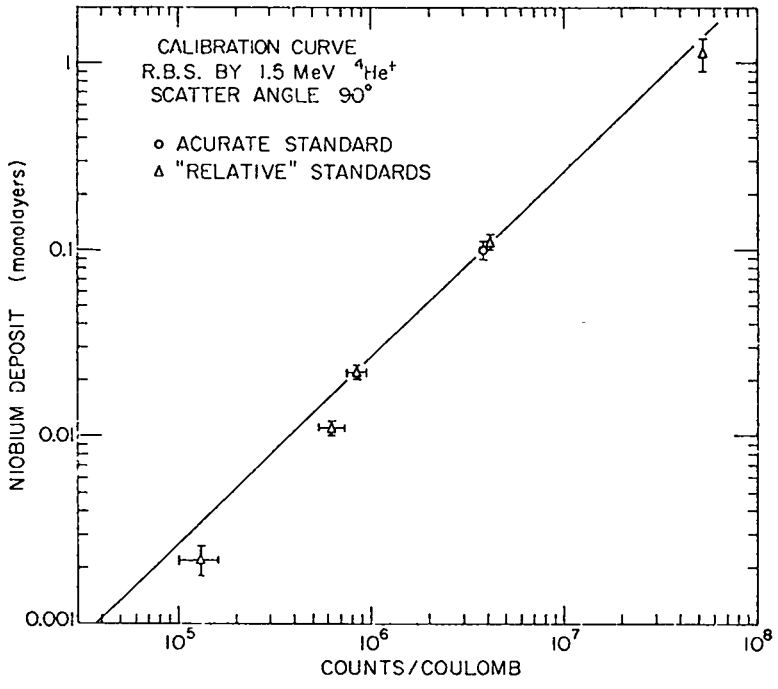
CALIBRATION CURVE
R.B.S. BY 1.5 MeV ⁴He⁺
SCATTER ANGLE 90°
o ACURATE STANDARD
Δ "RELATIVE" STANDARDS
NIOBIUM DEPOSIT (monolayers)
1
0.1
0.01
0.001
10⁵
10⁶
10⁷
10⁸
COUNTS/COULOMB

Fig. 6

ION MICROPROBE MASS ANALYZER

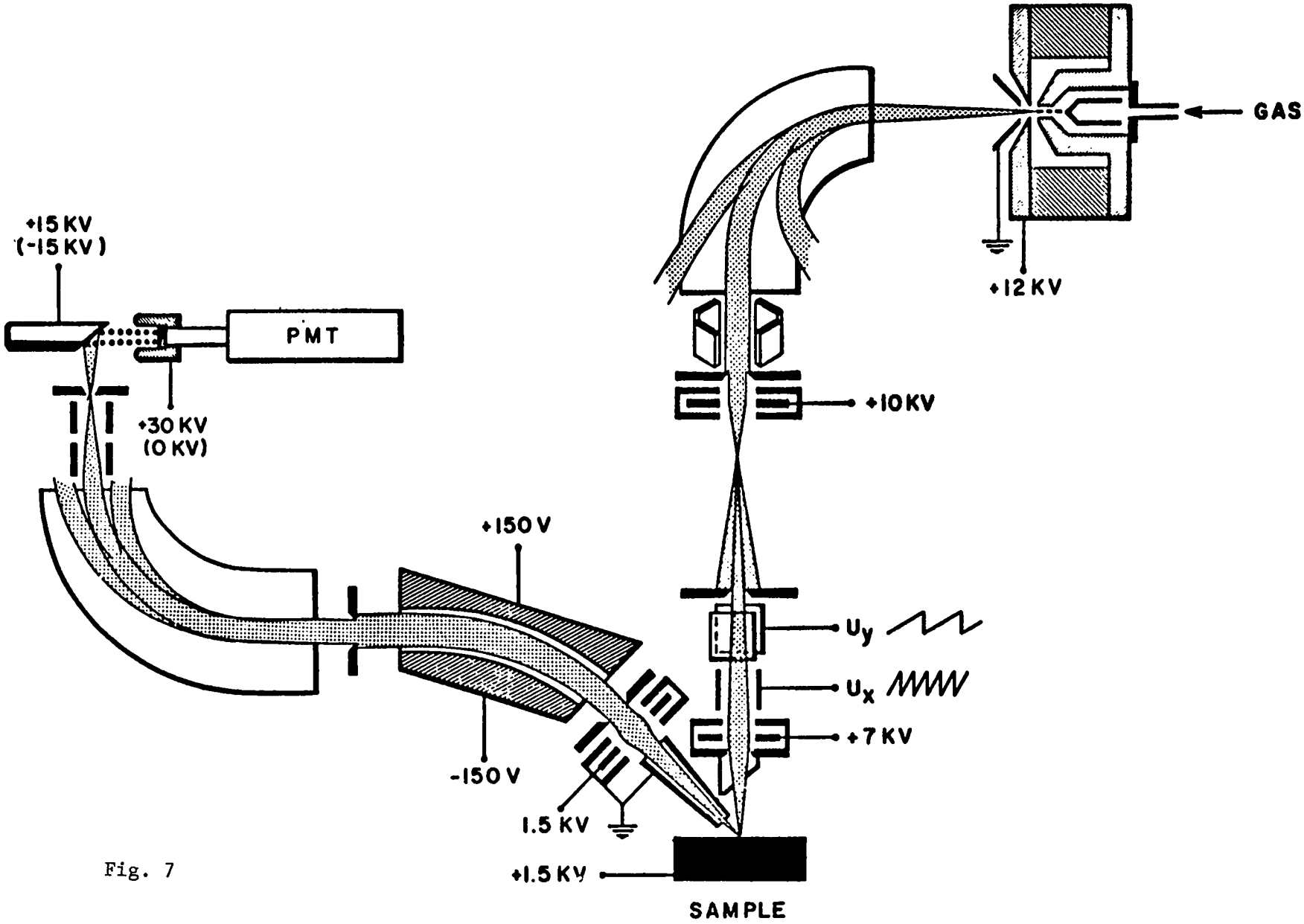

Fig. 7

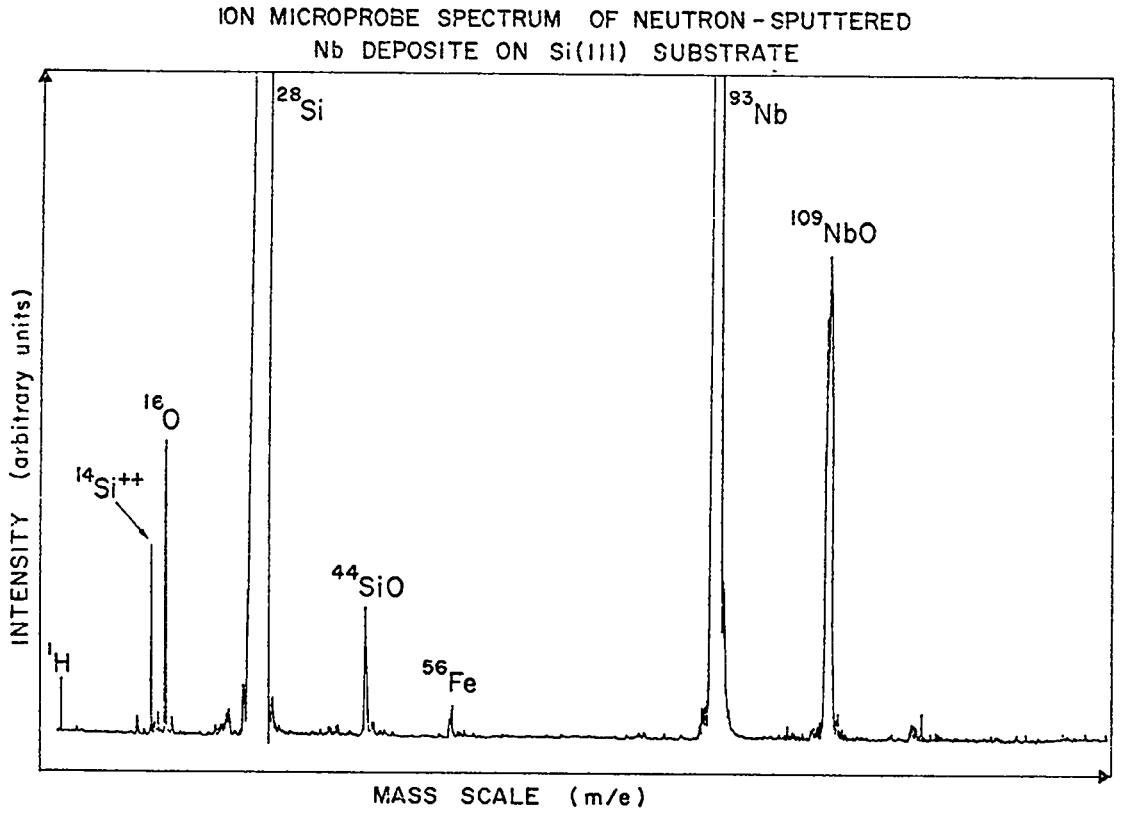
ION MICROPROBE SPECTRUM OF NEUTRON-SPUTTERED
Nb DEPOSITE ON Si(111) SUBSTRATE
INTENSITY (arbitrary units)
MASS SCALE (m/e)
^{28}Si
^{93}Nb
^{109}NbO
^{16}O
$^{14}Si^{++}$
^{44}SiO
^{56}Fe
^{1}H

Fig. 8

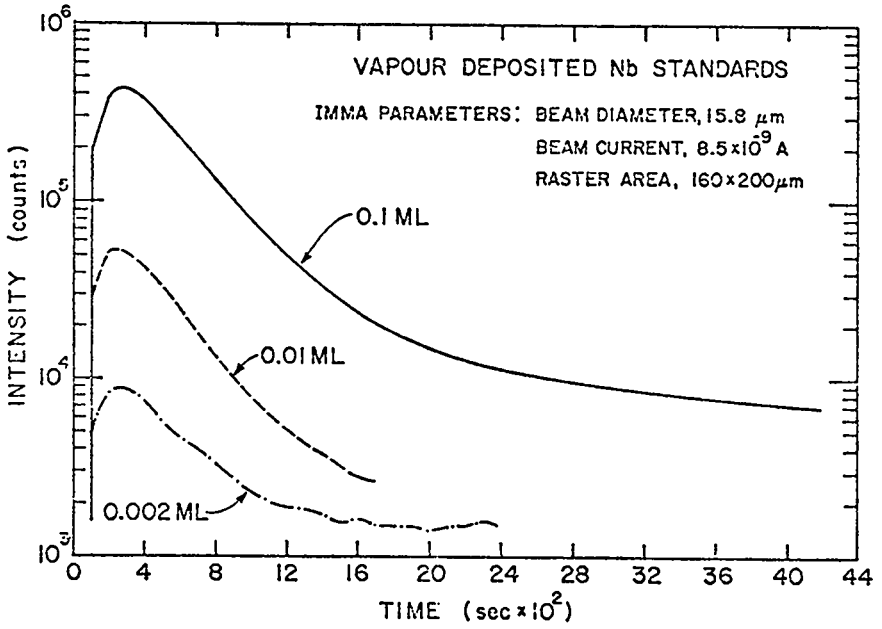
VAPOUR DEPOSITED Nb STANDARDS
IMMA PARAMETERS: BEAM DIAMETER, 15.8 μm
BEAM CURRENT, 8.5x10⁻⁹ A
RASTER AREA, 160x200μm
0.1 ML
0.01 ML
0.002 ML
INTENSITY (counts)
TIME (sec x 10²)
10⁶
10⁵
10⁴
10³
0
4
8
12
16
20
24
28
32
36
40
44

Fig. 9

THE ROLE OF AUGER ELECTRON SPECTROSCOPY AND SECONDARY ION MASS SPECTROSCOPY IN THIN FILM COMPOSITION ANALYSIS

by

R. W. Springer

Los Alamos Scientific Laboratory

ABSTRACT

Auger Electron Spectroscopy (AES), because of its surface sensitivity, is ideally suited to the elemental analysis of surface constituents. The technique, when combined with ion beam etching techniques, allows depth profiles yielding elemental distribution within the solid. Secondary Ion Mass Spectroscopy (SIMS), naturally accompanies depth profiling as the sputtered ions are mass analyzed. The SIMS spectra allow fingerprint analysis of the chemical state of the surface by fragment analysis. The limits and sensitivities of these tools along with recent attempts to quantify AES will be presented. Examples of application to sputter profiling will also be discussed.

Preparation of self-supporting Silver Sulphide Targets

M.A. SAETTEL
Centre de Recherches Nucléaires, Université Louis Pasteur
Strasbourg, France

The sulphurization of a thin silver layer is a technic which can be used for preparing self-supporting silver sulphide targets.

This paper describes a very simple method of obtaining self-supporting sulphur targets composed of silver sulphide, which are stable, of a fixed composition, using only a small amount of sulphur.

The method can easily be used for preparing self-supporting silver sulphide targets with isotopically-enriched sulphur.

1. INTRODUCTION

The preparation of sulphur targets is always difficult. The evaporation of the element or the compounds (zinc or cadmium sulphide) by heating them in a crucible, produces inhomogeneous targets, on account of the bad adherence to the backing material, and the efficiency of the method is very low. On the other hand, sulphur targets made from the element do not withstand the impact of the beam from an accelerator.

Engelbertink and Ollness (ref.1) propose a method of preparation of sulphur targets, by dissolving the sulphur in toluene and applying this solution, drop by drop, onto a silver foil : the sulphur reacts with the silver and produces silver sulphide. The reaction takes place at 60°C; at this temperature, the toluene evaporates easily. We have tried this method, but the homogeneity of the targets was not satisfying and their thicknesses were difficult to standardize.

Watson gives another interesting method for preparing sulphur targets on a thick silver backing. We have used the principle for obtaining self-supporting silver sulphide targets (ref.2).

2. PREPARATION OF SELF-SUPPORTING SILVER SULPHIDE TARGETS

2.1. Principle

The sulphur reacts easily with silver at 150°C. A thin silver layer of a fixed thickness is placed above a small amount of sulphur, which totally transfoms the silver layer into silver sulphide.

2.2. Procedure

The silver is evaporated by means of a tantalum crucible on glass-slides covered with a layer of baryum chloride (about 50µg/cm^2) The salt is evaporated in the same vacuum enclosure as the silver. The thickness of the layer is measured with a calibrated sensor head connected to a deposit monitor during evaporation.

A small amount of sulphur (about 200µg) is placed in a tungsten crucible covered with alumina. This type of crucible has been chosen, because there is no reaction possible between the two materials.

The reaction takes place in a drying-oven at 150°C, where the silver layer on the glass-slide is placed on the crucible containing the sulphur. The distance between the silver layer and the sulphur is about 3mm.

The chemical reaction

$$2Ag + S \rightarrow Ag_2S$$

starts and a brownish stain appears on the contact glass side. When the sulphur has completely passed through the silver layer, the target is brown and the reaction can be considered as being finished.

If the silver layer remains too long a time upon the sulphur, the target will increase in area, but will not contain an excess of sulphur.

The reaction takes place easily in an oven, when both, the silver layer and the sulphur are at the same temperature. The sulphurization is more difficult in the atmosphere, when only the crucible containing the sulphur is heated.

After about four minutes, a silver layer of 100µg/cm^2 is saturated in sulphur. The diameter of the target was about 10mm.

When the reaction is finished, the target is removed from the slide by floating it on distilled water, and put on a target frame.

2.3. The efficiency of the method

With 200µg of sulphur, we have made seven targets of 150µg/cm^2 of silver sulphide, by saturating silver layers of 125µg/cm^2. The efficiency of the method is about 70%, and the success of obtaining self-supporting targets 90%.

3. THICKNESS OF THE TARGETS

The thickness of the silver layer is known during the evaporation by means of the calibrated sensor head. When the sulphurization takes place, we assume that the silver layer will be saturated in sulphur and that the composition of the silver sulphide target will be stoichiometric.

The silver and the silver sulphide targets were weighed and the results corresponded to our calculations from the formula of chemical silver sulphide.

However, the thicknesses of the targets were checked by measuring the stopping-power of the targets, and their composition determined by elastic scattering of alpha particles.

3.1. Stopping-power of the targets

A silver layer of 120µg/cm^2 has been saturated with sulphur. The thicknesses of the silver, sulphur, and silver sulphide corresponding targets have been measured using the energy loss of alpha particles.

The testing system includes a silicon surface barrier detector having a resolution of 18 keV and a multi-channel analyser.

The 5,5 MeV alpha particles from the ^{241}Am source interact with the target and lose energy according to the composition and the thickness of the material traversed.

The amount of energy lost, called $\frac{dE}{dx}$, for α particles at 5,5 MeV, is

given in the stopping-power tables for different elements (ref.3)

$$Ag : \frac{dE}{dx} (keV/\mu g\text{-}cm^{-2}) = 302.10^{-3}$$

$$S : \frac{dE}{dx} (keV/\mu g\text{-}cm^{-2}) = 541.10^{-3}$$

In the case of the compound Ag_2S, it was calculated from the preceeding relations and we found :

$$Ag_2S : \frac{dE}{dx} (keV/\mu g.cm^{-2}) = 334.10^{-3}$$

First, we measured the thicknesses of the silver target and then that of the silver sulphide prepared using the same silver layer.

When we compare the position of the Am peak obtained with the silver target to that with the silver sulphide target, the energy difference between both, converted in $\mu g/cm^2$ represents the amount of sulphur which satures the silver layer.

Using the theoretical relations, we can calculate the thickness in $\mu g/cm^2$ of several silver, sulphur and silver sulphide corresponding targets.

The results are given in the following table :

	keV	$\mu g/cm^2$
Ag	38 ± 2	126 ± 6
S	11 ± 2	20 ± 2
Ag_2S	49 ± 2	146 ± 6

The thicknesses obtained correspond perfectly to the stoichiometric formula of the silver sulphide and prove that there is no excess of sulphur on the target.

3.2. Determination of target composition by elastic scattering of alpha particles (ref.4)

A very sensitive method of determination of targets components is the

study of elastic scattering of charged particles. A knowledge of the energy and the cross-section of the scattered particles permits qualitative and quantitative analysis of the target. Quantities of element down to 0,1µg/cm^2, as well as of trace elements can be detected through this process.

From systematic analysis of silver sulphide targets of 17 to 115 g/cm^2, we conclude that :

- the saturation of the silver layer with sulphur is independant of the thickness of the former
- the only relative important contaminant present is 0,5µg/cm^2 of oxygen for a target of 17µg/cm^2 on a 10µg/cm^2 carbon backing
- and the targets are reproductible.

The energy and the elastic scattering cross-section of 10 MeV incident alpha particles were measured at an angle of 30° with a surface barrier localisation detector in the focal plane of a Buechner spectrometre.

Fig.1 and 2 represent the spectra of silver sulphide targets with natural sulphur and 80% enriched ^{34}S respectively, obtained in the same experimental conditions. That, about forty channels separate two neighbouring peaks of ^{32}S and ^{34}S, shows the precision of the method. The following table gives the values obtained :

	Ag µg/cm^2	S µg/cm^2	S (theoretical calculation) µg/cm^2
Spectre 1	19,9	2,9	3
Spectre 2	17,2	2,9	2,8

The results are compatible within 10% of the stoichiometric composition of the targets.

4. CONCLUSION

Unsing this method, we have made many self-supporting silver sulphide targets isotopically enriched with ^{32}S, ^{34}S and ^{36}S.

The minimum thickness that is possible to produce without backing is about 60µg/cm^2 of silver sulphide, which means, saturating a silver layer of about 50µg/cm^2. Below this, the silver can be evaporated on a thin carbon layer (for instance of 10µg/cm^2) and it is sulphurized in the same way as described above. There does not seem to be an upper-limit for the target thickness : self-supporting silver sulphide targets (sulphur content being 3,5% enriched ^{36}S), of 500 and 900µg/cm^2 were prepared without difficulties.

The targets were strong, stable, pure and needed for their preparation a small amount of sulphur isotope, which in terms of the usual cost-price, is nevertheless appreciable.

REFERENCES

1) G.A.P. Engelbertink and J.W Olness "Beta Decay of ^{38}S", Phys. Rev. C, Vol.3, n° 1, January 1971

2) D.D. Watson "Simple Method for Making Sulphur targets", Rev. of Sc. Instr., Vol.37, n° 11, November 1966

3) C.F. Williamson, J.P. Boujot, J. Picard "Tables of Range and Stopping Power of Chemical Elements for charged particles of Energy 0,05 to 500 MeV", Rapport C.E.A., R 3042, 1966, Centre d'Etudes Nucléaires de Saclay.

4) The analysis of the targets was realized by B. Bilwes, Laboratoire des Basses Energies, C R N Strasbourg

FIGURE CAPTIONS

Fig.1 Position-Spectrum obtained at 30° by elastic scattering of 10 MeV α-particles on a 17μg/cm^2 natural silver sulphide target on a 10μg/cm^2 carbon backing.

Fig.2 Position-Spectrum obtained at 30° by elastic scattering of 10 MeV α-particles on 17μg/cm^2 80% ^{34}S enriched silver sulphide target on a 10μg/cm^2 carbon backing.

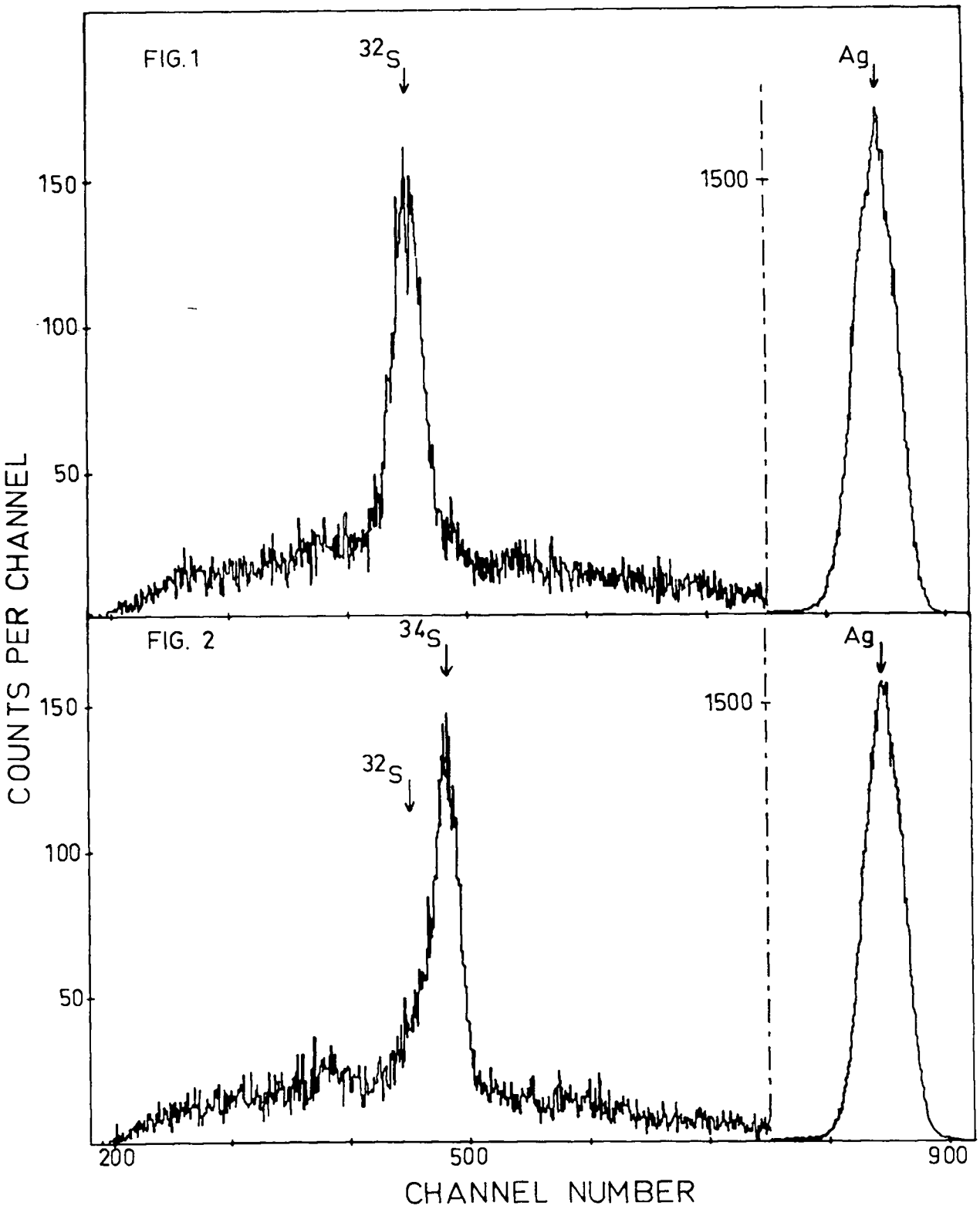
FIG. 1
32S
Ag
1500
150
100
50
FIG. 2
34S
32S
Ag
1500
150
100
50
COUNTS PER CHANNEL
200
500
900
CHANNEL NUMBER

REPRODUCIBILITY AND ACCURACY IN THE PRODUCTION AND THICKNESS MEASUREMENT OF EVAPORATED CARBON FILMS*

John O. Stoner, Jr. and Stanley Bashkin

Physics Department, University of Arizona*

Tucson, Arizona

ABSTRACT

Although the optical and electrical properties of carbon films evaporated from arcs in vacuo vary substantially with variations in technique, we have found it possible to monitor the thicknesses of such films to indicate accurately (typically ± 10%) their carbon content. In order to develop films with surface densities greater than about 100 $\mu g/cm^2$, for which the optical transmittance is too small to be used, we have used "witness" slides that indicate the amount of carbon added to coatings initially having surface densities of 80-100 $\mu g/cm^2$.

*Supported in part by NSF, ONR, and NASA

We make carbon films to be used as self-supporting targets for a variety of purposes: beam-foil spectroscopy, ion strippers, x-ray windows, optical filters, and backings for other target materials. Our thinnest carbon foils have surface densities less than 1.0 $\mu g/cm^2$; the thickest have surface densities greater than 300 $\mu g/cm^2$. We make these by the method suggested by Dearnaley (1960), evaporating from a carbon arc *in vacuo* onto soaped and polished microscope slides.

For many applications, it is necessary to know the surface densities of the carbon layers. A non-destructive method that we have used successfully is to measure the optical transmittance at λ5461 Å of the carbon film of interest. We had previously (Stoner, 1969) calibrated this quantity vs. carbon surface density, over the range 0-70 $\mu g/cm^2$. The determination is good to approximately $\pm$ 10% or $\pm$ 1 $\mu g/cm^2$, which is good enough for most purposes. By constructing multiple carbon coatings whose components' surface densities were found optically in this way, we have been able to extend the calibration to about 110 $\mu g/cm^2$. Above this surface density, at which the transmittance is less than 0.01%, such measurements become rapidly more difficult and unreliable because of the low levels of stray light that may be tolerated.

We have been able to make carbon layers with known surface densities in the range 120-300 $\mu g/cm^2$ by evaporating in several cycles. After the first cycle, during which we deposit 90-100 $\mu g/cm^2$ of carbon, we measure the surface densities directly by the transmittance method. We then replace the same slides in the evaporator, placing uncoated "witness" slides next to them, and again evaporate 90-100 $\mu g/cm^2$ (or

as needed). The original slides now have coatings that are too thick to transmit measurable amounts of light, but the amount of carbon added to each can be found by interpolation of measurements on the witness slides. We expect to have cumulative errors in the resulting thickness determinations, and usually estimate them as ± 20% in the surface densities.

It was not until recently that we found a review (McClintock and Orr, 1973) that points out that the optical transmittance of a carbon film is not a reliable measure of its surface density! Presumably our success in using this method is due to the fact that we always use the same evaporation technique. We have sometimes obtained verifications of our determinations from scattering and energy-loss measurements (Fig. 1).

Although measuring the surface density of a carbon film via its transmittance is easy when the film is outside the evaporator, it is not so easy while the film is being formed inside the evaporator. The carbon arc source emits both intense light and carbon vapor, and these interfere with the monitoring process.

In order to measure the progress of evaporation in situ, we have explored the possibility of measuring the electrical resistance of a carbon film as it is formed. For this purpose we make a monitor slide by gluing two parallel copper wires 32 mm apart to a 25.4 x 76.2 mm microscope slide. We then paint colloidal graphite over these wires, leaving a square, uncoated region 25.4 x 25.4 mm (Fig. 2). The resistance between the wires is monitored by an ohmmeter during the evaporation. This resistance is usually reliable to about ± 20% in indicating the carbon surface density (Fig. 3). Occasionally, we observe

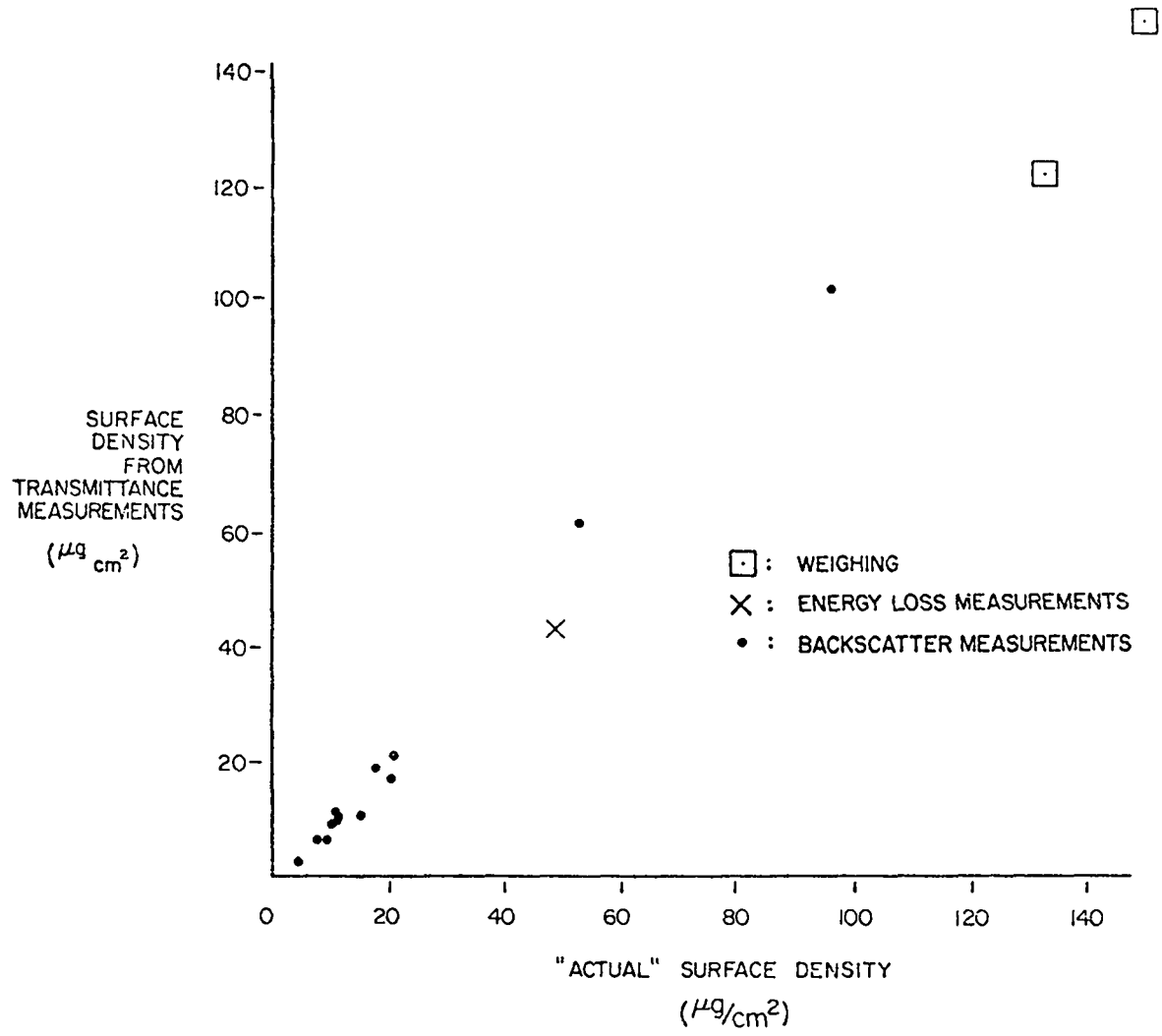

Fig. 1 Measurements by weighing, energy losses, and backscattering rates verify that the transmittance measurements provide useful indicators of surface densities of carbon foils (from private communication from B. Curnutte).

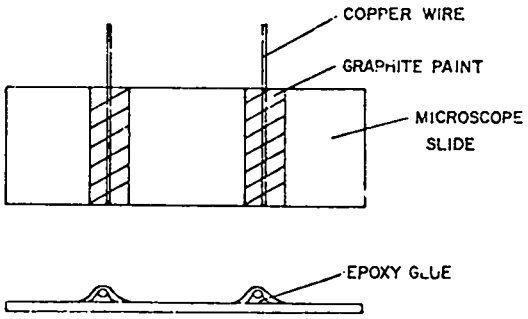

Fig. 2 Monitor slides used for resistive measurements of carbon-foil surface densities.

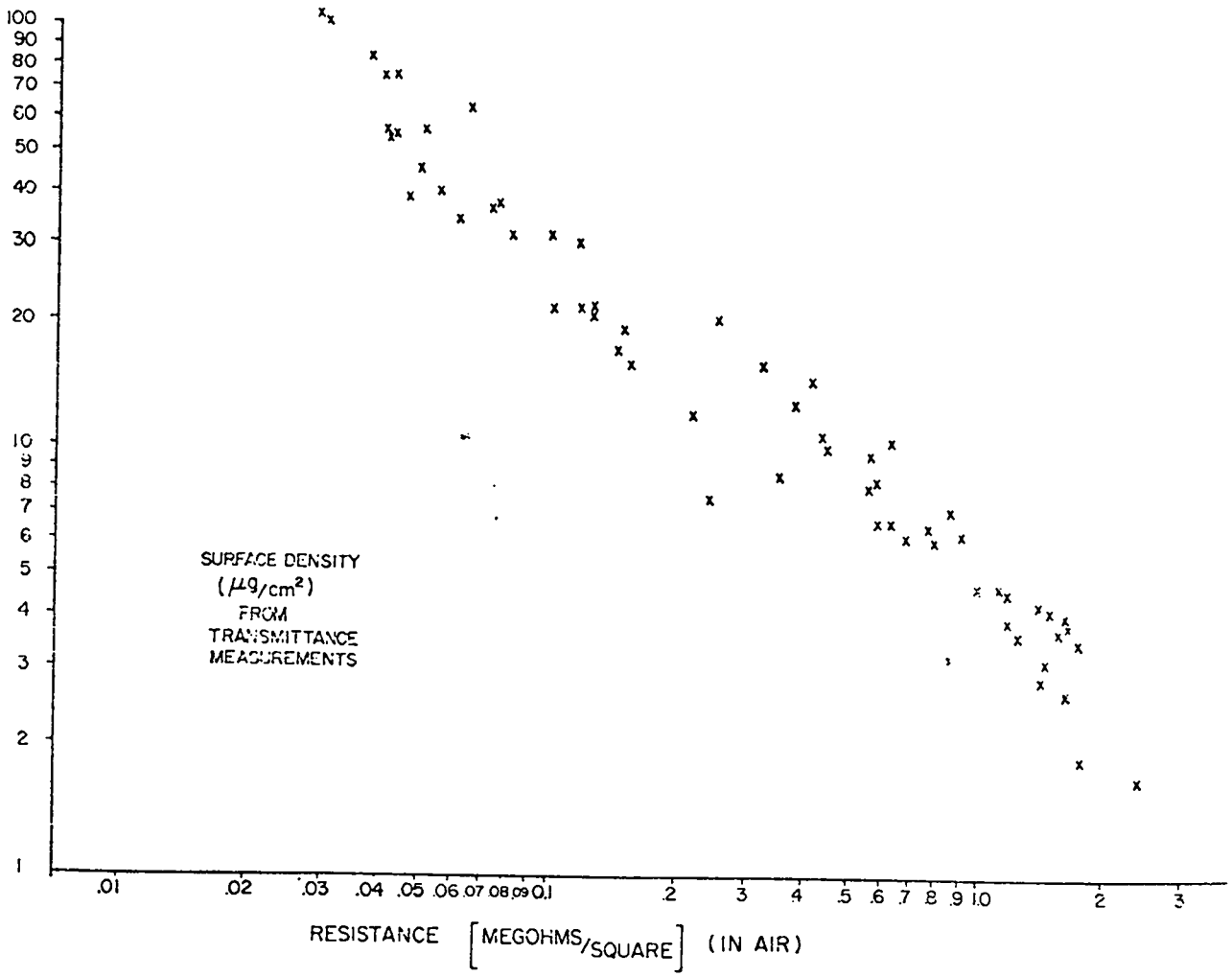

Fig. 3 Resistance vs. surface density for carbon foils.

anomalously-high resistance values, and have in some cases been able to associate them with pressures that were unusually high during evaporation. Over the range of surface density 2-100 $\mu g/cm^2$, our data are consistent with an approximate resistivity of 1.5 ohm-cm, which is much greater than that for carbon or graphite, and is consistent with others' measurements on carbon films (see McClintock and Orr, 1973). As others have found, however, the reproducibility of such measurements depends critically on the conditions of evaporation, and the resistance method does not appear to be a precise way of providing surface-density values.

Below about 2 $\mu g/cm^2$ the resistance monitor fails. Its behavior is erratic and suggests reaction of the freshly-deposited films with residual gas in the evaporator. Since carbon is known to evaporate as C, C_2, and C_3, all highly reactive (Schaeffer and Pearson, 1969), this is not surprising. It may also help explain why "carbon" films have a hydrogen component, typically 1.2 g/cm^2, roughly independent of total thickness (Stoner, 1969 and Curnutte, private communication).

References

G. Dearnaley, 1960, Rev. Sci. Instrum. 31, 197 .

I. S. McClintock and J. C. Orr, 1973, Chemistry and Physics of Carbon, P. L. Walker and P. A. Thrower, editors, Vol. 11, (Marcel Dekker).

R. Schaeffer and R. K. Pearson, 1969, J. Am. Chem. Soc. 91, 2153.

J. O. Stoner, Jr., 1969, J. Appl. Phys. 40, 707.

A Method for the Preparation of Selenium Foils

J.L. Gallant

Atomic Energy of Canada Limited

Chalk River Nuclear Laboratories

Chalk River, Ontario, Canada K0J 1J0

ABSTRACT

A characteristic of allotropic selenium is its brittleness at room temperature. It is therefore impossible to prepare foils of this metalloid by conventional means. However when immersed in distilled water at 80°C selenium becomes very soft and can be rolled. An evaporated film can be released from its substrate by this procedure.

DISCUSSION SUMMARY

VAPOR DEPOSITION OF LARGE AREA NpO_2 AND UO_2 DEPOSITS - H. L. Adair

The substrate for UO_2 was 0.015-in.-thick titanium at 200°C heated by quartz iodide lamps. The bonding of actinide oxide deposits to titanium is good when Ti is heated to ~ 200°C.

Synchronization of evaporation rates from the two guns: a quartz crystal monitor calibration was established for the deposits on the rotating drum. When the lower end of the desired range was reached, the evaporation was stopped, and the test plates at each side of the drum were weighed. Compensation was then made by heating whichever gun needed to evaporate more.

The UO_2 system is in an open lab, not in a glove box. The roughing pump exhausts to an absolute filter. Respirators are worn when the system is opened. The systems have to be decontaminated for different isotopes.

Electron gun power is ~ 100 mA at 6 to 7 kV for UO_2. Rotating drum speed is 50 rpm. U_3O_8 is heated in vacuum to convert to UO_2 and outgas at the same time.

ALTERNATIVES TO THIN CARBON FOILS FOR USE IN STRIPPING HEAVY ION BEAMS D. Ramsay

There are discrepancies in the data on heating of stripper foils. Some experiments use a furnace, some radiant heating. A hot tungsten filament near the carbon would cause electron flow through the target foil. The increased current density could offset an effect due to heating.

Annealing of damage does not occur at the beam spot temperatures normally reached.

Experiments with liquid strippers at the Univ. of Washington were described. A rapidly rotating wheel is dipped into diffusion pump oil, throwing up a continuous hydrocarbon film. Five to ten $\mu g/cm^2$ has been reached.

THE PREPARATION OF NITROGEN-15 TARGETS - J. D. Stinson

Less carbon contamination than reported is indicated when the targets are analyzed by spark spectroscopy. The reported carbon is from Van de Graaff experiments where carbon is always present.

Alloying of Ti with the W boat is not a problem in this case because of the small loadings required.

REDUCTION TECHNIQUES FOR ISOTOPIC MATERIALS - J. M. Heagney

Hydrogen reduction of chromium oxide is fairly difficult. The hydrogen must be pure, and a high temperature, > 1350°C, is required. Most reductions require at least 1 hr; possibly 2 hrs are needed for Cr. Reoxidation of Cr may occur on cooling if any water vapor is present in the hydrogen. Carbon can be used for simultaneous reduction-evaporation of Cr. The carbon used is filings from spectroscopic carbon rod.

A method reported for lead oxide is to heat it with rice starch. The starch decomposes to make carbon, which reduces the oxide to lead.

Lead nitrate can be simultaneously reduced and evaporated in a pinhole boat, but the substrate has to take a fairly high temperature.

Cadmium has been simultaneously reduced with carbon and evaporated onto a substrate seeded with a very thin layer of Be or other material that matches the crystal structure of Cd.

Rare earth oxides are often reduced with thorium reductant. After one redistillation lanthanum may be a worse contaminant from reduction than Th. To use La successfully, use a low temperature and long time.

Zinc may be cleaned up with white silver solder flux. Zinc with flux on top is heated in a conical tube to the flux melting point. The flux is washed off after cooling.

DEUTERATED TITANIUM TARGETS ON THIN BACKINGS - A. Méens

Source to substrate distance was 15 cm.

TARGETS OF SILICON OXIDE AND VANADIUM OXIDE ENRICHED IN ^{18}O ON VARIOUS BACKINGS - A. Méens

The silane is at atmospheric pressure. Cleaning of silane from the vacuum system must be complete before admitting air because silane is highly explosive.

Anodic oxidation makes stronger targets. The described method is not for self-supporting foils.

Direct oxidation of silicon with ^{18}O might be done, but a temperature > 1000°C is required.

PREPARATION OF ISOTOPICALLY ENRICHED MERCURY TARGETS - H. J. Maier

Targets can be made up to 15 to 20 mm in diameter.

The targets are cooled while in use. (Amalgam targets are even more sensitive to warm-up dissociation.) They are cooled from the edges by connecting to a copper block with silver paint. The copper block is cooled to -80°C; the target is probably at about -50°C.

A METHOD FOR STRETCHING ULTRATHIN POLYPROPYLENE FILMS - D. M. Barrus

Thickness of the films is measured by x-ray transmission and by the weighing of a known area on a microbalance. Uniformity is accurately observed by visual examination of color fringes.

Conduction of nichrome coating begins at 50 Å.

The films suffer radiation damage in about 1 hr in a flux of 10^7 photons/sec.

PREPARATION OF ULTRATHIN POLYETHYLENE FILMS BY FILM CASTING - B. S. Cranfill

Standard pre-cleaned slides are used. No special cleaning is needed except wiping free of dust.

PLASTIC-BONDED TARGETS OF CARBON 13 AND SILICON - R. K. Rohwer

The 8% binder required for carbon is probably inherent for carbon. The binder amount for silicon might be reduced to 3% if the particles were carefully screened. The amount needed depends on particle surface area, with 3% binder routine.

THICK TARGETS FOR IN-BEAM HYPERFINE STRUCTURE STUDY - D. Ramsay

The holder ring was split to prevent eddy currents in the ring from rf. There was no problem with the sheet foil.

A RAPID AND ACCURATE METHOD FOR MEASURING THE THICKNESS OF EXTREMELY THIN TARGETS - P. Maier-Komor

Sodium fluoride was used as a parting agent because of high humidity, which causes difficulty with Teepol. NaF is evaporated in vacuum followed by the carbon evaporation. The carbon films must be pinhole free. Uniformity is not crucial because the beam spot is 5 to 8 mm in diameter. A laser of the appropriate wavelength is recommended for measuring uniformity in small areas.

This method is feasible for metal foils (Au, Al, Ag), but surface effects cause a problem. Nitrogen and oxygen are adsorbed on the metal surface in thicknesses dependent on the history of the foil. In carbon the gas content is all the way through the foil.

PRODUCTION OF FRACTIONAL ATOMIC LAYER STANDARDS OF NIOBIUM AND VANADIUM G. E. Thomas

There is too little material present for activation analysis.

The question was raised of the significance of 0.001 monolayer. It might be in islands rather than in a uniform layer. It could be scanned with an ion microprobe.

THE ROLE OF AUGER ELECTRON SPECTROSCOPY AND SECONDARY ION MASS SPECTROSCOPY IN THIN FILM COMPOSITION ANALYSIS - R. W. Springer

The beam profile is approximately Gaussian, with a spot variable from 100 μm to a few mm. Argon and xenon ions are produced in a simple ion gun and focused by an einzel lens.

In using SIMS, the ion beam and electron beam must be in perfect registry. If they are not, the electron beam hits the wrong part of the crater. A technique to eliminate the problem is to put deflector plates on the guns. The spectrometer is gated only when the beam is at the center of the crater.

If there is a question that preferential sputtering is taking place, an electron microprobe will show if the film is uniform to a depth of 1 μ. Then you can decide if preferential sputtering is occurring.

FOCUSED ION BEAM SPUTTERING APPARATUS - W. D. Riel

Commercial units are available from General Ionex and Danphysik. The reasons for the attractiveness of the process are as follows.

For high-vacuum evaporation of refractories or low-vapor pressure materials, sputtering will deposit without high temperature. Standard sputtering operates in a fairly high pressure with chance of contamination, using large amounts of sputtering material.

The focused beam system has a duoplasmatron source operating with Ar^+ or Kr^+, followed by an einzel lens that focuses the beam to a spot 2 to 5 mm in diameter. It operates at 10^{-6} torr or better and requires only small quantities of material. The beam is about 2 mA at 8000 to 20000 V.

The tradeoff for these advantages is speed. Deposition times are from one or two to many hours.

The isotopic material is placed in a beam stop of spectrographic grade graphite. Although the beam strikes only the charge, a halo strikes the graphite. In spite of carbon's low sputtering yield, considerable material is deposited, such as carbon and possibly contaminants adsorbed on the graphite. Duoplasmatrons are finicky and sometimes hard to operate stably for many hours. Tungsten filaments frequently burn out before the end of a long deposition. The method is promising but still has many problems.

The following comments were added in discussion.

Some materials, which would not make a self-supporting film, benefit from carbon deposition from the graphite stop because carbon content makes them self-supporting. Films may also be made of metals that are highly stressed when vacuum evaporated.

The tungsten contamination transferred to the substrate appears to be about 1%.

There is no alternative for this method for rare actinide oxides, which are available only in very small quantities.

Another possible method for beam generation is the Penning ion gauge source (PIG). This has a cold cathode, probably reducing the contamination problem. Beam spots of 1 mm are reported and more stable operation for long periods. The more finely focused beam should have less halo and less destruction of carbon substrate films.

The General Ionex machine has an ion-exchange canal that produces a neutral beam. This prevents charge build-up on nonconducting sputtering materials.

Technics, Inc., makes a micro-ion milling machine for the semiconductor industry. It uses a cold cathode ion source, and the beam comes out focused to 1 mm without additional focusing. It is intended to operate at a high rate for secondary ion deposition.

Another possible alternative ion source is the high temperature surface ionization source developed at Livermore. The tip of a tungsten crucible is heated by electron bombardment. The temperature profile along the crucible axis regulates the rate of evaporation of the charge material. The load is about 2 mg of rare earth oxides, actinides, etc. It could be used with a simple extraction device and retardation lens and could deposit directly onto a substrate.

ROLLING OF METAL TARGETS - W. Perry

Large and expensive rolling mills are not required to make useful targets. One can roll many useful foils down to the 1 to 5 mg/cm^2 region with a small bench-type manually operated mill.

Molybdenum: Powder can be used to roll targets 25 to 30 mg/cm^2. For thinner foils, machine a carbon crucible, melt Mo powder into a ball with an electron gun, crack off the carbon crucible. The ball is good feed stock for rolling. Hand mill rolls to less than 1 mg.

The following results were added in discussion.

Cadmium: Can be rolled down to 5 to 6 mg/cm^2 between 20-to 25-mil mylar sheets.

Calcium: Can be rolled to 700 $\mu g/cm^2$ in a mill in a glove box with flowing filtered argon. The foils are good at 1 mg/cm^2, somewhat oxidized at 700 $\mu g/cm^2$.

In addition to stainless steel, spring steel sheet has been found useful for pack rolling.

Tungsten sheet, 0.003 to 0.005 in., is good for pack rolling, is very hard with a good polish, and can be used many times. Tungsten is not suitable for rolling very thin targets because of its crystal structure.

Palladium: A problem is welding of palladium to the pack when trying for less than 500 $\mu g/cm^2$. This can be avoided by making three to five passes at the same setting before going thinner.

Uranium: 1 mg/cm^2 is about the limit. Since oxidation of U limits its rollability, it is useful to roll, electropolish (sulfuric acid removes oxide), roll again (or roll in Ar). Be careful not to generate too much heat in rolling.

Uniformity may be poor in rolling a small quantity of a separated isotope with few passes--the target is thick in the center, thinner at the edges. Instead of rolling, the material can be pressed between two highly polished flats of cobalt tungsten carbide from a machine shop.

PREVENTION OF STRESS IN FOILS BY SUBSTRATE HEATING - J. C. Gursky

Some information on this topic is available in Thin Film Phenomena by Chopra. Tensile stress causes fracture of thin films and compressive stress causes buckling. Tension decreases with increasing substrate temperature, goes to zero, and in some cases changes to compression with still higher temperature. The temperature referred to is that of the substrate at the time of deposition. Later annealing in this range of 400°C and less does not seem to affect the residual stresses.

The crossover from tensile to compressive stress is related to melting point. It occurs at lower temperatures for lower melting materials. Thus, from the limited experimental evidence available, the crossover point is about 210°C for nickel, 100°C for copper, and about 300°C for iron. This is roughly correlated with empirical results of unstressed or less stressed films deposited on substrates heated to these temperatures. The following table gives some temperatures that have produced good films. Since the stripping agent also influences film structure, this is also given, along with the method of evaporation. Substrates are 1" x 3" glass microscope slides. The electron gun evaporations usually require a minimum ball size of 200 to 300 mg, which is feasible for inexpensive isotopes but not for rare ones. Inorganic stripping agents are vacuum evaporated, 20 to 40 $\mu g/cm^2$.

Radiant heating of the substrate from 5 cm or so distance can be done with a semi-cylindrical furnace heater element or a flat diffusion pump heater element.

TABLE I

Element	Substrate Temp., °C	Stripping Agent	Method of Evaporation	Minimum Thickness, $\mu g/cm^2$
Chromium	375 - 400	KCl	e-gun, sublimes	60
Cobalt	300	KI	e-gun	100
Copper	100	Contrad, KI	Mo boat	50
Gold	100	Contrad	Mo boat	70
	No heat	CsI	Mo boat	45
Iron	325	KI	e-gun or Al_2O_3-coated Mo boat	70 - 80
Manganese	100			100 on carbon backing
Molybdenum	300	KI or NaCl	e-gun	100
Nickel	250 - 300	KI	e-gun	40
Palladium	200	CsI	e-gun, min. ball 50 mg	80
Platinum	350 - 400	KI	e-gun	150
Titanium	230 - 260	KI	e-gun	50
(Following results were added in discussion)				
Pd	350 - 400	NaCl		70 - 80
B	250	NaCl		50 or less
Ge	No heat	Betaine	e-gun	70 - 300
Ge	No heat	NaCl	W boat	
Si	360	$BaCl_2$ on Nickel plate		30 - 250

One possible alternative to substrate heating is a very slow evaporation rate that has given unstressed films of WO_3 and Ti (30 $\mu g/cm^2$ with Betaine parting agent).

Another is to coat the slide with parlodion. This permits the evaporated film to move and relieve stress.

Another suggestion was to evaporate directly onto a formvar or other film mounted on a target frame. This was successful with strontium.

WHAT ARE YOU WORKING ON? - W. D. Riel

This is a compendium of actual or possible solutions to specific target problems.

Irving Feigenbaum reported that in a study of fluorine in food and other organic materials, the ground-up powders were pressed in aluminum cups at about 15 tons and made useable Van de Graaff targets.

Laszlo Csihas described a system for making isotopic oxygen targets. The isotopic gas is introduced into a small chamber containing 30 $\mu g/cm^2$ nickel foils mounted on target frames. The gas is frozen by introduction of liquid nitrogen, then the chamber is pumped out and the oxygen permitted to warm up by removing the liquid nitrogen. A small projector light with focal length of 1-1/2 in. is shined on the center of a nickel foil and oxidation proceeds, leaving a supporting area of nickel around the edges.

A problem exists with evaporating LiF so that it bonds with any base layer such as carbon. It flakes badly when the thickness is three to four mg/cm^2 on stainless steel. Etching of the surface and glow discharge cleaning don't improve the sticking. One possibility is sputtering, which inherently produces a better-adhering film. A thin layer of LiF might be sputtered, followed by vacuum evaporation of the rest of the thick layer. It might also be possible to bond LiF to stainless steel by pressure. Another suggestion that helps bonding with thinner LiF is to do all parts of the process slowly--slow cooldown, vent to about 1/3 atmosphere of inert gas for an hour or so, vent slowly to atmosphere.

The sticking of calcium fluoride was improved in 200 $\mu g/cm^2$ thickness by heating the substrate to 150°C.

ATTENDEES - VISITORS

H. L. Adair
Isotope Research Materials
Oak Ridge National Laboratory
Oak Ridge, Tennessee 37830

Robert B. Anderl
EG&G Idaho, Inc.
Idaho National Engineering Lab.
Idaho Falls, Idaho 83401

Laszlo Csihas
University of Pennsylvania
209 S. 33 St. E-1
Philadelphia, Pennsylvania 19174

Edith B. Fehr
Physics Department
Nuclear Structure Laboratory
Yale University
New Haven, Connecticut 06511

Irving L. Feigenbaum
Bldg. 901A
Tandem Van de Graaff
Brookhaven National Laboratory
Upton, L.I., New York 11973

Donald J. Hammond
Medi-Physics, Inc.
5801 Christie Avenue
Emeryville, California 94608

Joanne M. Heagney
Micro Matter Company
197 - 34th East
Seattle, Washington 98112

Joseph S. Heagney
Micro Matter Company
197 - 34th East
Seattle, Washington 98112

Joaquín Hernández
Cyclotron Institute
Texas A and M University
College Station, Texas 77843

T. A. Hodges
TRIUMF
University of Victoria
Victoria, B.C., Canada

Frank J. Karasek
MSD 212 H-118
Argonne National Laboratory
9700 S. Cass Avenue
Argonne, Illinois 60439

Charles I. Krieger
Bldg. 362 B002
Argonne National Laboratory
9700 S. Cass Avenue
Argonne, Illinois 60439

Bill Lozowski
Indiana University
Cyclotron Facility
Milo B. Sampson Lane
Bloomington, Indiana 47401

Hans-Jörg Maier
Sektion Physik
4ER Universitat Munchen
8046 Garching-Am Coulombwall 1
West Germany

Peter Maier-Komor
Techn. Universitat Munchen
D 8046 Garching Bei Munchen
West Germany

Andrée Méens
Centre de Recherches Nucléaire
Laboratoire PNPA
67037 Strasbourg - CEDEX
France

Wayne L. Perry, Station 49
Atomic Energy of Canada Ltd.
Chalk River Nuclear Labs.
Chalk River, Ontario
Canada